New ionization and tagging methods for mass spectrometry

THÈSE N^{O} 8273 (2017)

PRÉSENTÉE LE 11 DÉCEMBRE 2017
À LA FACULTÉ DES SCIENCES DE BASE
LABORATOIRE D'ÉLECTROCHIMIE PHYSIQUE ET ANALYTIQUE
PROGRAMME DOCTORAL EN CHIMIE ET GÉNIE CHIMIQUE

ÉCOLE POLYTECHNIQUE FÉDÉRALE DE LAUSANNE

POUR L'OBTENTION DU GRADE DE DOCTEUR ÈS SCIENCES

PAR

Xiaoqin ZHONG

acceptée sur proposition du jury:

Prof. C. Heinis, président du jury
Prof. H. Girault, directeur de thèse
Dr A. Rodolphe, rapporteur
Dr J.-M. Busnel, rapporteur
Dr N. Lion, rapporteur

ÉCOLE POLYTECHNIQUE
FÉDÉRALE DE LAUSANNE
Suisse
2017

To my family and friends

致我的亲人和朋友

Acknowledgements

First of all, I would like to sincerely appreciate my thesis advisor Prof. Hubert Girault for his constant and precious guidance, both in science and life. Motivated by his creativity and passion in science, I have experienced an interesting research life in the past four years, which I will benefit from and cherish throughout my future career. Inspired by his freedom in life and prudence in science, I learned an exceptional lesson about the interdependence between work and leisure. Especially, his optimism and wisdom have encouraged me to overcome difficulty and depression in everyday research.

I warmly thank Prof. C. Heinis as my jury president, Dr. N. Lion, Dr. J. Busnel and Dr. R. Antoine for accepting to be my jury members, reading and correcting my thesis.

I would like to deeply thank Dr. Liang Qiao. Without his selfless help and fruitful discussion, this thesis would not be accomplished. He helped me adapt to the big family of LEPA in the beginning and guided me into the research field of analytical chemistry particularly mass spectrometry. I will never forget how patient and detailed he taught me how to use mass spectrometry, solve experimental problems and write a professional paper. His modest attitude and open mind in science have influenced me most.

I would also thank the helpful discussion with Dr. Natalia Gasilova about my projects and collaboration in solving mechanical problems. I am surprised by her super carefulness, logical analysis and strong responsibility for everything related. She influenced me a lot in amending my mistakes and shortcomings.

I would like to thank the help from mechanical and electronic workshops in ISIC of EPFL, especially Frédéric Gumy from LEPA. I also thank LEPA secretary Madame Patricia Byron-Exarcos. She is professional in paper work and so passionate in life that I am happy to talk with her. I also want to thank secretary Anne Lene Odegaard in ISIC for her assistance with all administrative routines.

I devoted my special thanks to Tzu-En Lin, Yingdi Zhu and Fangting Zhang. We had lunch together almost every day and shared girls' secrets in daily life. They are so pretty, friendly, and of course excellent in scientific research. I also thank all the former and current LEPA colleagues, especially grateful to Haiqiang Deng, Yan Deng, Shuai Yang, Smirnov Evgeny, Jovic Milica, Alexandra Bondarenko, Battistel Alberto, Amstutz Véronique, Piwek Justyna, Atek Imene, for their help and kindness either in research or in daily life.

I really appreciated the friendships with several Chinese friends, including Jiangman Zhao, Meng Lin, Cuiyun Shao, Qiu Liu, Yang Sun and Wei Yan. With them, my weekends and holidays became colorful and funny. We had countless dinners, shared complaints or crazy ideas, and did many other things together, such as skiing and travelling. I really hope they enjoy the time with me, as I enjoy hanging out with them.

I especially thank to one of my best friends, Shenghan Zhang. He accompanied me through a very tough period during the preparation of this thesis. We talked about everything almost everyday and cared for each other. We have many aspects in common, especially the drawbacks, but we encouraged each other to become more mature. I wish we could cherish this precious friendship forever.

I would give my sincerest thank to my ex-boyfriend, Shiwei Zhou. During the past 9 years either together or separated, he took care of me a lot and gave me unconditional understanding and supporting. Our characters are different but partially complementary, and through him I have seen a fancy world from another aspect, which is full of love, curiousness and empathy for everybody and everything.

Finally but most importantly, I addressed my deepest thank to my family, especially my father Yuannan Zhong. He brought me up and gave me the opportunity of receiving good education. Though we quarrel often and do not know how to express our emotions well, I understand he has done his best to love me. I also thank to my mother for giving me life to experience the world and finish this thesis.

Abstract

Mass spectrometry (MS) is an essential detection tool in bioanalytical chemistry owing to its exceptional selectivity and sensitivity, paired with rapid analyte identification and quantification. In this thesis, two classical MS and a newly developed ionization method are employed, including matrix-assisted laser desorption/ionization (MALDI) MS, electrospray ionization (ESI) MS and electrostatic spray ionization (ESTASI) MS.

To meet the emerging challenges in bioanalytical chemistry, from disease diagnosis to drug development, new MS-based analytical methods ought to be developed with respect to high sensitivity, throughput, speed, as well as sample consumption and experimental simplification. For these purposes, this thesis presents four analytical strategies combined with MS detection for improved analytical performance in different research fields.

Two classical analytical tools, thin layer chromatography (TLC) and 384-well plate, were coupled with ESTASI-MS respectively. In ESTASI-TLC-MS, ESTASI was applied to extract and identify a wide range of molecules of different polarities and chemical structures from both hydrophilic or hydrophobic silica plates with high sensitivity and minimal sample consumption in the femtomole range. In 384-well plate ESTASI-MS, the commercial 384-well plate could work as a container and an emitter for sample spray ionization, without any liquid delivery system or any additional interface. This approach provides fast and high throughput analyses for the large batches of reactions, such as enzyme assay and drug metabolism. Tyrosinase-catalyzed tyrosine oxidation in the presence or absence of inhibitors and cytochrome P450-catalyzed metabolic reactions of two drugs were studied respectively.

To improve analysis sensitivity, two strategies, mass barcoded gold nanoparticles (Mb-AuNPs) for MALDI-MS signal amplification and microfabricated on-chip spyhole (Ø 10-12 μm) emitter for nanoelectrospray (spyhole-nanoESI), were developed, leading to a low sample consumption and high analysis efficiency. Mb-AuNPs combined with magnetic separation were applied for multiplex cow's milk allergy diagnosis in a component-resolved manner. IgE antibodies (Abs) could be extracted from a patient's blood serum by the formation of a sandwich structure between allergenic proteins-coated Mb-AuNPs and anti-human IgE Abs-functionalized magnetic beads (MBs). Detection of Mb-AuNPs by MALDI-MS provides a limit of detection (LOD) down to picograms per milliliter level for specific IgE Abs from only 1 μL of patient's blood serum. To take advantages of microfluidics in low

sample consumption and easy integration, a novel interface of spyhole-nanoESI was designed for coupling microfluidics with MS and showed an improved sensitivity than standard ESI. This disposable microchip coupled with MS/MS shows potential application in cancer diagnosis by the successful detection of a small cell lung cancer biomarker in 1 μL of human serum at the extensive stage, without any complicated sample preparation steps.

Key words: matrix-assisted laser desorption ionization, electrospray ionization, electrostatic spray ionization, nanoelectrospray ionization, mass spectrometry, thin layer chromatography, signal amplification, gold nanoparticles, 384-well plate, microfluidic chip, allergy, cancer biomarker, drug metabolism.

Résumé

La spectrométrie de masse (MS) est un outil de détection essentiel en chimie bioanalytique en raison de sa sélectivité et de sa sensibilité exceptionnelle, avec une identification et une quantification rapides des analytes. Dans cette thèse, on utilise trois types de spectromètre de masse avec une source désorption/ionisation laser assistée par matrice (MALDI), une source d'ionisation par électronébulisation (ESI) et une source d'ionisation par nébulisation électrostatique (ESTASI).

Pour répondre aux défis émergents dans les applications de la chimie bioanalytique, du diagnostic médical au développement de médicaments, les méthodes de spectrométrie tirent avantage de la sensibilité, du débit, et de la vitesse, ainsi que de la faible consommation d'échantillons et de la simplification expérimentale. Cette thèse présente diverses stratégies analytiques utilisant la MS comme méthode de détection pour améliorer les performances analytiques dans différents domaines de recherche.

Deux outils analytiques classiques, une chromatographie en couche mince (TLC) et une plaque de 384 puits ont été couplés avec ESTASI-MS respectivement. Dans ESTASI-TLC-MS, ESTASI a été appliqué pour extraire et identifier une large gamme de molécules de différentes polarités et structures chimiques à partir de plaques de silice hydrophiles ou hydrophobes avec une sensibilité élevée et une consommation minimale d'échantillon dans la gamme de la femtomole. Dans l'approche plaque-ESTASI-MS, une plaque commerciale de 384 puits plaque a été utilisée comme récipient et comme émetteur pour l'ionisation par électronébulisation d'échantillons, sans système de fluidique ni aucune interface supplémentaire. L'approche fournit des analyses rapides et à haut débit pour les nombreux lots de réactions, tels que le dosage enzymatique et le métabolisme médicamenteux. L'oxydation de la tyrosine catalysée par la tyrosinase en présence ou en l'absence d'inhibiteurs et les réactions métaboliques catalysées par la cytochrome P450 de deux médicaments ont été étudiées respectivement.

Pour améliorer la sensibilité à l'analyse, deux stratégies, les nanoparticules d'or modifiées avec des code-barres massiques (Mb-AuNPs) pour l'amplification du signal de MALDI-MS et l'émetteur sur puce (spyhole, Ø 10-12 μm) pour la nanoélectronébulisation (spyhole-nanoESI), ont été développées pour une faible consommation d'échantillons et une efficacité élevée d'analyse. Les Mb-AuNPs combinées avec la séparation magnétique ont été

appliqués pour le diagnostic multiplex de l'allergie au lait de vache d'une manière résolue par les composants. Les anticorps (Abs) IgE ont été extraits du sérum sanguin d'un patient par la formation d'une structure en sandwich entre les Mb-AuNPs recouvertes de protéines allergènes et les billes magnétiques (MBs) fonctionnalisées avec des anticorps IgE. La détection de Mb-AuNPs par MALDI-MS fournit une limite de détection (LOD) de l'ordre de picogrammes par millilitre pour des IgE Abs spécifiques dans seulement 1 μL de sérum sanguin du patient. Pour profiter des avantages de la microfluidique dans une faible consommation d'échantillons et une intégration facile, une nouvelle interface de spyhole-nanoESI a été conçue pour coupler la microfluidique avec la MS et a montré une sensibilité améliorée par rapport à l'ESI standard. Ce microchip jetable couplée à la MS/MS montre une application potentielle dans le diagnostic du cancer par la détection réussie d'un biomarqueur de cancer du poumon en petites cellules dans 1 μL de sérum humain au stade étendu, sans étapes de préparation d'échantillon compliquées.

Mots-clés: désorption/ionisation laser assistée par matrice, ionisation par électronébulisation, ionisation par nébuliseur électrostatique, ionisation par nanoélectronébulisation, spectrométrie de masse, chromatographie sur couche mince, amplification du signal, nanoparticules d'or, plaque de 384 puits, microfluidique, allergie, biomarqueur du cancer, métabolisme médicamenteux.

List of abbreviations

Abs	Antibodies
APCI	Atmospheric pressure chemical ionization
AuMPs	Gold microparticles
AuNPs	Gold nanoparticles
CE	Capillary electrophoresis
CHCA	α-cyano-4-hydroxy-transcinnamic acid
CI	Chemical ionization
CID	Collision-induced dissociation
CRM	Charge residue model
DAN	1,5-diaminonaphthalene
DBS	Dried blood spot
DEP	Direct electrospray probe
DESI	Desorption electrospray ionization
DHB	2,5-dihydroxybenzoic acid
2D-PAGE	Two-dimensional polyacrylamide gel electrophoresis
ECD	Electron capture dissociation
EDD	Electron-detachment dissociation
EESI	Extractive electrospray ionization
EI	Electron ionization
ELDI	Electrospray-assisted laser desorption ionization
ELISA	Enzyme-linked immunosorbent assay
ESI	Electrospray ionization
ESTASI	Electrostatic spray ionization
ETD	Electron transfer dissociation
FAB	Fast atom bombardment
FD-ESI	Fused-droplet ESI
GC	Gas chromatography
HPLC	High performance liquid chromatography
HTS	High-throughput screening
IEF-GE	Isoelectric focusing based gel electrophoresis

IEM	Ion evaporation model
IPG	Immobilized pH gradient
IR	Infrared radiation
LA-ESI	Laser ablation electrospray ionization
LEPA	Laboratory of physical and analytical electrochemistry
LIAD-ESI	Laser-induced acoustic desorption/electrospray ionization
LOD	Limit of detection
LSI	Liquid secondary ion
MALDI	Matrix-assisted laser desorption/ionization
MBs	Magnetic beads
microESI	Micro-electrospray ionization
MS	Mass spectrometry
MSI	Mass spectrometry imaging
m/z	Mass-to-charge ratio
nanoESI	Nano-electrospray ionization
PDMS	Polydimethylsiloxane
PET	Polyethylene terephthalate
PESI	Probe electrospray ionization
PMMA	Poly(methyl methacrylate)
PTM	Post-translational modification
RP	Reverse phase
SA	Sinapic acid
SCX	Strong cation exchange
SPE-GEMS	Solid-phase extraction-gradient elution-MS
SSP	Surface-sampling probe
TOF	Time of flight
TSP	Thermospray
TLC	Thin layer chromatography
UPLC	Ultra performance LC
UV	Ultraviolet

List of symbols

C	Concentration	mol/L
d	Distance	m
ε_0	Vacuum permittivity	F/m
Ø	Diameter	m
P_L	Laplace pressure	Pa
P_E	Electrostatic pressure	Pa
q	Charge	C
r	Radius	m
γ	Surface tension	N/m
t	Time	min
U	Voltage	Volt
V	Volume	m^3
ϑ	Angle	°
σ	Surface charge density	C/m^2

Table of Contents

CHAPTER I.

Introduction

1.1. Mass spectrometry ion source

1.1.1. General introduction

Since the observation of anode rays by Goldstein in 1886,[1] mass spectrometry (MS) research started and progressed continuously. The progress has led to advent of new instruments and expanded the applications from isotope research and organic molecule detection to solving biochemical issues.[2,3] A typical MS instrument contains three main parts: ion source, mass analyzer and detector. The masses within a sample could be simultaneously determined by ionizing the chemical species with an ion source, separating them according to their mass-to-charge ratios (*m*/*z*) with a mass analyzer, and detecting them with a detector. From a mass spectrum, the elemental, isotopic composition and chemical structures could be elucidated.

It is critical to choose a proper ion source for a MS depending on what types of samples to be analyzed and various ion sources have been introduced consecutively for different purposes. In 1918, Dumpster introduced the first ion source of electron ionization (EI) by bombarding salts with electrons.[4] As a hard ionization technique, EI is predominantly coupled with gas chromatography (GC) for the gas analysis and gives an extensive fragmentation. 50 years later, a complimentary technique of chemical ionization (CI) was discovered by Munson and Field with less fragmentation, through colliding the gas phase analytes with reagent gas ions coexisting in the source for proton transfer, adduct formation or charge transfer.[5]

To analyze liquid samples, atmospheric pressure chemical ionization (APCI) was firstly introduced by Horning and collaborators in 1974[6] and has become a popular interface for coupling liquid chromatography (LC) with MS.[7] Later on, fast atom bombardment (FAB),[8] liquid secondary ion (LSI)[9] and thermospray (TSP)[10] were successively described. Both FAB and TSP were widely applied as interfaces for LC-MS until the beginning of 1990s, when it began to be replaced by atmospheric pressure ionization methods, especially

with the advent of electrospray ionization (ESI) technique.[11,12] Fenn and Aleksandrov established ESI as a powerful ion source in 1980s and Fenn received the Nobel Prize in Chemistry for ionizing large biological molecules with ESI.[13,14] Since then, ESI has become an essential technique for the proteomics studies mainly due to its soft character and easy coupling with separation methods.

For analyzing solid samples, the ion source usually combines both desorption and ionization (DI) processes. Currently, there are more than 25 described DI techniques, each with their own advantages and disadvantages for specific classes of samples and mainly classified into two catalogues. One type is under vacuum and another type, known as ambient ionization techniques, operates at atmospheric pressure with minimal sample preparation. As one of the two most widely used soft ionization techniques together with ESI, matrix-assisted laser desorption/ionization (MALDI) was developed by Franz Hillenkamp, Michael Karas and co-workers in 1985.[23] Tanaka shared the Nobel Prize of Chemistry in 2002 with Fenn for his contribution in ionizing intact biomolecules as large as 34 kDa with MALDI.[16,17]

In analytical chemistry, the most recent applications are oriented towards biochemical studies, such as proteome, metabolome, drug discovery and metabolism, with the two primary ion sources of ESI and MALDI. In this thesis, different analytical methods are developed based on ESI and MALDI MS, and therefore the detailed introductions of ESI and MALDI will be given in the following parts.

1.1.2. Matrix-assisted laser desorption ionization

Since MALDI was introduced in 1988,[17] it has become a powerful and widely used ion source for analyses of a broad range of large, non-volatile and thermally labile compounds such as proteins, oligonucleotides, polymers and large inorganic molecules. This method is characterized by high throughput, easy sample preparation, high tolerance to contaminations, soft ionization of intact molecules with little fragmentation, and giving mainly singly charged ions. Therefore, it has been widely applied for polymer science, biochemistry, microbiology, and medicine development.

1.1.2.1 Principle

The MALDI process involves two steps, co-crystallization of sample and matrix, laser irritation induced sample desorption and ionization. The sample to be analyzed is deposited on a conductive plate together with proper matrix solutions for crystallization. To obtain a

homogeneous sample distribution and geometry, the most commonly used methods for sample preparation include the dried droplet method, thin layer method, and sandwich method with a matrix to analyte ratio of 1000:1 or larger.[18] The analyte molecules are embedded throughout the matrix so that they are mostly isolated from one another. The matrix plays an important role in sample co-crystallization and strong optical absorption in ultraviolet (UV) or infrared radiation (IR) range.[19] Matrices employed for MALDI are normally small organic species and suitable matrix is determined to some extent by trial and error. Some common matrices such as 2,5-dihydroxybenzoic acid (DHB), α-cyano-4-hydroxy-transcinnamic acid (CHCA), and sinapic acid (SA) are particularly suited to nitrogen (337 nm) and Nd-YAG lasers (355 nm).[20]

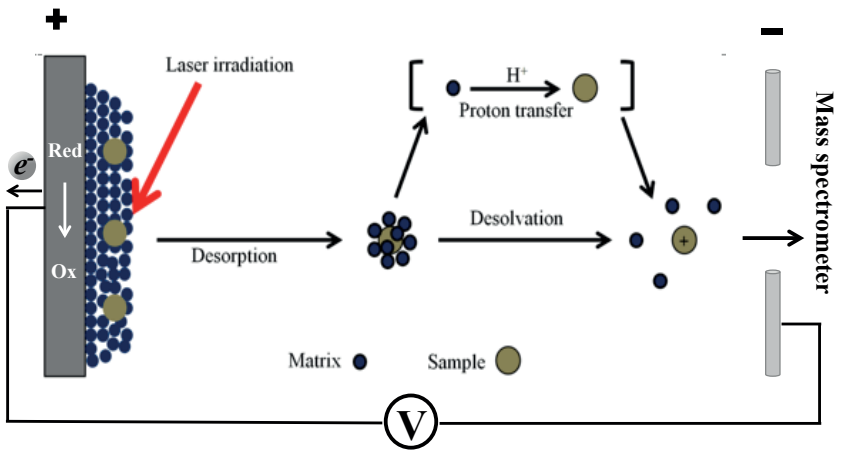

Figure 1.1. Schematic representation of a MALDI source in positive ionization mode. Figure adapted from " Mass Spectrometry: Principles and Applications", 3rd edition, de Hoffmann *et al*., John Wiley & Sons Ltd. © 2007.

The second step occurs under vacuum conditions in the MALDI source and combines photo-ablation and photo-ionization, as shown in Figure 1.1. Upon intense laser irradiation over a short duration, a photochemical process takes place and its exact mechanism is not completely elucidated.[21,22] The rapid heating of sample crystals through laser irradiation-induced excitation of matrix molecules causes localized sublimation of matrix crystals entraining intact analytes into the gas phase.[23] During this process, when and how the ions are produced are still not fully understood.[19,24] The most widely accepted mechanism suggested that the ionization happened through proton transfer from matrix molecules in solid sample crystals before desorption or from photo-ionized matrix molecules in the gas-phase plume.

MALDI is a high frequency pulsed ion source and produces mainly singly charged

ions with large values of *m*/*z*. The analyzer of time of flight (TOF) is fast, theoretically not limited by *m*/*z* values and thereby very suitable for MALDI.[25] The gas phase ions in MALDI are extracted and accelerated towards the field-free TOF tube under a constant electric field between the plate and the detector. The counter ions are driven back to the target plate under the electrostatic field. The initially obtained velocities of ions are reversely related with *m*/*z* values and determine the total time taken to reach the detector after passing through a known length of TOF tube. By measuring the time of flight, *m*/*z* values of ions could be easily obtained. The most important drawback of a TOF analyzer is poor resolution, which is proportional to the flight path and time. To improve the mass resolution, two important strategies were developed by reducing the kinetic energy spread with delayed pulsed extraction[26] or an electrostatic reflector[27] to increase the path length. In a delayed pulsed extraction mode, the ions with same *m*/*z* values but different energies could be separated in the field-free region. The initially less energetic ions receive more kinetic energy and join the initially more energetic ions at the detectors. While with a reflectron TOF, the kinetic energy spread could be reduced by creating a retarding field behind the field-free region. The ions with more kinetic energy will penetrate the reflectron more deeply for a longer time inside and thereby reach the detector at the same time as slower ions with the same *m*/*z*.

1.1.2.2 Quantification

Quantitative analysis with MALDI was considered as improbable due to the low shot-to-shot reproducibility and strong dependence on sample preparation process. There is a poor correlation between uncorrected signal intensity and analyte amount. But, there are still several ways to optimize the experiment conditions and design experiments that allow for meaningful quantitative comparisons by MALDI.[28] For relative quantification, a fixed amount of internal standard with similar chemical or physical properties as the analyte of interest was added into samples and the relative peak intensity or area of an individual analyte to the internal standard is calculated. To obtain the absolute amount of analyte in a sample, a calibration curve requires to be constructed with a constant amount of the internal standard and varying amounts of a single specific analyte of interest. Consequently, the constant of proportionality for one analyte can be deduced to convert the ion intensity ratios to absolute amounts of analytes. When the matrix is rather complex or highly variable between samples and the analyte exists in a low abundance, known amounts of the standard analytes are added to assist the establishment of the calibration curve. The utility of an

internal standard is not necessary for a sample giving a mass spectrum with quite constant relative signal intensities. In this case, a method called profile analysis is utilized to obtain useful information from the changes of relative signal intensities between similar samples. The differences of mass spectra between distinct populations could be examined reproducibly by using classification algorithms and this method has been commonly applied for MALDI protein profiling.[29–31]

1.1.2.3 LDI-MS signal amplification with mass barcodes

The analysis sensitivity and mass accuracy with laser desorption ionization (LDI)-MS are greatly depending on analyte type, concentration and sample complexity. The limits of detection (LODs) of peptides and proteins with MALDI-MS are in practice somewhere between femtomoles and picomoles.[32,33] The nucleic acids (DNA or RNA) are not so easy to be analyzed because of easy fragmentation and strong bonds between phosphodiester group and alkali metal atoms. In clinical diagnostics, the abnormal expression of an early stage disease-related biomarker is normally at an ultralow level in rather complex biofluids, which makes the direct LDI-MS identification challenging. Thus, many efforts have been devoted to concentrate the targets specifically and apply LDI-MS signal amplification strategies to realize the ultrasensitive and even single-molecule detection.

Instead of detecting targets, a surrogate molecule, namely mass barcode here, is designed, grafted onto a surface in a large excess amount over the target analytes, and applied for different applications with LDI-MS.[34,35] With the development of nanotechnology and nanoscience, nanomaterials hold great promise in signal amplification as carriers for high loading of mass barcodes, due to the large surface-to-volume ratio and easy synthesis. Among various nanomaterials, gold nanoparticles (AuNPs) are widely used due to the strong UV energy absorption, size and morphology-controlled synthesis, good biocompatibility, and easy modification of biomolecules for targeting.[36]

Alkanethiols are the most widely used mass barcodes to date because they can be detected easily by LDI-MS and synthesized conveniently with unique structures and distinct masses.[37,38] Besides, several polyethylene glycol units (PEG, $-CH_2CH_2O-$) could be incorporated into mass barcodes, acting as surfactants to reduce unspecific adsorption of analytes onto AuNPs. The mass barcodes could be readily attached to AuNPs through the formation of stable gold-thiol bonds, which could be cleaved efficiently upon laser irradiation. To improve the desorption/ionization efficiency of mass barcodes, some matrices, such as

1,5-diaminonaphthalene (DAN) or CHCA were added and proved to have a signal enhancement.[35,39]

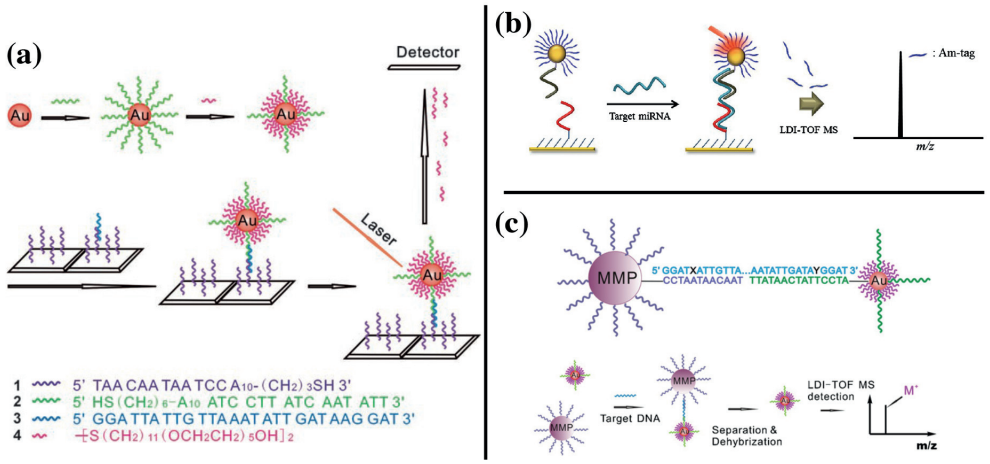

Figure 1.2. Mass barcoded AuNPs and AuMPs for DNA sensing on different surfaces: **(a)** silica wafer chip, **(b)** gold chip, and **(c)** magnetic beads. Figure (a) from Angew. Chem. Int. Ed., **2008**, 47, 5009-5012; figure (b) from Analytical Biochemistry, **2013**, 434, 199-201; figure (c) from Talanta, **2011**, 85, 1698-1702.

The mass barcoded AuNPs (Mb-AuNPs) could be applied for different purposes, including biosensing and tissue imaging. Qiu *et al.* demonstrated the use of Mb-AuNPs to amplify the LDI-MS signals from DNA hybridization events on biochips or magnetic beads, as shown in Figure 1.2(a) and (c).[40,41] Firstly, AuNPs were tagged with mass barcodes of alkanethiols as well as probe DNA strands. Capture DNA strands were covalently immobilized on a silica wafer chip or magnetic beads and then hybridized with target DNA strands, followed by washing to remove free target DNA. Next, hybridization of probe DNA on AuNPs with the overhanging target DNA sequence caused AuNPs to be captured on the chip. A single DNA binding event led to the detection of multiple mass barcodes directly on the biochip or in the elutant from magnetic beads with LDI-MS, which therefore provided LODs of DNA as low as 100 pM on biochips or 1 fM on magnetic beads. Multiplex DNA assays could also be realized using various mass barcodes with different numbers of PEG units. Similarly, Yeo *et al.* used larger Au microparticles (AuMPs), 2 μm in diameter, to load more mass barcodes (Mb-AuMPs) and lowered the LOD of a microRNA to 1 fM on a gold chip, in Figure 1.2(b).[42]

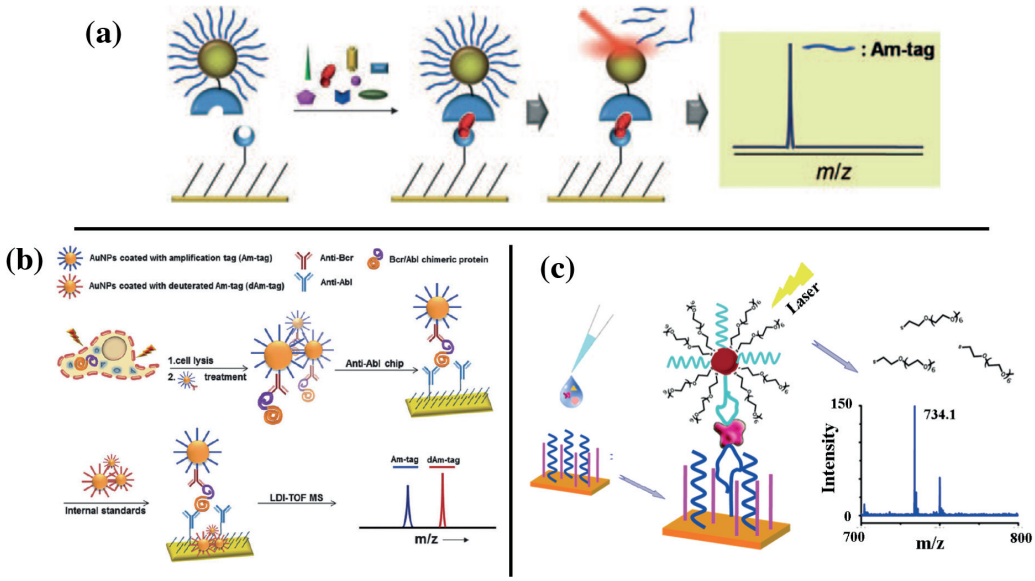

Figure 1.3. Mass barcoded AuNPs for protein assays on gold plates: **(a)** Au microparticles were used to futher enhance signal amplification effect; **(b)** relative quantification of proteins from cell lysates; **(c)** protein isolation with aptamer functionalized Mb-AuNPs from human serum or cell lysates. Figure (a) from Angew. Chem. Int. Ed., **2008**, 47, 9518-9521; figure (b) from Chem. Commun., **2014**, 50, 4831-4834; figure (c) from Anal. Chem., **2016**, 88, 6767-6772.

Coupling Mb-Au particles with LDI-MS can provide the protein analysis over a wide *m*/*z* range with a good sensitivity. Yeo *et al.* also applied Mb-AuMPs for protein analysis in a sandwich assay format on a gold plate, in Figure 1.3(a).[43] The LOD was as low as 1 aM with a wide dynamic range from 1 aM to 1 pM. For the quantification purpose, deuterium-substituted Mb-AuNPs were deposited together with captured AuNPs probes as internal standards.[44,45] With this approach, two protein biomarkers from cell lysates were quantified successfully, in good agreements with western blotting results, in Figure 1.3(b).[45] For the target proteins with two affinity ligands of aptamers, a similar sandwich assay could also be formed to isolate the targets specifically. With this principle, thrombin and epithelial cell adhesion molecule (EpCAM) in human serum or cell lysate were detected with a superior sensitivity over the traditional enzyme-linked immunosorbent assay (ELISA), in Figure 1.3(c).[46]

Besides the bioassays, the surface functionalized AuNPs also hold great potential for drug delivery through efficient cellular uptake. Rotello's group demonstrated a series of cell-related applications with surface modified AuNPs. The cellular uptake or distribution of AuNPs can be tracked through the detection of mass barcodes by LDI-MS,[47,48] as shown in Figure 1.4(a) and (b). The characteristic mass barcode MS signals allow side-by-side comparisons of cellular uptake efficiencies of AuNPs with different surface chemical and

physical parameters. In one set of experiments, the uptake of four different Mb-AuNPs by mammalian kidney cells was simultaneously identified and quantified at levels as low as 30 pmol.[49] Multiplex imaging of different Mb-AuNPs in tissues could also be performed with LDI-MS imaging (LDI-MSI) by the same group.[50] With the inkjet printing technique, the Mb-AuNPs could be used as the security inks to print patterns that should be profiled only through LDI-MSI, which provides great potential for a wide range of anti-counterfeiting applications, as shown in Figure 1.4(c).[51]

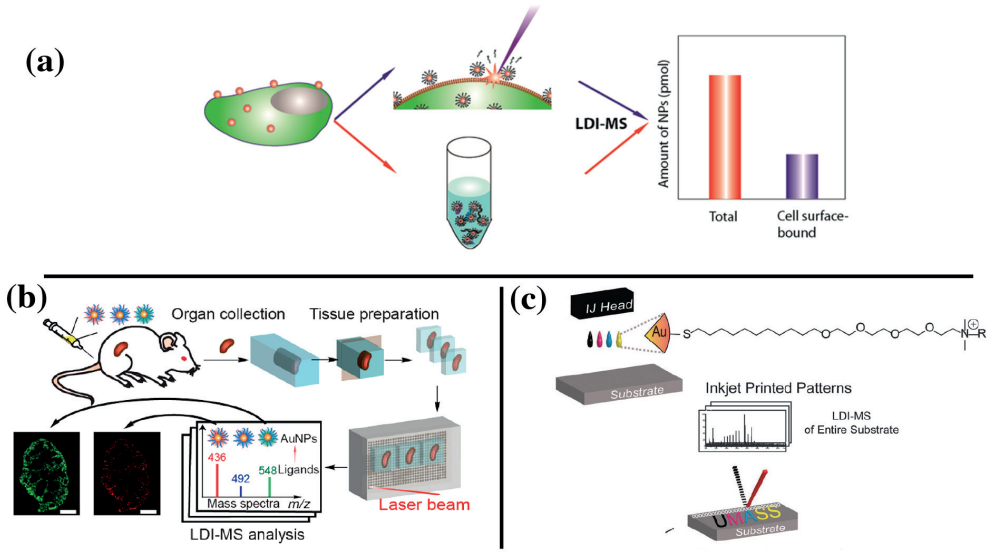

Figure 1.4. Mass barcoded AuNPs for cell applications with LDI-MS and MSI: **(a)** identification and quantification of Mb-AuNPs uptaken by cells; **(b)** LDI-MSI of multiplex Mb-AuNPs in tissues; **(c)** LDI-MSI of printed patterns with Mb-AuNPs as inks. Figure (a) from ACS Nano, **2016**, 10, 6731-6736; figure (b) from J. Am. Chem. Soc., **2013**, 135, 12564-12567; figure (c) from Chem. Commun., **2012**, 48, 4543-4545.

Other than polyethylene glycol molecules, plasmid-expressed peptides on AuNPs[52] or gold cluster ions themselves generated by LDI-MS have also been reported as mass barcodes for bioassays,[53] heavy metal ion detection,[54] bacteria and tumor cell detection, or tissue imaging.[55]

1.1.3. Electrospray ionization

In the late 16th century, the Taylor cone formed by a water droplet in the presence of an electric field was observed by Gilbert,[56] which was clearly related to electrosprays. The electrospray process was described by Nollet[57] in 1750 and then pictured for the first time by Zeleny[58] in the early 20th century. Although the electrospray of gas-phase polystyrene ions

and their subsequent detection by MS were first reported by Dole in 1968,[12] it was only in the 1980s that electrospray was established as a powerful technique to softly ionize biological macromolecules for MS analyses by Fenn[13] and Aleksandrov[59] and came to be commercialized. Since then, electrospray has become an essential ionization technique for proteomics study mainly due to its soft character and easy coupling with separation methods.

1.1.3.1 Principle

The exact mechanism of ESI has been studied theoretically and experimentally.[60,61] A typical ESI process operated in a positive mode is depicted generally in Figure 1.5. When a potential difference is applied between an electrode in solution flowing through a capillary and a counter-electrode, *e.g.* mass spectrometer placed in the air outside facing the capillary outlet, the solution/air interface at the capillary tip is polarized into a shape of Taylor cone,[11] resulting from the balance between the electrostatic pressure of

$$P_{\mathrm{E}} = \frac{q^2}{32\pi^2 r^4 \varepsilon_0}$$

where ε_0 is the permittivity of vacuum, q is the charge on the droplet and r is its radius, and the Laplace pressure of

$$P_{\mathrm{L}} = 2\gamma/r$$

where γ is the surface tension of the liquid. If the applied voltage is sufficiently high, charges will greatly accumulate up to a point until P_{E} is larger than P_{L}.[61] The tip of the Taylor cone becomes unstable, leading to the spray of individual charged droplets into gas phase. The onset voltage (U_{on}) of electrospray can be obtained as:

$$U_{\mathrm{on}} \approx \sqrt{\frac{r\gamma \cos 49}{2\varepsilon_0}} \times \ln \frac{4d}{r}$$

where 49$^{\mathrm{o}}$ is the half-angle of the Taylor cone,[11] d is the distance between the emitter tip and MS inlet.[62] From this equation, the onset voltage could be reduced by using a smaller ESI emitter, a shorter distance between emitter tip and MS inlet and solvents with lower surface tensions. Organic solvents, *e.g.*, methanol, acetonitrile and propanol are routinely added into aqueous samples for efficient ESI-MS analysis.

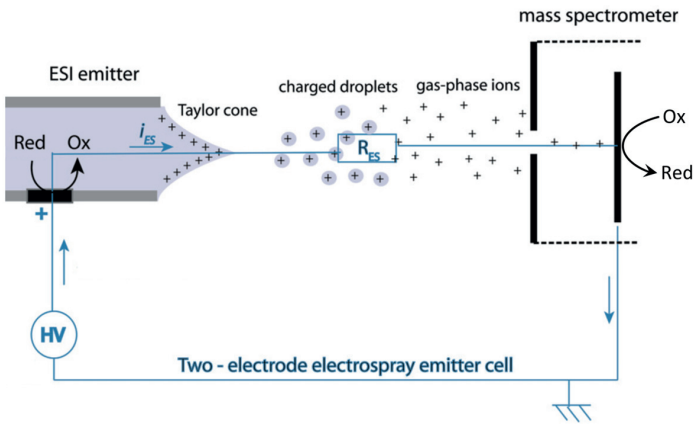

Figure 1.5. Classical electrospray ionization process. Figure from Annu. Rev. Anal. Chem., **2010**, 3, 231-254.

Once in the gas phase, the P_E of the charged droplets is increasing to an upper limit, which is known as the Rayleigh limit and reached when P_E equals P_L, due to the solvent evaporation. When the charge is larger or the radius is smaller, the droplets will break up to form smaller charged droplets continuously until the gas-phase ions are generated. The formation process of gas-phase ions is usually explained by two theories, the charge residue model (CRM) proposed by Dole[12,63] and the ion evaporation model (IEM) by Iribarne and Thomson.[64] The CRM suggests that the solvent evaporation and droplet fission events repeat constantly until only one charged analyte molecule remains in a droplet. The IEM considers that when the radius of charged droplets reduces to be smaller than 10 nm, the small ions can be directly evaporated or ejected out of the droplet. Nevertheless, it's generally accepted that both models regulate the formation of gas-phase ions, where CRM produces mainly large ions while IEM contributes the generation of small ions. The ions then enter the MS inlet and are eventually detected by the MS analyzer, providing a spectrum of *m*/*z* peaks.

1.1.3.2 Micro/nano-electrospray ionization: principle

Since Smith *et al.* found the detection sensitivity could be markedly increased at a lower flow rate down to 200 nL/min,[65] the concept of micro-electrospray was introduced by Emmett and Caprioli one year later.[66] The capillary needle was packed with C_{18} for liquid chromatography and optimized by HF etching to be 50 μm in inner diameter, which allowed the flow rate as low as 300 nL/min and yielded picomole per liter sensitivity for peptides and nanomole per liter sensitivity for proteins.

In the same year, a theoretical model was established by Wilm and Mann to explain the advantage of micro-electrospray ionization (microESI) and an equation was drawn to predict the proportionality between the two-thirds power of the flow rate and the size of the emission zone at the Taylor Cone tip from which smaller charged droplets are ejected, as following:

$$r = \left(\frac{\rho}{4\pi^2 \gamma \tan\left(\frac{\pi}{2} - \vartheta\right)\left[\left(\frac{U_a}{U_T}\right)^2 - 1\right]} \right)^{1/3} \times (\mathrm{d}V/\mathrm{d}t)^{2/3}$$

where r is the radius of the emission region at the Taylor Cone tip, γ is the surface tension of the liquid, ϑ refers the liquid cone angle (for the classical Taylor Cone model $\vartheta = 49.3^{\circ}$), ρ is the liquid density, U_T and U_a present the threshold voltage and applied voltage respectively, and $\mathrm{d}V/\mathrm{d}t$ means the flow rate.[61]

This formula provided guidance for the construction of a more sensitive ionization source and they verified this model experimentally with a modified ion source for microESI. To allow small flow rates and thus decrease r, a gold-coated glass capillary with an opening diameter of 1-3 μm at the tip was constructed to obtain a stable electrospray. They operated the analysis at a very low flow rate less than 25 nL/min to really achieve nano-electrospray ionization (nanoESI) and obtained an excellent sensitivity with an overall ion transmission efficiency of 8×10^{-4}.[61] Nowadays, the microESI refers to the flow rate between 100 to 1000 nL/min, while nanoESI operates at a far slower flow rate less than 100 nL/min.[67,68]

The ionization efficiency can be generally determined by the specific surface charge, which means the surface charge number per unit amount of analytes obtained when the Rayleigh limit is reached for every initial droplet emitted from the Taylor Cone, according to the equation of:

$$\frac{\text{surface charge number}}{\text{sample amount}} = \frac{4\pi r^2 \sigma}{\frac{4}{3}\pi r^3 \mathrm{C}} = \frac{3\sigma}{r\mathrm{C}} = 6\frac{\sqrt{\gamma \varepsilon_0}}{\mathrm{C}}\frac{1}{r^{3/2}}$$

where σ is surface charge density, ε_0 is vacuum permittivity, r is the radius of the initial charged droplet, γ refers to the surface tension of the liquid and C presents the analyte concentration.

A larger proportion of analyte molecules could be ionized for MS detection when the initial droplets are smaller. Also, the smaller primary droplets need fewer steps to shrink through evaporation, undergo Coulomb fission and finally form gas phase ions. All these

factors make nanoESI more sensitive than traditional MS and microESI. The strong ion suppression is a common phenomenon when analyzing complex samples with a high concentration of surface-active molecules by conventional MS. However, the problem could be alleviated evidently by nanoESI, which is presumably due to the higher ionization efficiency of analytes.

Besides the high ionization efficiency and high tolerance to contaminants, the rather low flow rate would in itself be beneficial by providing a long measurement time with a tiny amount of sample. This extremely economic sample consumption makes nanoESI very suitable to couple with separation methods for proteomic or metabolic studies with a limited volume of complicated biosamples.

1.1.3.3 ESI-related ambient ionization techniques

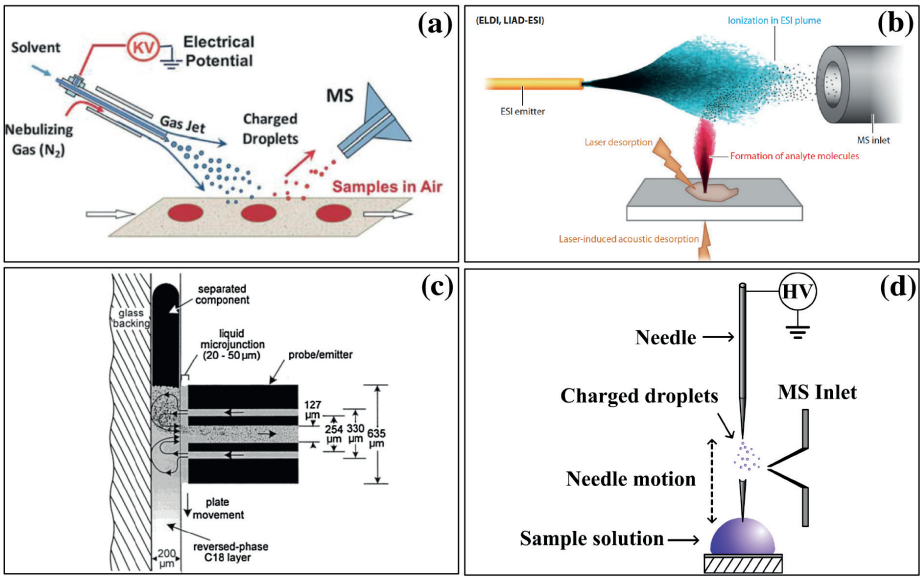

Figure 1.6. Various ESI-derived ambient ion sources: **(a)** ESI for desorption ionization; **(b)** ESI for post-ionization after laser-induced desorption of samples from surfaces; **(c)** ESI from a surface sampling probe with a liquid microjunction; **(d)** ESI from a solution sampling probe with a stainless needle. Figure (a) from Science, **2004**, 306, 471-473; figure (b) from Annu. Rev. Anal. Chem., **2010**, 3, 43-65; figure (c) from Anal. Chem., **2002**, 74, 6216-6223; figure (d) from Rapid Commun. Mass Spectrom., **2007**, 21, 3139-3144.

The advent and development of ambient ion sources went back to one decade ago and were to retain the highly specificity while greatly reducing the complexity of sample preparation or operation to improve the analysis speed and simplicity, which especially benefit the *in-situ* analysis and could find many applications in forensic analysis or clinical diagnosis. Combining ESI and different sampling strategies, ambient ionization can be

achieved through a one-step "desorption/extraction ionization" or a two-step "desorption/extraction and then ionization" procedure. Depending on these criteria, various ESI-derived ion sources could be classified into three types, ESI for desorption ionization, ESI for post-ionization and ESI directly from sampling probes, and summarized as follows.

ESI for desorption ionization. Integrating desorption and electrospray ionization in one step, desorption electrospray ionization (DESI) has been developed by Cooks *et al.* in 2004.[69] Figure 1.6(a) presents a conceptual diagram of DESI for surface sample analysis, where charged droplets generated by ESI were directed onto a sample surface with the assistance of a high-pressure sheath gas for desorption and ionization. The analyte-pickup process involves initial wetting of the surface to dissolve analytes and then projection of subsequent droplets resulting in the emission of secondary charged microdroplets containing analyte molecules.[70–72] Because of the lack of sample pretreatment in principle, DESI holds the advantage in *in-situ* surface analysis, including the imaging of intact biological tissue and detection of active ingredients in tablets, industrial polymers, peroxide-based explosive chemicals and warfare agents, untreated bacteria cultures, alkaloids in plant tissues and so forth.[73–78] *In-situ* analyses by DESI often require the development of portable mass spectrometers for a variety of public safety applications.

ESI for post-ionization. In these techniques, a sample spray or plume was generated and then delivered into an ESI plume for analyte molecule extraction and post-ionization. Different strategies, including thermal evaporation, pyrolysis, pneumatic or ultrasonic nebulization, laser desorption, or laser-induced acoustic desorption, have been applied to assist the generation of a sample spray or plume.

The fused-droplet ESI (FD-ESI) technique was developed to characterize large analytes, such as peptides and proteins.[79] A probe nebulizes the aqueous sample solution ultrasonically or pneumatically in the absence of high voltage to form fine mists, which are then conducted into the ESI plume. The polarities of the solutions used to produce the sample mists and the ESI droplets should be close so that they can fuse efficiently. Because of the sample fusion process, the salt tolerance of FD-ESI is much higher than in conventional ESI analyses.[80,81] Similarly, a method named extractive electrospray ionization (EESI) was developed in Cooks' group for online droplet-droplet extraction followed with MS detection. It is useful for characterizing both volatile and nonvolatile compounds and has been used to analyze urine, serum, milk, perfume and so forth.[82–84] Analytes can also be desorbed by

blowing the solid sample surface with heated gas stream for subsequent ionization in the ESI plume. This technique is known as neutral desorption extractive ESI and the desorbed analyte molecules can be transported efficiently over distances greater than 1m for remote analysis. Volatile components have been detected from human breath and other biological samples.[85,86]

Various laser irradiation-assisted ESI techniques were developed, such as electrospray-assisted laser desorption ionization (ELDI)[87] and laser-induced acoustic desorption/electrospray ionization (LIAD-ESI),[88] as shown in Figure 1.6(b). For ELDI, the analyte molecules are desorbed by irradiating the sample surface with the pulsed UV laser and are then positioned in an ESI plume for ionization. A related technique named liquid ELDI-MS was also developed to characterize chemicals or monitor (bio)-chemical reactions directly from solutions by adding small amount of fine carbon powders into the solution to adsorb laser energy.[89] Several other similar ionization methods, including matrix-assisted laser desorption electrospray ionization (MALDI-ESI)[90] and laser ablation electrospray ionization (LA-ESI)[91] with an IR laser, were subsequently developed. Additionally, a heated stream of high-velocity N_2 gas or acoustic waves generated by laser irradiation in LIAD-ESI can thermally evaporate or mechanically desorb analyte molecules into the ESI plume for further ionization.

ESI from sampling probes. Different from desorbing or extracting analytes sampled on a surface into an ESI plume for ionization, a direct sampling/ionization method becomes increasingly popular by performing ESI directly with the sampling probes as emitters, which avoids desorption/extraction steps and thus further accelerates the analysis speed. The original or modified sampling probes are usually sharp in tip and the sampled analytes on the probes could be directly sprayed into gas phase ions by delivering solutions and applying a high voltage to the conductive-coated probes.

Several direct sampling/ionization techniques have been developed and differ in sampling probes. The direct electrospray probe (DEP) method developed by Shiea *et al.* generates electrospray from a sample droplet pre-deposited on a small metal ring subjected to a high voltage, which is useful for rapid analysis of dirty samples or of samples only available in extremely small volumes.[92] Afterwards, several different solid probes, including copper wires, optical fibers, graphite fibers coiled with a copper or platinum wire, a glass rod and a nanostructured tungsten oxide surface, have been introduced.[93,94] Based on DEP, probe electrospray ionization (PESI) method was further developed by applying a stainless needle

with a diameter of 4 μm to pick up as little as 4 pL of sample solutions on a surface automatically through a motor-driven motion followed by ESI process, in Figure 1.6(d).[95]

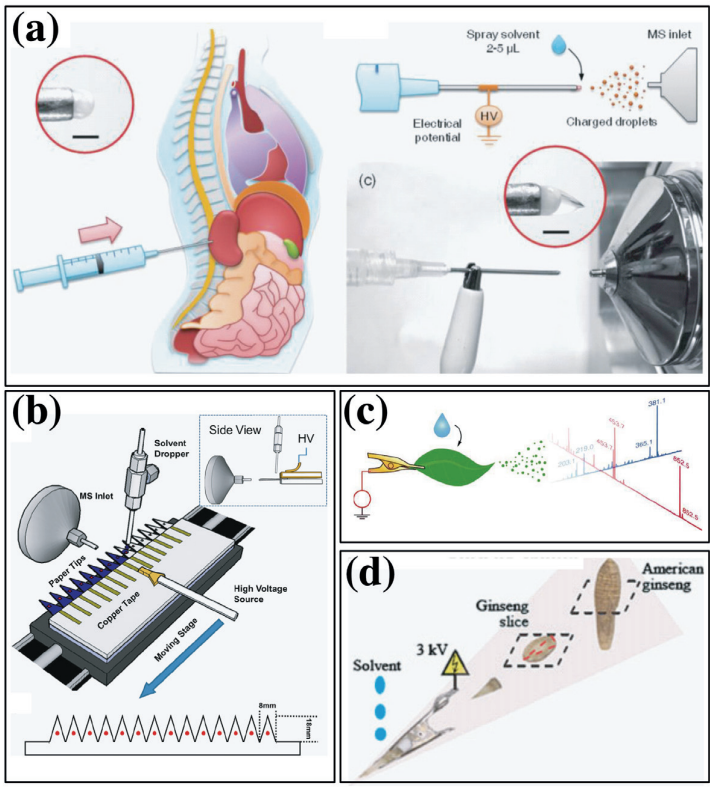

Figure 1.7. Different sampling probes for ESI: **(a)** Needle biopsy on tissue for direct ESI; **(b)** High-throughput paper spray-MS Platform; **(c)** Leaf for direct ESI; **(d)** Wetted ginseng tissue for ESI. Figure (a) from Anal. Chem., **2011**, 83, 9221-9225; figure (b) from Clin. Chim. Acta., **2013**, 420, 28-33; figure (c) from Anal. Chem., **2011**, 83, 7608-7613; figure (d) Rapid Commun. Mass Spectrom., **2011**, 25, 2837-2843.

To sample solid analytes on a surface for direct ionization, another kind of efficient probe called surface-sampling probe (SSP) has been developed for the *in-situ* surface analysis, where a liquid microjunction is formed between the probe and surface to extract soluble chemicals and then delivered into an integrated ESI emitter for subsequent MS analysis, shown in Figure 1.6(c).[96,97] Recently, a paper spray was introduced for MS analysis of dried blood spot (DBS) on a triangular section of chromatography paper by Cooks' group.[98] After being wetted by a mixture solution of methanol and water, the wet paper was applied with a high voltage to induce ESI at the triangular tip. A high-throughput device with multiple angles for loading multiple samples was developed by Ouyang *et al.* to achieve a relatively fast analysis speed of 7 s per sample, in Figure 1.7(b).[99] Analogous to paper spray,

several other probes, such as leaf,[100] wooden tip,[101] tissue,[102] and biopsy needle[103] could also induce ESI and find a wide range of applications in blood, drug and food safety, as shown in Figure 1.7(a), (c) and (d).

1.1.4. Electrostatic spray ionization: principle

In traditional ESI-MS, a direct current high voltage is applied between an electrode contacting the solution in a microchannel or a capillary and the mass spectrometer. Recently, Cooks *et al.* have reported a contactless method to generate a pulsed spray.[104,105] A pulsed high voltage waveform was applied on an electrode 2 mm away from a nanospray emitter to induce voltage inside the emitter. Similarly, Zhang *et al.* have used alternating current high voltages to perform a contactless spray, where the charge states of peptides were controllable.[106] In comparison with classical ESI, the high voltage was not directly applied to the sample solution, and no electrode reaction could occur, which is an advantage when electrochemical reactions during conventional ESI need to be avoided.

Herein, Girault's group developed a contactless pulsed spray technique named as electrostatic spray ionization (ESTASI) and comprehensively investigated its working mechanism, which is of interest for the development of new ambient ionization techniques and for opening up a wide range of applications for mass spectrometry analysis.[107] Sample solution will be deposited as a droplet on an insulating substrate. A disc electrode is placed behind the substrate and against the MS inlet. The droplet position on the substrate is precisely adjusted to be always in line with the electrode and MS inlet. A pulsed high voltage will be generated by amplifying square wave voltage pulses with a high voltage amplifier and applied to the electrode to induce ESTASI. The electrical setup is equivalent to two capacitors in series, as described previously in Figure 1.8. One capacitor is composed of electrode-insulating substrate-sample droplet. Another capacitor is at the tip of Taylor cone and is sample solution-air-mass spectrometer. The charging-discharging process of these two capacitors will induce ESTASI. When the voltage is at maximum, the positive charge will accumulate at the tip of spray emitter to the Rayleigh limit. When the electrostatic pressure is increasing and larger than the surface tension due to the solvent evaporation, the positive charged droplets will break up into smaller droplets continuously until the gas-phase ions are generated. In this case, the second capacitor can be considered as a leaky capacitor with a diode in parallel and cause an excess amount of negative charges remaining in the sample solution, which will prevent the continuous spray of positive charge. To alleviate this

problem, the square wave voltage value is then transited to 0 to discharge both capacitors and induces the spray of anions until the system returns back to be electroneutral, wherein the first capacitor acts as the power supply. Alternating electrostatic spray of cations and anions can be realized by repeating the charging-discharging process.

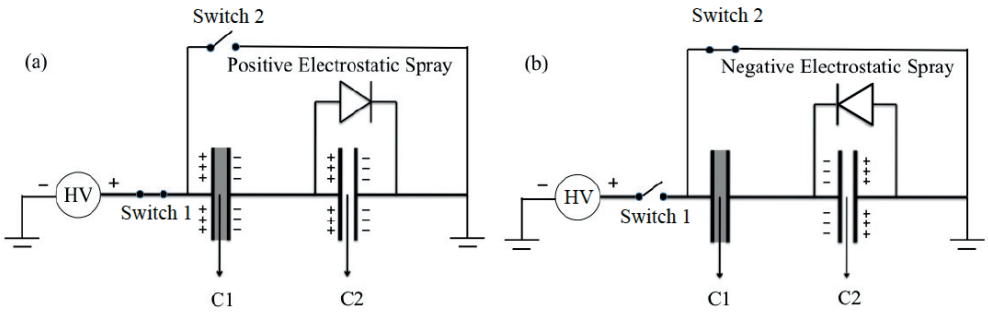

Figure 1.8. Equivalent circuit of the ESTASI during the charging-discharging process. Figure from Anal. Chem., **2012**, 84, 7422-7430.

ESTASI has been successfully demonstrated with different geometries including polymer coated silica capillaries, disposable plastic micropipette tips, polyimide microchips, polyacrylamide gel strip, and tissues.[107–109] Because of its very convenient connection with many analytical techniques, ESTASI-MS is ideally suited for bioanalytical studies.

1.2. Selected ESI-MS based applications

1.2.1. Coupling with separation methods

1.2.1.1 ESI-MS coupled with separation methods

In order to analyze a complex mixture, for example biofluids or nature products, a separation technique is usually coupled with the MS to reduce the ion suppression effect and the complexity of the mass spectrum for easy interpretation. Compared to MALDI-MS, ESI-MS holds great advantage of easy interfacing to separation systems for liquid sample analyses. Chromatography and electrophoresis are the two representative separation methods.

ESI is by nature very easy to be on-line connected with LC systems with continuous flows and has been widely used for bottom-up proteomics, pharmacokinetics and drug development.[110] In proteomics, the proteins/peptides are first desalted and fractionated by a LC system and then online analyzed by MS or tandem MS. The most widely used separation modes for LC are reverse phase (RP) and strong cation exchange (SCX). When analyzing

high-complicity and large-scale proteomics samples, multidimensional separation is usually performed with a 2D LC system combining RP and SCX. Depending on the column diameter and the packing particles size, various flow rates could be used ranging from submicroliter per minute to milliliter per minute and the separation efficiency or peak resolution could be improved by high performance LC (HPLC) or ultra-performance LC (UPLC).[111]

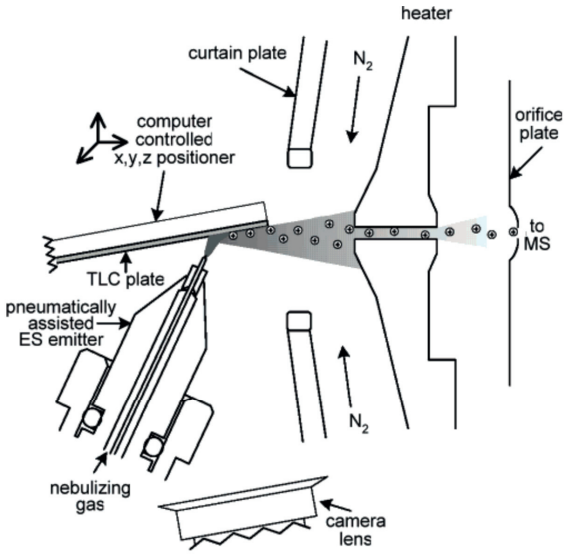

Figure 1.9. Schematic illustration of the TLC/DESI-MS. Figure from Anal. Chem., 2005, 77, 1207-1215.

As another important chromatography technique, thin layer chromatography (TLC) is simple, cost-effective, and easy-to-operate for routine separation of non-volatile mixture. MS could be interfaced with TLC through a direct or indirect sampling mode. Conventionally, the indirect sampling is based on the extraction of compounds from a TLC plate and requires a number of labor-intensive and time-consuming processes, including locating, extraction, filtration and concentration of the compounds.[112,113] While these shortcomings have been overcome with the development of ambient ion sources for direct sampling of TLC for MS analysis since the late 1960s. Several ESI related ambient ionization methods have been widely used for the direct coupling of TLC with MS. Van Berkel *et al.* exploited the SSP to sample organic compounds from TLC plate directly for MS analysis.[96] Similarly, Luftmann *et al.* developed a plunger-based extraction device for TLC-ESI MS.[97] Various laser irradiation-assisted ESI techniques for TLC-MS were developed, such as ELDI[114] and LIAD-ESI.[115] In addition, charged or neutral droplets were also used for the direct sampling of TLC plates. For example, DESI has already been introduced to couple TLC with MS in 2005,

where the charged solvent droplets induced by ESI were directed to a TLC plate at an optimal angle to sample and ionize analytes on the plate, in Figure 1.9.[116] Today, commercial TLC-MS interfaces are available from CAMAG (Muttenz, Switzerland)[117] and PROSOLIA (Indianapolis, IN).[118]

As the classical proteomic methodology, two-dimensional polyacrylamide gel electrophoresis (2D-PAGE) is a powerful separation tool allowing simultaneous resolution of thousands of proteins based on two independent protein characteristics.[119] Molecules are more effectively separated in 2D electrophoresis than in 1D electrophoresis, where molecules are separated linearly through isoelectric focusing based gel electrophoresis (IEF-GE) in the first dimension and then separated orthogonally to the first electropherogram according to the molecular weight in the second dimension. The protein spots were then stained and extracted for MS identification, which were time-consuming and cause sample loss. In 2002, OFFGEL electrophoresis was introduced by Girault's group to separate proteins or peptides according to their isoelectric points and collect the separated components in liquid fractions for LC-MS analysis, making sample recovery much easier than with traditional gels.[120] OFFGEL electrophoresis has been commercialized by Agilent Technologies since 2006, named as OFFGEL 3100 fractionator.[121]

Another typical electrophoresis-based separation technique for MS coupling is capillary electrophoresis (CE) due to its fast speed, high resolution and small sample volume.[122] Coupling CE with ESI is not so easy as LC due to the mismatches of flow rate and electric current. CE applied a higher voltage than that in ESI, therefore the CE current must be decoupled from ESI by grounding the ESI emitter to avoid the electrical current mismatch. The commercial interface from Agilent applies a high voltage inside the MS whilst grounding the ESI emitter tip, making it easier to decouple the CE current from ESI. To avoid the necessary sample dilution for MS analysis with conventional ESI source, the nanoESI is ideal to couple with CE since the flows in CE are typically in the range of nanoliters per minute.

1.2.1.2 ESTASI-MS coupled with separation methods

The ESTASI-MS cannot only analyze liquid droplets on a flat surface, but also dried samples deposited on a surface or inside a porous matrix, where the latter needs to drop an acidic solution to the substrate to dissolve or extract samples for ESTASI. Therefore, ESTASI has been used as an interface between MS and various separation techniques, such as CE and IEF.[107,109] After CE separation, the fractions were directly collected on an

insulating polymer plate. After drying all the droplets, the polymer plate was placed between the electrode and MS inlet. A droplet of an acidic buffer was deposited on each sample spot to dissolve the samples for ESTASI-MS detection.

ESTASI-MS has also been adapted to IEF-GE, where an immobilized pH gradient (IPG) strip containing fractions of proteins or peptides and supported on a thin piece of insulating polymer layer was placed in front of the MS inlet, as shown in Figure 1.10. Upon the application of acidic buffer and a high voltage pulse, the samples under the very acidic droplet can be positively charged and extracted from the gel to the droplet by the electric field. This droplet sprayed into charged microdroplets when the electrostatic pressure of the droplet was larger than the Laplace pressure. This direct coupling of ESTASI-MS with IEF-GE improves the detection sensitivity and demonstrates a more powerful method compared with the classic methods for the proteins or peptides analysis.

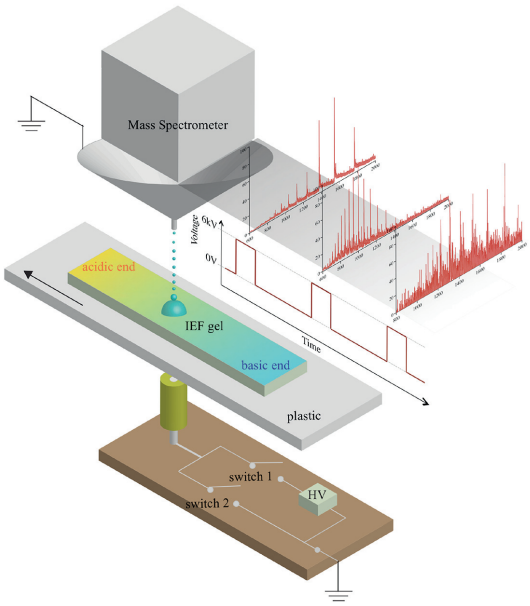

Figure 1.10. Schematic representation of ESTASI-MS coupled with IEF-GE. Figure from Anal. Chem., **2013**, 85, 4745-4752.

1.2.2. Coupling with microtiter plates

High-throughput screening (HTS) is a powerful method for scientific experiments, especially used in drug discovery and biochemical or biological research, which allows conducting millions of chemical, genetic, or pharmacological tests within a single run analysis and improving analysis efficiency greatly.[123,124] The key labware or testing vessel of

HTS is the microtiter plate with multiple wells as small test tubes and widely used for combinatorial chemistry and drug development. Coupled with MS, accurate qualification and quantification could be obtained for different applications of enzymatic assays, inhibitor screening assays and drug metabolism assays.[125]

A liquid transfer system is normally required to probe samples with a capillary in Figure 1.11(a),[126] or with an autosampler from the microtiter plates for MS analysis, such as the commercial TriVersa NanoMate by Advion,[127] where the fractions of LC are collected in a microtiter plate and then an ESI chip aspirates the sample liquid for later analysis by nanoESI-MS. To overcome the disadvantage of low throughput with the single probe autosampler, a multi-probe autosampler was developed by Kassel *et al.* to greatly shorten the total analysis time of a whole 96-well plate from 48 min to 12 min.[128] Later on, the analysis time of a 96-well plate was further reduced to 5 min by Morand *et al.*[129] Though the improved throughput with the multi-probe autosampler, the cross contamination between wells is inevitable and washing steps are necessary when transferring the sample from one well to another. To overcome this shortcoming, avoiding using auto-samplers is another option, wherein each well on a microtiter plate was modified and integrated with an ESI emitter, such as disposable micropipette tips in Figure 1.11(b).[130]

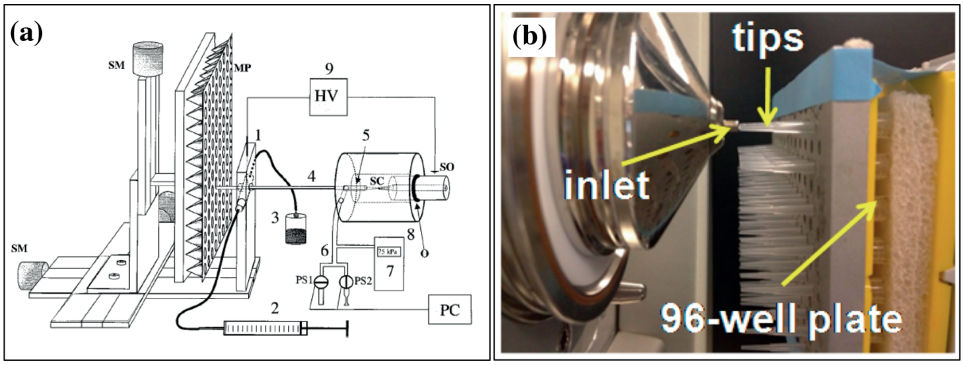

Figure 1.11. MS coupled with microtiter plates. **(a)** Direct-infusion with a capillary from microtiter plates for ESI-MS analysis; **(b)** Microtiter plates modified with multiple pipette tips for high throughput solvent assisted inlet ionization (SAII) MS analysis. Figure (a) from Anal. Chem., **2001**, 73, 1449-1454; figure (b) from Anal. Chem., **2014**, 86, 1000-1006.

1.2.3. Coupling with microfluidics : interface

Microfluidic chip or so called "Lab-on-chip" has been greatly used in analytical and bioanalytical chemistry since the introduction of microfluidics in the beginning of 1980s. It refers to a miniaturized analytical device that integrates multiple functions on a single chip to

process fluids constrained to a microscale and thus shows advantages of low sample consumption, reduced analysis time, high throughput and potential for automation and portability. Compared with various detection methods based on spectroscopy and electrochemistry, MS provides label-free, sensitive and high throughput characterization of analyte and thus becomes an essential detection tool in microfluidic-based bioanalysis. Compatible with low sample consumption in microfluidics, micro/nanoESI is an ideal MS interface for integration with microfluidic chips as it provides good detection sensitivity at nanoscale flow rates.

Three types of interfacing approaches have been developed for coupling microfluidic chips with micro/nanoESI-MS and presented in Figure 1.12.[131] The simplest way is to spray directly from chips and such an interface was firstly reported in 1997 with a chip containing 9 microfluidic channels.[132] The performance of direct electrospray from microchannel is limited by the eluent spreading due to the hydrophilic and blunt edge of the glass chip. To prevent liquid spreading, the channel exit could be chemically treated to be more hydrophobic.[133]

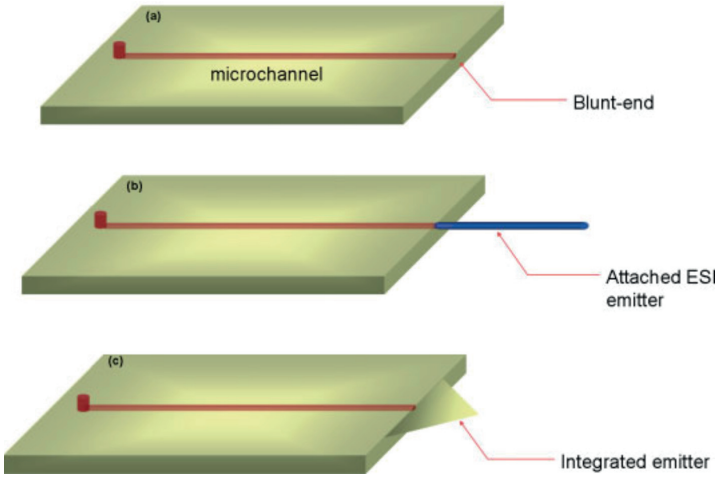

Figure 1.12. ESI for coupling microfluidic chips with MS from: **(a)** a blunt-end chip, **(b)** an attached emitter, and **(c)** an integrated emitter. Figure from J. Mass. Spectrom., **2009**, 44, 579-593.

An alternative interfacing approach is to spray samples from an external emitter attached onto the chip channel.[134] A fused silica capillary pulled to a fine point is typically inserted into or glued to a microfluidic chip for sample infusion and micro/nanoESI.[135] However, the device was usually limited to continuous sample infusion and suffered from difficulties in alignment. A drilling procedure with a 200 μm tungsten carbide bit was

developed to make a hole for emitter attachment with a low dead volume connection between the emitter and microfluidic chip.[136] Sub-attomole detection limits for peptides was reported by inserting a nanospray tip of 5 μm in i.d. into a hole perpendicular to the cover of the chip.[137] Liquid junctions could also realize the connection between a removable emitter and the microfluidic chip and was maintained with a maker-up buffer between the on-chip CE channel and emitter.[138] Although being simple and stable, the attached emitters cause dead volumes and deteriorate on-chip separation performance.

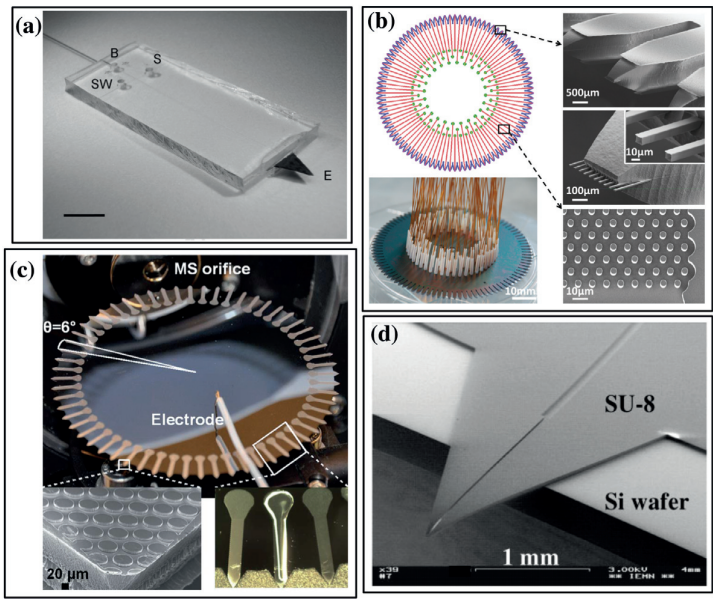

Figure 1.13. ESI for coupling microfluidic chips with MS from integrated emitters of: **(a)** a graphite-coated PDMS microchip tip, **(b)** a 96-capillary array, **(c)** a platform with 60 silicon microchip tips, and **(d)** nib-like tips fabricated using the negative photoresist SU-8. Figure (a) from Electrophoresis, **2005**, 26, 4674-4683; figure (b) from Anal. Chem., **2011**, 83, 6082-6089; figure (c) from Lab Chip, **2011**, 11, 3011-3014; figure (d) from Electrophoresis, **2003**, 24, 3640-3647.

Instead, microfabricated emitters can be integrated on microfluidic chips with a precise and reproducible microfabrication procedure to avoid the dead volume and make the interfacing simpler and laborless. As examples in Figure 1.13(a) and (d), integrated emitters have been constructed on a large variety of substrates, including polydimethylsiloxane (PDMS),[139] polycarbonate (PC),[140] polyethylene terephthalate (PET),[141] poly(methyl methacrylate) (PMMA),[142] polyimide (PI),[143] SU-8,[144] as well as silicon and glass.[145,146] Two multi-nozzle emitter array chips were developed for monolithic integration of SiO_2-based multi-nozzle emitters with microfluidic channels, as shown in Figure 1.13(b).[147] A wafer-scale microfluidic platform with 60 identical micropillar emitter arrays was constructed and

fixed on a computer controlled rotating table in front of an MS analyzer to realize high throughput MS analysis of 60 samples in 8 min, as shown in Figure 1.13(c).[148] A commercial device (Agilent, CA) has also been developed using a multilayer PI chip with an integrated spray tip formed by laser ablation.[149,150]

Girault's group has a long history in fabricating microfluidic chips by laser ablation since 2001 and hyphenating them with ESI-MS.[141,151] The microchip could work as both a microreactor and an ESI emitter at the channel exit. Contrary to the PET-based chip, the wetting problem at the flat edge of the channel is easily eliminated by using PI as the chip substrate and cutting it into a pointed tip as an emitter. Various functional microfluidic chips have also been developed to realize many types of applications, *e.g.*, tagging of cysteine and phosphopeptide,[152] protein desalting with an on-chip PVDF membrane,[152] micro-mixing[153] and on-chip reaction studies, including binding of Cu^{2+} to β-amyloid,[154] tyrosine nitration,[155] and oil-water interface reactions.[156] Proteins and peptides could be supercharged in the Taylor cone sprayed from two adjacent microchannels.[157] A microchip with C_8 or C_{18}-coated magnetic beads trapped in the microchannel has also been designed, namely solid-phase extraction-gradient elution-MS (SPE-GEMS), for effective desalting, enrichment, sequential elution and ESI-MS detection of peptide mixtures for proteomic studies.[158] Later on, C_8 or C_{18}-coated magnetic beads were replaced by C_8-functionalized mesoporous magnetic microspheres to selectively enrich and analyze large hydrophobic peptides, matching the desired mass bin of the extended bottom-up proteomic approach.[159]

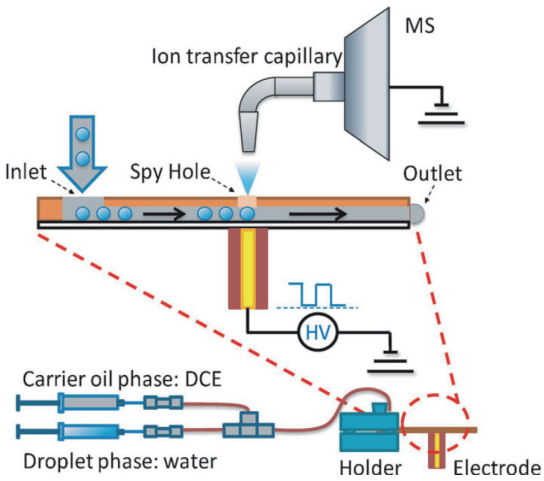

Figure 1.14. On-chip spyhole coupled with ESTASI-MS for droplet-based microfluidics. Figure from Angew. Chem., **2014**, 126, 4497-4501.

Recently, we have also realized the spray from a "spy hole" on a microfluidic channel in a direction orthogonal to the flow stream, in Figure 1.14. Oil/water droplets were introduced to the system and high voltage would only be applied when the water droplets pass below the spy hole to induce ESTASI-MS for monitoring droplet-based microfluidic reactions.[160]

1.2.4. Ambient mass spectrometry imaging

Mass spectrometry imaging (MSI) is a label free and high throughput technique to investigate the *in-situ* spatial distribution of peptides, proteins, biomarkers, or metabolites on a surface or in a tissue.[161] In a typical MSI process, localized mass spectra are recorded sequentially on regular grid points and the spatial distribution is obtained by plotting the measured relative intensities of individual *m*/*z* data with respect to their local positions.

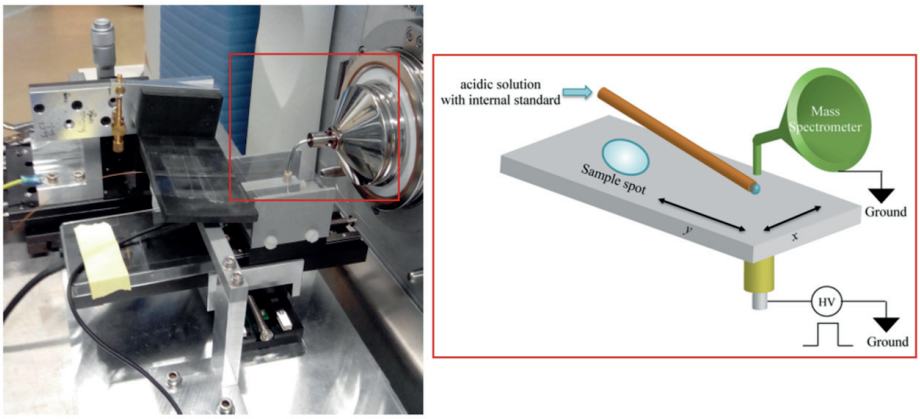

Figure 1.15. Schematic representation of the setup for ESTASI-MSI. Figure from Anal. Chem., **2014**, 86, 2033-2041.

The well-developed and commonly used methods in this field are MALDI-MSI and SIMS imaging.[161,162] In general, MALDI-MSI can reach a spatial resolution of 10 μm, but it suffers limitations such as the influence of matrix molecules on the detection in low *m*/*z* regions and the limited quantitative analysis. In contrast to vacuum ionization MSI, the most representative ambient MSI method is based on DESI, which has been applied in imaging of both artificial sample surfaces and biological tissues.[163,164] The spatial resolution of DESI is usually at 180-220 μm, which is limited by the large mist size generated by ESI.[165] It has been recently reduced to 40 μm under particular operating conditions. Another limitation of DESI-MSI is the relatively low sensitivity compared to MALDI-MSI in the analysis of

biological tissue with complex matrice conditions. Recently, to exploit the outstanding property of ESTASI for *in-situ* surface analysis, we have recently constructed an ESTASI-MSI setup to image peptides, proteins and cells distributed on a plastic plate, making it an alternative strategy to realize MSI as compared to LDI and DESI. It shows tolerance to the presence of salts, provides quantitative analyses with an internal standard, and holds an optimized lateral spatial resolution better than 110 μm.[166]

The setup used for ESTASI-MSI is illustrated in Figure 1.15.[166] The ion transfer capillary of MS inlet was modified into an "L" shape to scan a level surface. A disc electrode (200 μm in diameter) is placed behind the insulating plate and connected to a pulsed high voltage to induce ESTASI. A fused silica capillary was in contact with the sample surface to deliver an acidic solution under constant flow rate to dissolve samples from the surface for ESTASI MS analysis. The surface to be scanned is fixed on an *x*, *y*-stage that is controlled by LABVIEW software to move under the ion transfer capillary and fused silica capillary. Several important parameters should be optimized to obtain best MS signal, including distance between the sample surface and the ion transfer capillary, angle between the fused silica capillary and the sample surface, flow rate of the acidic solution and parameters of pulsed HV.

1.2.5. Bottom-up proteomics

The terminology of proteomics was coined in 1994 and devoted to the large-scale study of proteins, including expression, cellular localization, interactions, post-translational modifications (PTMs) and turnover as a function of time, space, and cell type.[167] Development of MS-based technologies for peptide/protein separation, detection, quantification and bioinformatics data analysis have driven the progress of proteomics.

To fit the performance and mass range of available MS analyzers, two approaches, bottom-up and top-down proteomics, are used for characterizing proteins. Top-down protein analysis refers to the characterization of intact proteins and has some potential advantages for PTM and protein isoform determination.[168] However, gas-phase fragmentation and the difficulties in protein fractionation and ionization have limited the wide application of top-down proteomics. In contrast, bottom-up proteomics is used to identify a protein by analyzing peptides obtained from the proteolysis of the protein.[169] In a typical experiment, the peptide mixture is fractionated and subjected to LC-MS/MS analysis. Peptides are identified by

MS/MS through fragmentation and compared to theoretical results of *in silico* proteolysis. Protein inference is achieved by assigning the identified peptide sequences to proteins.

1.2.5.1 Tandem mass spectrometry

Tandem MS is a crucial technique in proteome research to determinine peptide sequence and structural information by generating numerous fragments of precursor ions and could be realized in space, such as TOF-TOF, or in time, such as ion trap. A typical procedure of tamdem MS includes first the selection of precursor ions, then the fragmentation and finally the scan of fragments. Various methods, *e.g.*, collision-induced dissociation (CID),[170] electron capture dissociation (ECD),[171] electron transfer dissociation (ETD),[172] and electron-detachment dissociation (EDD),[173] could be applied to activate the precursor ions for fragmentation.

Among these techniques, CID is most popular and widely used in quadruple, ion trap and time of flight mass spectrometers partly owing to the ease of implementation. Normally, *b*- and *y*-type ions are generated by CID through two stages. In first stage, the selected ions collide with the neutral gas at high speeds and are activated into exicited states by transfering the kinetic energy into internal energy. The second stage is unimolecular decomposition of the activated ion. CID is an 'ergodic' ion activation method and the energy is redistributed over the chemical bonds of peptides. Therefore the amide bonds with lowest energy is preferencially disscoiated and ions of *b*- and *y*-type fragments are generated. The high energy CID could cleave the peptide side-chains to produce more types of fragments. Due to the removal of side-chains, the main drawback of CID is losing informations of PTM sites on peptides. As the complementary technologies, ETD/ECD can generate *c*, *z*-fragmentation by attracting electrons and keep peptide modifications, thereby suitable for PTM studies. Conversely, EDD can induce *a*, *x*-fragmentation through the oxidization of the nitrogen on the peptide backbone by losing one electron.

1.2.5.2 Clinical application: sample processing

The MS-based proteomics is an indispensable tool for clinic use by characterizing disease-specific biomarkers from clinical samples, such as plasma and tissues from patients. It provides great values for early diagnosis, treatment optimization and progress monitoring during treatment. The biofluids including blood,[174] urine,[175] cerebrospinal fluid,[176] nipple aspirate fluid[177] and bile[178] are common sources for biomarkers. As an alternative to

biofluids, use of tumor tissues as a source of biomarkers is also crucial for cancer biology. Intact proteins could be extracted from formalin-fixed and paraffin-embedded tissues and provide a great potential for biomarker studies using millions of stored specimens.[179]

Among these sources, blood is considered the optimal source for biomarker discovery due to the virtual contact of blood with all organism cells. However, plasma proteins show a big complexity and a wide dynamic range, up to 9 orders of magnitude.[180] The complexity of the serum proteome brings technical limitations for its use in clinical proteome analysis. Therefore, for a more comprehensive proteome study of low abundance proteins, it is critical to adjust the protein dynamic range. In the case of plasma, the most abundant proteins are mainly serum albumin and thus can be easily and specifically depleted prior to LC-MS analysis by immunoaffinity or chemical-based approaches. Antibody-coated columns are applied to capture most of high abundance proteins and improve the proteomic coverage of clinical samples.[181] The significant shortcomings of antibody depletion methodologies are the high cost and limited binding capacity of only several microliter sample amounts. Alternatively, various chemicals including sodium chloride and ethanol,[182] acetonitrile,[183] the disulfide reducing agents of DTT and TCEP,[184] and ammonium sulfate,[185] could selectively precipitate abundant albumin proteins to improve depletion throughput and proteomic depth.

Combinatorial ligand library is another cheaper and more holistic approach to collect the captured proteins for analysis, wherenin a large collection of ligands from the combinatorial hexapeptide library are conjugated onto beads and bind to a wide range of proteins.[186] The approximately equimolar amounts of the ligands could equalize the protein concentrations and thus benefit the bottom-up proteomics study. More recently, the proteins could also be digested by a protease and then a molecular weight cutoff filter was exploited to remove the abundant peptides.[187] The remaining undigested or partially digested proteins existing in less abundance were then digested to completion for analysis, resulting in a great improvement of identified protein number, sequence coverage and quantification of low abundant proteins.

Although the sample complexity could be greatly reduced by protein depletion, the remaining protein mixture still requires efficient separation to improve identification efficiency and accuracy. The commonly used separation methods including 2D-PAGE, LC, off-gel and CE have been described in the part of ESI coupling with separation methods. For protein separation, 2D gel-based proteomics is a mature technology that has been employed in proteomics for over three decades and is still a powerful tool to study bacterial proteomics

with low complexity, and protein with PTMs. Combined with LC-MS/MS, 2D gel could be reduced to 1D gel to separate complex protein mixture according to their molecular weight. This methodology has been standardardized as gel enhanced LC-MS to represent the hybrid gel and LC-MS analysis.[188]

Recently, a great deal of work attempts to discover potential biomarkers with bottom-up proteomics method based on glycopeptide/glycoprotein structures, since alteration of cellular glycosylation is known to be disease-related and most protein biomarkers used clinically are glycosylated. Various types of lectin chromatography[189] and a covalent method using hydrazide[190] are commonly used for glycoproteins enrichment. The glycan isoforms could be differentiated by structure-specific chromatography based on porous graphitized carbon and hydrophilic interaction.[191]

Despite the discovery of many new potential markers using proteomics, only a few biomarkers have been developed into clinical applications for disease screening, due to several limitations, such as false discovery or the lack of standardization of workflow, appropriate biospecimens, bioinformatics *et al.*. However, the advances in MS-based proteomics technology will benefit the biomarker development, from discovery to clinical application.

1.3. Thesis outline

This thesis containing four chapters focuses on two major aspects, direct coupling of various analytical tools with ESTASI-MS and MS sensitivity improvement for bioanalytical applications. Chapter II and III describe the direct coupling of ESTASI-MS with TLC and 384-well plate to expand the applications of ESTASI-MS in various research fields. In Chapter II, ESTASI-TLC-MSI is presented for the identification and imaging of different types of compounds separated on either hydrophilic or hydrophobic silica plates. Chapter III describes a 384-well plate as an emitter for ESTASI-MS. With this setup, enzyme assay and drug metabolism studies were performed in a high throughput and fast way.

The MALDI-MS and ESI-MS signal intensities were greatly improved with two different strategies, as reported in Chapter IV and V respectively. Chapter IV employed Mb-AuNPs for the multiplex separation and sensitive probing of specific IgE antibodies (Abs) from allergic patient blood serum, combined with magnetic separation in a sandwich immunoassay format and MALDI-MS detection of the large amount of mass barcodes. In Chapter V, a novel interface of spyhole between MS and microfluidic chip was created by laser ablation as a nanoESI emitter. The ultrahigh sensitivity provided by the disposable microchip coupled with MS/MS offers the potential application in cancer diagnosis with limited sample amount and simplified experimental procedure. Finally, Chapter VI concluded this thesis generally and described the future perspectives with the presented techniques.

1.4. References

(1) Goldstein, E. *Berl. Ber.* **1886**, *39*, 691.

(2) Reinders, J.; Lewandrowski, U.; Moebius, J.; Wagner, Y.; Sickmann, A. *Proteomics* **2004**, *4* (12), 3686–3703.

(3) Silas G. Villas-Bôas; Mas, S.; Åkesson, M.; Smedsgaard, J.; Nielsen, J. *Mass Spectrom. Rev.* **2005**, *24* (5), 613–646.

(4) A. J. DEMPSTER. *Phys. Rev.* **1918**, *11*, 316–325.

(5) Munson, M. S. B.; Field, F. H. *J. Am. Chem. Soc.* **1966**, *88* (12), 2621–2630.

(6) Horning, E. C.; Horning, M. G.; Carroll, D. I.; Dzidic, I.; Stillwell, R. N. *Anal. Chem.* **1973**, *45* (6), 936–943.

(7) TAYLOR, L.; JOHNSON, R.; RASO, R. *J. Am. Soc. Mass Spectrom.* **1995**, *6* (5), 387–393.

(8) Barber, M.; Bordoli, R. S.; Sedgwick, R. D.; Tyler, A. N. *J. Chem. Soc., Chem. Commun.* **1981**, *0*, 325–327.

(9) Processes, I.; Stoll, R. G.; Harvan, D. J. *Int. J. Mass Spectrom. Ion Process.* **1984**, *61* (1), 71–79.

(10) Blakley, C.; Carmody, J.; Vestal, M. *Anal. Chem.* **1980**, *52* (11), 1636–1641.

(11) Taylor, G. *Proc. R. Soc. A Math. Phys. Eng. Sci.* **1964**, *280* (1382), 383–397.

(12) Dole, M.; Mack, L. L.; Hines, R. L.; Mobley, R. C.; Ferguson, L. D.; Alice, M. B.; Malcolm Dole, L. L. M.; Marck, L. L.; Hines, L.; Mobley, R. C.; Ferguson, L. D.; Alice, M. B. *J Chem.Phys.* **1968**, *49* (5), 2240–2249.

(13) Yamashita, M.; Fenn, J. B. *J Phys.Chem.* **1984**, *88* (20), 4451–4459.

(14) Fenn, J. B.; Mann, M.; Meng, C. K.; Wong, S. F.; Whitehouse, C. M. *Science (80-.).* **1989**, *246* (4926), 64–71.

(15) Karas, M.; Karas, M.; Hillenkamp, F.; Hillenkamp, F.; Bachmann, D.; Bachmann, D. *Anal.Chem.* **1985**, *57* (14), 2935–2939.

(16) Karas, M.; Bachmann, D.; Bahr, U.; Hillenkamp, F. *Int. J. Mass Spectrom. Ion Process.* **1987**, *78*, 53–68.

(17) Tanaka, K.; Waki, H.; Ido, Y.; Akita, S.; Yoshida, Y.; Yohida, T. *Rapid Commun. Mass Spectrom.* **1988**, *2* (8), 151–153.

(18) Garaguso, I.; Borlak, J. *Proteomics* **2008**, *8* (13), 2583–2595.

(19) Zenobi, R.; Knochenmuss, R. *Mass Spectrom. Rev.* **1998**, *17* (5), 337–366.

(20) Stump, M. J.; Fleming, R. C.; Gong, W.-H.; Jaber, A. J.; Jones, J. J.; Surber, C. W.; Wilkins, C. L. *Appl. Spectrosc. Rev.* **2002**, *37* (3), 275–303.

(21) Knochenmuss, R. *J. Mass Spectrom.* **2002**, *37* (8), 867–877.

(22) Karas, M.; Krüger, R. *Chem. Rev.* **2003**, *103* (2), 427–439.

(23) Dreisewerd, K. *Chem. Rev.* **2003**, *103* (2), 395–425.

(24) Knochenmuss, R.; Zenobi, R. *Chem. Rev.* **2003**, *103* (2), 441–452.

(25) Wolff, M. M.; Stephens, W. E. *Rev. Sci. Instrum.* **1953**, *24* (8), 616–617.

(26) Wiley, W. C.; McLaren, I. H. *Rev. Sci. Instrum.* **1955**, *26* (12), 1150–1157.

(27) Mamyrin, B. A.; Karataev, V. I.; Shmikk, D. V; Zagulin, V. A. *Sov. Phys.-JETP.* **1973**, *37* (1), 45–48.

(28) Duncan, M. W.; Roder, H.; Hunsucker, S. W. *Briefings Funct. Genomics Proteomics* **2008**, *7* (5), 355–370.

(29) Jones, L. E.; Carney Doebbeling, C. *Eur. J. Cancer Care (Engl).* **2003**, *18* (2), 165–173.

(30) Rubin, R. B.; Merchant, M. *Am. Clin. Lab.* **2000**, *19* (8), 28–29.

(31) Petricoin, E. F.; Ornstein, D. K.; Paweletz, C. P.; Ardekani, A.; Hackett, P. S.; Hitt, B. A.; Velassco, A.; Trucco, C.; Wiegand, L.; Wood, K.; Simone, C. B.; Levine, P. J.; Linehan, W. M.; Emmert-Buck, M. R.; Steinberg, S. M.; Kohn, E. C.; Liotta, L. A. *J.Natl.Cancer Inst.* **2002**, *94* (20), 1576–1578.

(32) Vorm, O.; Roepstorff, P.; Mann, M. *Anal. Chem.* **1994**, *66* (19), 3281–3287.

(33) Martin, S. E.; Shabanowitz, J.; Hunt, D. F.; Marto, J. A. *Anal. Chem.* **2000**, *72* (18), 4266–4274.

(34) Gong, W.; Elitzin, V. I.; Janardhanam, S.; Wilkins, C. L.; Fritsch, I. *J. Am. Chem. Soc.* **2001**, *123* (4), 769–770.

(35) Trevor, J. L.; Lykke, K. R.; Pellin, M. J.; Hanley, L. *Langmuir* **1998**, *14* (7), 1664–1673.

(36) Pilolli, R.; Palmisano, F.; Cioffi, N. *Anal. Bioanal. Chem.* **2012**, *402* (2), 601–623.

(37) Prime, K.; Whitesides, G. *Science (80-.).* **1991**, *252* (5009), 1164–1167.

(38) Mrksich, M.; Whitesides, G. M. In *Poly(ethylene glycol)*; 1997; Vol. 680, pp 361–373.

(39) Su, J.; Mrksich, M. *Angew. Chemie - Int. Ed.* **2002**, *41* (24), 4715–4718.

(40) Qiu, F.; Jiang, D.; Ding, Y.; Zhu, J.; Huang, L. L. *Angew. Chemie - Int. Ed.* **2008**, *47* (27), 5009–5012.

(41) Qiu, F.; Gu, K.; Yang, B.; Ding, Y.; Jiang, D.; Wu, Y.; Huang, L. L. *Talanta* **2011**, *85* (3), 1698–1702.

(42) Seo, H.; Kim, S.; Kim, J. Il; Kang, H.; Jung, W.; Yeo, W. S. *Anal. Biochem.* **2013**, *434* (1), 199–201.

(43) Lee, J. R.; Lee, J.; Kim, S. K.; Kim, K. P.; Park, H. S.; Yeo, W. S. *Angew. Chemie - Int. Ed.* **2008**, *47* (49), 9518–9521.

(44) Nam, J.; Yoo, M.; Yeo, W. *BioChip J.* **2015**, *9*, 124–129.

(45) Hong, S.-H.; Kim, J. Il; Kang, H.; Yoon, S.; Kim, D.-E.; Jung, W.; Yeo, W.-S. *Chem. Commun.* **2014**, *50* (37), 4831–4834.

(46) Du, R.; Zhu, L.; Gan, J.; Wang, Y.; Qiao, L.; Liu, B. *Anal. Chem.* **2016**, *88* (13), 6767–6772.

(47) Yan, B.; Yesilbag Tonga, G.; Hou, S.; Fedick, P. W.; Yeh, Y. C.; Alfonso, F. S.; Mizuhara, T.; Vachet, R. W.; Rotello, V. M. *Anal. Chem.* **2014**, *86* (13), 6710–6714.

(48) Zhu, Z. J.; Tang, R.; Yeh, Y. C.; Miranda, O. R.; Rotello, V. M.; Vachet, R. W. *Anal. Chem.* **2012**, *84* (10), 4321–4326.

(49) Hou, S.; Sikora, K. N.; Tang, R.; Liu, Y.; Lee, Y. W.; Kim, S. T.; Jiang, Z.; Vachet, R. W.; Rotello, V. M. *ACS Nano* **2016**, *10* (7), 6731–6736.

(50) Yan, B.; Kim, S. T.; Kim, C. S.; Saha, K.; Moyano, D. F.; Xing, Y.; Jiang, Y.; Roberts, A. L.; Alfonso, F. S.; Rotello, V. M.; Vachet, R. W. *J. Am. Chem. Soc.* **2013**, *135* (34), 12564–12567.

(51) Creran, B.; Yan, B.; Moyano, D. F.; Gilbert, M. M.; Vachet, R. W.; Rotello, V. M. *Chem. Commun.* **2012**, *48* (48), 4543–4545.

(52) Zhou, X.; Cao, P.; Tian, Y.; Zhu, J. *J. Am. Chem. Soc.* **2010**, *132* (12), 4161–4168.

(53) Li, Y. J.; Chiu, W. J.; Unnikrishnan, B.; Huang, C. C. *ACS Appl. Mater. Interfaces* **2014**, *6* (17), 15253–15261.

(54) Weng, C. I.; Cang, J. S.; Chang, J. Y.; Hsiung, T. M.; Unnikrishnan, B.; Hung, Y. L.; Tseng, Y. T.; Li, Y. J.; Shen, Y. W.; Huang, C. C. *Anal. Chem.* **2014**, *86* (6), 3167–3173.

(55) Huang, R.-C.; Chiu, W.-J.; Po-Jung Lai, I.; Huang, C.-C. *Sci. Rep.* **2015**, *5*, 10292.

(56) Gilbert, W. *De Magnete, Magneticisque Corporibus, et de Magno Magnete Tellure*, 1ère.; Peter Short: London, 1628.

(57) Nollet, J. A. *Recherches sur les causes particulières des phénomènes électriques*, 1ère.; Chez les frères Guerin: paris, 1749.

(58) Zeleny, J. *Phys. Rev.* **1914**, *3* (2), 69–91.

(59) Publishers, B. V; Alexandrov, M. L.; Shkurov, V. A.; Gall, L. N.; Krasnov, N. V; Nikolaev, V. I.; Pavlenko, V. A. *Int. J. Mass Spectrom. Ion Process.* **1983**, *54*, 231–235.

(60) Kebarle, P.; Verkcerk, U. H. *Mass Spectrom. Rev.* **2009**, *28* (6), 898–917.

(61) Wilm, M. S.; Mann, M. *Int. J. Mass Spectrom. Ion Process.* **1994**, *136*, 167–180.

(62) Eyring, C. F.; MacKeown, S. S.; Millikan, R. A. *Phys. Rev.* **1928**, *31* (5), 900–909.

(63) Mack, L. L.; Kralik, P.; Rheude, A.; Dole, M. *J. Chem. Phys.* **1970**, *52* (10), 4977.

(64) Iribarne, J. V; Thomson, B. A. *J. Chem.Phys.* **1976**, *64* (6), 2287–2294.

(65) Gale, D. C.; Smith, R. D. *Rapid Commun. Mass Spectrom.* **1993**, *7* (11), 1017–1021.

(66) Emmett, M. R.; Caprioli, R. M. *J. Am. Soc. Mass Spectrom.* **1994**, *5* (7), 605–613.

(67) Wilm, M.; Mann, M. *Anal. Chem.* **1996**, *68* (1), 1–8.

(68) Gibson, G. T. T.; Mugo, S. M.; Oleschuk, R. D. *Mass Spectrom. Rev.* **2009**, *28* (6), 918–936.

(69) Takáts, Z.; Wiseman, J. M.; Gologan, B.; Cooks, R. G. *Science* **2004**, *306* (5695), 471–473.

(70) Venter, A.; Sojka, P. E.; Cooks, R. G. *Anal. Chem.* **2006**, *78* (24), 8549–8555.

(71) Costa, A. B.; Cooks, R. G. *Chem. Commun.* **2007**, No. 38, 3915–3917.

(72) Costa, A. B.; Graham Cooks, R. *Chem. Phys. Lett.* **2008**, *464*, 1–8.

(73) Leuthold, L. A.; Mandscheff, J. F.; Fathi, M.; Giroud, C.; Augsburger, M.; Varesio, E.; Hopfgartner, G. *Rapid Commun. Mass Spectrom.* **2006**, *20* (2), 103–110.

(74) Cotte-Rodríguez, I.; Cooks, R. G. *Chem. Commun. (Camb).* **2006**, No. 28, 2968–2970.

(75) Laskin, J.; Heath, B. S.; Roach, P. J.; Cazares, L.; Semmes, O. J. *Anal. Chem.* **2012**, *84* (1), 141–148.

(76) Garcia-Reyes, J. F.; Jackson, A. U.; Molina-Diaz, A.; Cooks, R. G. *Anal. Chem.* **2009**, *81* (2), 820–829.

(77) Wiseman, J. M.; Ifa, D. R.; Zhu, Y.; Kissinger, C. B.; Manicke, N. E.; Kissinger, P. T.; Cooks, R. G. *Proc. Natl. Acad. Sci. U. S. A.* **2008**, *105* (47), 18120–18125.

(78) Nyadong, L.; Hohenstein, E. G.; Galhena, A.; Lane, A. L.; Kubanek, J.; Sherrill, C. D.; Fernández, F. M. *Anal. Bioanal. Chem.* **2009**, *394* (1), 245–254.

(79) Shiea, J.; Chang, D. Y.; Lin, C. H.; Jiang, S. J. *Anal. Chem.* **2001**, *73* (20), 4983–4987.

(80) Chang, D. Y.; Lee, C. C.; Shiea, J. *Anal. Chem.* **2002**, *74* (11), 2465–2469.

(81) Chen, H.; Venter, A.; Cooks, R. G. *Chem. Commun.* **2006**, 2042–2044.

(82) Gu, H.; Chen, H.; Pan, Z.; Jackson, A. U.; Talaty, N.; Xi, B.; Kissinger, C.; Duda, C.; Mann, D.; Raftery, D.; Cooks, R. G. *Anal. Chem.* **2007**, *79* (1), 89–97.

(83) Chingin, K.; Chen, H.; Gamez, G.; Zhu, L.; Zenobi, R. *Anal. Chem.* **2009**, *81* (1), 123–129.

(84) Marquez, C. A.; Wang, H.; Fabbretti, F.; Metzger, J. O. *J. Am. Chem. Soc.* **2008**, *130* (51), 17208–17209.

(85) Chen, H.; Wortmann, A.; Zhang, W.; Zenobi, R. *Angew. Chemie - Int. Ed.* **2007**, *46* (4), 580–583.

(86) Chen, H.; Yang, S.; Wortmann, A.; Zenobi, R. *Angew. Chemie - Int. Ed.* **2007**, *46* (40), 7591–7594.

(87) Shiea, J.; Huang, M. Z.; Hsu, H. J.; Lee, C. Y.; Yuan, C. H.; Beech, I.; Sunner, J. *Rapid Commun. Mass Spectrom.* **2005**, *19* (24), 3701–3704.

(88) Cheng, S. C.; Cheng, T. L.; Chang, H. C.; Shiea, J. *Anal. Chem.* **2009**, *81* (3), 868–874.

(89) Shiea, J.; Yuan, C.-H.; Huang, M.-Z.; Cheng, S.-C.; Ma, Y.-L.; Tseng, W.-L.; Chang, H.-C.; Hung, W.-C.

Anal. Chem. **2008**, *80* (13), 4845–4852.

(90) Sampson, J. S.; Hawkridge, A. M.; Muddiman, D. C. *J. Am. Soc. Mass Spectrom.* **2006**, *17* (12), 1712–1716.

(91) Nemes, P.; Vertes, A. *Anal. Chem.* **2007**, *79* (21), 8098–8106.

(92) Hong, C. M.; Lee, C. T.; Lee, Y. M.; Kuo, C. P.; Yuan, C. H.; Shiea, J. *Rapid Commun. Mass Spectrom.* **1999**, *13* (1), 21–25.

(93) Jeng, J.; Shiea, J. *Rapid Commun. Mass Spectrom.* **2003**, *17* (15), 1709–1713.

(94) Kuo, C. P.; Yuan, C. H.; Shiea, J. *J. Am. Soc. Mass Spectrom.* **2000**, *11* (5), 464–467.

(95) Jackson, P.; Attalla, M. I. *Rapid Commun. Mass Spectrom.* **2010**, *24* (24), 3567–3577.

(96) Van Berkel, G. J.; Sanchez, A. D.; Quirke, J. M. E. *Anal. Chem.* **2002**, *74* (24), 6216–6223.

(97) Luftmann, H. *Anal. Bioanal. Chem.* **2004**, *378* (4), 964–968.

(98) Wang, H.; Liu, J.; Graham Cooks, R.; Ouyang, Z. *Angew. Chemie - Int. Ed.* **2010**, *49* (5), 877–880.

(99) Shen, L.; Zhang, J.; Yang, Q.; Manicke, N. E.; Ouyang, Z. *Clin. Chim. Acta* **2013**, *420*, 28–33.

(100) Liu, J.; Wang, H.; Cooks, R. G.; Ouyang, Z. *Anal. Chem.* **2011**, *83* (20), 7608–7613.

(101) Hu, B.; So, P. K.; Chen, H.; Yao, Z. P. *Anal. Chem.* **2011**, *83* (21), 8201–8207.

(102) Chan, S. L. F.; Wong, M. Y. M.; Tang, H. W.; Che, C. M.; Ng, K. M. *Rapid Commun. Mass Spectrom.* **2011**, *25* (19), 2837–2843.

(103) Liu, J.; Cooks, R. G.; Ouyang, Z. *Anal. Chem.* **2011**, *83* (24), 9221–9225.

(104) Huang, G.; Li, G.; Cooks, R. G. *Angew. Chemie - Int. Ed.* **2011**, *50* (42), 9907–9910.

(105) Huang, G.; Li, G.; Ducan, J.; Ouyang, Z.; Cooks, R. G. *Angew. Chem. Int. Ed. Engl.* **2011**, *50*, 2503–2506.

(106) Peng, Y.; Zhang, S.; Gong, X.; Ma, X.; Yang, C.; Zhang, X. *Anal. Chem.* **2011**, *83* (23), 8863–8866.

(107) Qiao, L.; Sartor, R.; Gasilova, N.; Lu, Y.; Tobolkina, E.; Liu, B.; Girault, H. H. *Anal. Chem.* **2012**, *84* (17), 7422–7430.

(108) Tobolkina, E.; Qiao, L.; Roussel, C.; Girault, H. H. *Talanta* **2014**, *130*, 377–381.

(109) Qiao, L.; Tobolkina, E.; Liu, B.; Girault, H. H. *Anal. Chem.* **2013**, *85* (9), 4745–4752.

(110) Kelleher, N. L.; Lin, H. Y.; Valaskovic, G. a; Aaserud, D. J.; Fridriksson, E. K.; McLafferty, F. W. *J. Am. Chem. Soc.* **1999**, *121* (4), 806–812.

(111) Churchwell, M. I.; Twaddle, N. C.; Meeker, L. R.; Doerge, D. R. *J. Chromatogr. B Anal. Technol. Biomed. Life Sci.* **2005**, *825* (2), 134–143.

(112) Meisen, I.; Pater-Katalinić, J.; Müthing, J. *Anal. Chem.* **2004**, *76* (8), 2248–2255.

(113) Lee, C. S.; Kim, Y. G.; Joo, H. S.; Kim, B. G. *J. Mass Spectrom.* **2004**, *39* (5), 514–525.

(114) Lin, S. Y.; Huang, M. Z.; Chang, H. C.; Shiea, J. *Anal. Chem.* **2007**, *79* (22), 8789–8795.

(115) Cheng, S. C.; Huang, M. Z.; Shiea, J. *Anal. Chem.* **2009**, *81* (22), 9274–9281.

(116) Van Berkel, G. J.; Ford, M. J.; Deibel, M. A. *Anal. Chem.* **2005**, *77* (5), 1207–1215.

(117) http://www.camag.com/en/tlc_hptlc/products/evaluation_documentation_tlc-ms_bioluminenscence/tlc-ms_interface_2.cfm.

(118) http://www.prosolia.com/products/flowprobe.

(119) O'Farrell, P. H. *J. Biol. Chem.* **1975**, *250* (10), 4007–4021.

(120) Ros, A.; Faupel, M.; Mees, H.; Van Oostrum, J.; Ferrigno, R.; Reymond, F.; Michel, P.; Rossier, J. S.;

Girault, H. H. *Proteomics* **2002**, *2* (2), 151–156.

(121) Hörth, P.; Miller, C. a; Preckel, T.; Wenz, C. *Mol. Cell. Proteomics* **2006**, *5* (10), 1968–1974.

(122) Olivares, J. A.; Nguyen, N. T.; Yonker, C. R.; Smith, R. D. *Anal. Chem.* **1987**, *59* (9), 1230–1232.

(123) Koehn, F. E.; Carter, G. T. *Nat. Rev. Drug Discov.* **2005**, *4* (3), 206–220.

(124) Fitch, W. L. *Mol. Divers.* **2002**, *4* (1), 39–45.

(125) Süßmuth, R. D.; Jung, G. *J Chromatogr B Biomed Sci Appl* **1999**, *725* (1), 49–65.

(126) Felten, C.; Foret, F.; Minarik, M.; Goetzinger, W.; Karger, B. L. *Anal. Chem.* **2001**, *73* (7), 1449–1454.

(127) https://advion.com/products/triversa-nanomate/.

(128) Wang, T.; Zeng, L.; Strader, T.; Burton, L.; Kassel, D. B. *Rapid Commun. Mass Spectrom.* **1998**, *12* (16), 1123–1129.

(129) Morand, K. L.; Burt, T. M.; Regg, B. T.; Chester, T. L. *Anal. Chem.* **2001**, *73* (2), 247–252.

(130) Wang, B.; Trimpin, S. *Anal. Chem.* **2014**, *86* (2), 1000–1006.

(131) Lee, J.; Soper, S. A.; Murray, K. K. *J. Mass Spectrom.* **2009**, *44* (5), 579–593.

(132) Xue, Q.; Foret, F.; Dunayevskiy, Y. M.; Zavracky, P. M.; McGruer, N. E.; Karger, B. L. *Anal. Chem.* **1997**, *69* (3), 426–430.

(133) Xue, Q.; Dunayevskiy, Y. M.; Foret, F.; Karger, B. L. *Rapid Commun. Mass Spectrom.* **1997**, *11* (12), 1253–1256.

(134) Barnidge, D. R.; Nilsson, S.; Markides, K. E. *Anal. Chem.* **1999**, *71* (19), 4115–4118.

(135) Figeys, D.; Ning, Y.; Aebersold, R. *Anal. Chem.* **1997**, *69* (16), 3153–3160.

(136) Bings, N. H.; Wang, C.; Skinner, C. D.; Colyer, C. L.; Thibault, P.; Harrison, D. J. *Anal. Chem.* **1999**, *71* (15), 3292–3296.

(137) Lazar, I. M.; Ramsey, R. S.; Sundberg, S.; Ramsey, J. M. *Anal. Chem.* **1999**, *71* (17), 3627–3631.

(138) Zhang, B.; Foret, F.; Karger, B. L. *Anal. Chem.* **2000**, *72* (5), 1015–1022.

(139) Svedberg, M.; Veszelei, M.; Axelsson, J.; Vangbo, M.; Nikolajeff, F. *Lab Chip* **2004**, *4* (4), 322–327.

(140) Tang, K.; Lin, Y.; Matson, D. W.; Kim, T.; Smith, R. D. *Anal. Chem.* **2001**, *73* (8), 1658–1663.

(141) Rohner, T. C.; Rossier, J. S.; Girault, H. H. *Anal. Chem.* **2001**, *73* (22), 5353–5357.

(142) Schilling, M.; Nigge, W.; Rudzinski, a; Neyer, a; Hergenroder, R. *Lab Chip* **2004**, *4* (3), 220–224.

(143) Yin, H.; Killeen, K.; Brennen, R.; Sobek, D.; Werlich, M.; Van De Goor, T. *Anal. Chem.* **2005**, *77* (2), 527–533.

(144) Le Gac, S.; Arscott, S.; Rolando, C. *Electrophoresis* **2003**, *24* (21), 3640–3647.

(145) Mellors, J. S.; Gorbounov, V.; Ramsey, R. S.; Ramsey, J. M. *Anal. Chem.* **2008**, *80* (18), 6881–6887.

(146) Schultz, G. A.; Corso, T. N.; Prosser, S. J.; Zhang, S. *Anal. Chem.* **2000**, *72* (17), 4058–4063.

(147) Mao, P.; Wang, H. T.; Yang, P.; Wang, D. *Anal. Chem.* **2011**, *83* (15), 6082–6089.

(148) Sainiemi, L.; Nissilä, T.; Kostiainen, R.; Ketola, R. a; Franssila, S. *Lab Chip* **2011**, *11* (17), 3011–3014.

(149) Yin, H.; Killeen, K. *Journal of Separation Science*. 2007, pp 1427–1434.

(150) Vollmer, M.; Hörth, P.; Rozing, G.; Couté, Y.; Grimm, R.; Hochstrasser, D.; Sanchez, J. C. *J. Sep. Sci.* **2006**, *29* (4), 499–509.

(151) Gobry, V.; Van Oostrum, J.; Martinelli, M.; Rohner, T. C.; Reymond, F.; Rossier, J. S.; Girault, H. H. *Proteomics* **2002**, *2* (4), 405–412.

(152) Prudent, M.; Rossier, J. S.; Lion, N.; Girault, H. H. *Anal. Chem.* **2008**, *80* (7), 2531–2538.

(153) Abonnenc, M.; Dayon, L.; Perruche, B.; Lion, N.; Girault, H. H. *Anal. Chem.* **2008**, *80* (9), 3372–3378.

(154) Lu, Y.; Prudent, M.; Qiao, L.; Mendez, M. a; Girault, H. H. *Metallomics* **2010**, *2* (7), 474–479.

(155) Qiao, L.; Lu, Y.; Liu, B.; Girault, H. H. *J. Am. Chem. Soc.* **2011**, *133* (49), 19823–19831.

(156) Me, M. A.; Prudent, M.; Su, B.; Girault, H. H. **2008**, *80* (24), 9499–9507.

(157) Miladinović, S.; Fornelli, L.; Lu, Y.; Piech, K.; Girault, H.; Tsybin, Y. *Anal. Chem.* **2012**, *84* (11), 4647–4651.

(158) Gasilova, N.; Qiao, L.; Momotenko, D.; Pourhaghighi, M. R.; Girault, H. H. *Anal. Chem.* **2013**, *85* (13), 6254–6263.

(159) Gasilova, N.; Srzentić, K.; Qiao, L.; Liu, B.; Beck, A.; Tsybin, Y. O.; Girault, H. H. *Anal. Chem.* **2016**, *88* (3), 1775–1784.

(160) Gasilova, N.; Yu, Q.; Qiao, L.; Girault, H. H. *Angew. Chemie - Int. Ed.* **2014**, *53* (17), 4408–4412.

(161) Amstalden van Hove, E. R.; Smith, D. F.; Heeren, R. M. A. *J. Chromatogr. A*. 2010, pp 3946–3954.

(162) McDonnell, L. A.; Heeren, R. M. A. *Mass Spectrom. Rev.* 2007, pp 606–643.

(163) Eberlin, L. S.; Liu, X.; Ferreira, C. R.; Santagata, S.; Agar, N. Y. R.; Cooks, R. G. *Anal. Chem.* **2011**, *83* (22), 8366–8371.

(164) Ifa, D.; Jackson, A.; Paglia, G.; Cooks, R. *Anal. Bioanal. Chem.* **2009**, *394* (8), 1995–2008.

(165) Ifa, D. R.; Wu, C.; Ouyang, Z.; Cooks, R. G. *Analyst* **2010**, *135* (4), 669–681.

(166) Qiao, L.; Tobolkina, E.; Lesch, A.; Bondarenko, A.; Zhong, X.; Liu, B.; Pick, H.; Vogel, H.; Girault, H. H. *Anal. Chem.* **2014**, *86* (4), 2033–2041.

(167) Anderson, N. L.; Anderson, N. G. *Electrophoresis* **1998**, *19* (11), 1853–1861.

(168) Han, X.; Jin, M.; Breuker, K.; McLafferty, F. W. *Science* **2006**, *314* (5796), 109–112.

(169) Wolters, D. A.; Washburn, M. P.; Yates, J. R. *Anal. Chem.* **2001**, *73* (23), 5683–5690.

(170) Mitchell Wells, J.; McLuckey, S. A. *Methods Enzymol.* **2005**, *402*, 148–185.

(171) Zubarev, R.; Kelleher, N. L.; McLafferty, F. W. *J. Am. Chem. Soc.* **1998**, *120* (16), 3265–3266.

(172) Syka, J. E. P.; Coon, J. J.; Schroeder, M. J.; Shabanowitz, J.; Hunt, D. F. *Proc. Natl. Acad. Sci. U. S. A.* **2004**, *101* (26), 9528–9533.

(173) Kjeldsen, F.; Silivra, O. A.; Ivonin, I. A.; Haselmann, K. F.; Gorshkov, M.; Zubarev, R. A. *Chem. - A Eur. J.* **2005**, *11* (6), 1803–1812.

(174) Zhang, H.; Liu, A. Y.; Loriaux, P.; Wollscheid, B.; Zhou, Y.; Watts, J. D.; Aebersold, R. *Mol Cell Proteomics* **2007**, *6* (1), 64–71.

(175) Moon, P. G.; You, S.; Lee, J. E.; Hwang, D.; Baek, M. C. *Mass Spectrom. Rev.* **2011**, *30* (6), 1185–1202.

(176) Tumani, H.; Pfeifle, M.; Lehmensiek, V.; Rau, D.; Mogel, H.; Ludolph, A. C.; Brettschneider, J. *J. Neuroimmunol.* **2009**, *214* (1–2), 109–112.

(177) Alexander, H.; Stegner, A. L.; Wagner-Mann, C.; Du Bois, G. C.; Alexander, S.; Sauter, E. R. *Clin. Cancer Res.* **2004**, *10* (22), 7500–7510.

(178) Farina, A.; Dumonceau, J.-M.; Lescuyer, P. *Expert Rev. Proteomics* **2009**, *6* (3), 285–301.

(179) Hood, B. L.; Darfler, M. M.; Guiel, T. G.; Furusato, B.; Lucas, D. A.; Ringeisen, B. R.; Sesterhenn, I. A.; Conrads, T. P.; Veenstra, T. D.; Krizman, D. B. *Mol. Cell. Proteomics* **2005**, *4* (11), 1741–1753.

(180) Anderson, N. L. *Mol. Cell. Proteomics* **2002**, *1* (11), 845–867.

(181) Liu, T.; Qian, W.-J.; Mottaz, H. M.; Gritsenko, M. A.; Norbeck, A. D.; Moore, R. J.; Purvine, S. O.;

Camp, D. G.; Smith, R. D. *Mol. Cell. Proteomics* **2006**, *5* (11), 2167–2174.

(182) Colantonio, D. A.; Dunkinson, C.; Bovenkamp, D. E.; Van Eyk, J. E. *Proteomics* **2005**, *5* (15), 3831–3835.

(183) Kay, R.; Barton, C.; Ratcliffe, L.; Matharoo-Ball, B.; Brown, P.; Roberts, J.; Teale, P.; Creaser, C. *Rapid Commun. Mass Spectrom.* **2008**, *22* (20), 3255–3260.

(184) Warder, S. E.; Tucker, L. A.; Strelitzer, T. J.; McKeegan, E. M.; Meuth, J. L.; Jung, P. M.; Saraf, A.; Singh, B.; Lai-Zhang, J.; Gagne, G.; Rogers, J. C. *Anal. Biochem.* **2009**, *387* (2), 184–193.

(185) Mahn, A.; Ismail, M. *J. Chromatogr. B Anal. Technol. Biomed. Life Sci.* **2011**, *879* (30), 3645–3648.

(186) Thulasiraman, V.; Lin, S.; Gheorghiu, L.; Lathrop, J.; Lomas, L.; Hammond, D.; Boschetti, E. *Electrophoresis* **2005**, *26* (18), 3561–3571.

(187) Fonslow, B. R.; Stein, B. D.; Webb, K. J.; Xu, T.; Choi, J.; Park, S. K.; Iii, J. R. Y.; Yates, J. R.; Iii, J. R. Y.; Yates, J. R. *Nat. Methods* **2013**, *10* (1), 54–56.

(188) Lundby, A.; Olsen, J. V. *Methods Mol. Biol.* **2011**, *753*, 143–155.

(189) Mechref, Y.; Madera, M.; Novotny, M. V. *Methods Mol. Biol.* **2008**, *424*, 373–396.

(190) Tian, Y., Zhou, Y., Elliot, S., Aebersold, R., Zhang, H. *Nat Protoc.* **2007**, *2* (2), 334–339.

(191) Nwosu, C. C.; Seipert, R. R.; Strum, J. S.; Hua, S. S.; An, H. J.; Zivkovic, A. M.; German, B. J.; Lebrilla, C. B. *J. Proteome Res.* **2011**, *10* (5), 2612–2624.

CHAPTER II.

Ambient *in-situ* analysis and imaging of both hydrophilic and hydrophobic thin layer chromatography plates by electrostatic spray ionization mass spectrometry

Based on X. Zhong et al., RSC Adv., 2015, 5, 75395-75402.

Abstract

Electrostatic spray ionization (ESTASI) mass spectrometry imaging (MSI) recently developed to profile spatial distribution of chemical and biochemical molecules on an insulating surface under ambient conditions has been applied to extract and identify chemicals from silica gel surfaces. Both hydrophilic or hydrophobic silica plates have been imaged with a good resolution providing a direct identification of the samples. For the hydrophilic silica gel substrate, silanization of the plate before ESTASI-MS analysis was used to render the surface hydrophobic. ESTASI-MSI is shown to be a sensitive technique for the identification of a wide range of molecules of different polarities and chemical structures with minimal sample consumption in the femtomole range.

2.1. Introduction

Compared to vacuum ionization mass spectrometry imaging (MSI), ambient ionization MSI holds the advantages of minimal sample preparation, more flexible device design and *in-situ* analysis. The commonly used ambient ionization methods for MSI include desorption electrospray ionization (DESI),[1] laser ablation electrospray ionization (LAESI), desorption atmospheric pressure photoionization (DAPPI),[2] laser desorption atmospheric pressure chemical ionization (LD-APCI),[3] low-temperature plasma (LTP) mass spectrometry,[4] and liquid extraction surface analysis.[5] Recently, LEPA has developed a novel ambient MSI system based on the newly introduced technology named electrostatic spray ionization (ESTASI),[6] as described in § 1.1.4 and 1.2.4, and successfully imaged dried peptide spots and black dye patterns on polyimide substrates.[7] However, a major problem of ESTASI-MSI has been the low spatial resolution due to the tailing effect resulting from droplet based extraction of the weakly bound samples on insulating polymer substrates. The purpose of this work is to show that this drawback can be circumvented when imaging thin-layer chromatography (TLC) plates by ESTASI-MSI. The strong hydrophobic or hydrophilic affinity between samples and substrates minimizes the tailing effect. By optimizing the extraction buffer conditions, selective sampling from the substrates can be realized.

TLC, one of the earliest forms of chromatography for the separation of a wide range of samples,[8-12] is still widely used nowadays in food analysis, pharmaceutical research, forensic science, biochemistry, clinical chemistry, etc. The compounds separated by TLC are amenable to the post-chromatographic detection and profiling by typical methods such as optical visualization and spectroscopic measurements. However, these detection methods usually have poor specificity and are restricted by the chemical or optical properties of analytes. For these reasons, MS is a suitable technique to couple with TLC due to its rapid analysis, high specificity and structural characterization ability.[13,14] Various vacuum-based desorption ionization techniques have been applied to sample and ionize non-volatile or thermally labile compounds directly from TLC surfaces.[15-20] Nevertheless, the widespread application of vacuum-based TLC-MS techniques has been hindered by several problems such as the requirement of a high-vacuum apparatus, difficult detection of volatile or semi-volatile compounds and interference of matrix ions in the low mass range (< 700 Da) during MALDI-MS analysis. Interfacing TLC with ambient ionization MS without much sample pretreatment prior to MS analysis is more convenient in the view of fast analysis. Recently,

several ambient ionization methods, including ESI based techniques, as described in § 1.2.1.1,[21-27] APCI,[28] DART[29] and inductively coupled plasma ICP[30, 31] have been introduced for the direct coupling of TLC with MS. Among the ESI based techniques, desorption electrospray ionization (DESI) is a powerful technique and has been combined with TLC, where the charged solvent droplets induced by electrospray ionization were directed to the TLC plate to sample and ionize the analytes.[24] Then a closely related approach, named nano-DESI, was developed in 2010, which enables the separation of desorption and ionization events by providing two capillaries to form a solvent bridge to desorb analytes from substrates followed by ionization through self-aspirating nanospray.[27] Afterwards, tissue imaging was demonstrated by using this technique with good spatial resolution and high sensitivity.[32]

Here, ESTASI is coupled with TLC directly. Sample spots separated by TLC were profiled by ESTASI-MSI, including drug molecules on normal phase silica TLC plates and dyes on high performance reverse phase (HPRP) C_{18} silica plates. In the former case, the highly hydrophilic silica plates were modified by chlorotrimethylsilane after TLC separation to form hydrophobic surfaces for ESTASI-MS analyses. The HPRP C_{18} and the modified normal phase silica plates provide ideal substrates for *in-situ* characterization and accurate sample location by ESTASI-MS with efficient sample extraction, reduced tailing effect due to the hydrophobic-hydrophobic or hydrophilic-hydrophilic interactions between samples and TLC substrates and even the abilities of sample desalting to enhance the detection sensitivity. The TLC-ESTASI-MS is universal for a wide range of organic molecules with very different chemical properties and polarities. The sample consumption can be as low as 75 fmole of fluorescein on the HPRP C_{18} plate, or $\leq$33 fmole of enrofloxacin on the normal phase silica plate. In addition to the identification of sample spots, the TLC-ESTASI-MS strategy can also provide a separation profile of the samples on the plates in a line-scan mode, or even a distribution image of the spots in a 2D-scan mode, which is of great value when the samples are colourless and do not give a clear image under UV illumination on the TLC plates with fluorescent indicators.

2.2. Experimental section

2.2.1. Materials and methods

Methanol (99.9% HPLC grade), acetic acid (>99.9%), 4-acetamidophenol (98%), aspirin (99%) and chlorotrimethylsilane (≥98% GC grade) were obtained from Sigma-Aldrich (Schnelldorf, Switzerland). 25% aqueous ammonia and tetrahydrofuran (99.8%) were from VWR (Nyon, Switzerland). Ammonium acetate (98%) was obtained from Merck (Zug, Switzerland). Rhodamine B (99%), rhodamine 6G (99%), caffeine (98.5%), formic acid (99%) and acetonitrile (99.9% HPLC grade) were purchased from Acros Organics (Geel, Belgium). Fluorescein (Reag. Ph. Eur.), methylene blue (95%), sudan III (≥96%), crystal violet (AR grade) and ethyl acetate (99.9% HPLC grade) were obtained from Fluka (St. Gallen, Switzerland). Enrofloxacin (ENR, 98%), fleroxacin (FLE, 98%) and lomefloxacin (LOM, 98%) were purchased from TCI (Tokyo, Japan). Angiotensin I (NH_2-DRVYIHPFHL-COOH, 98%) was obtained from Bachem (Bubendorf, Switzerland). Deionized water (18.2 MΩ cm) was purified by an alpha Q Millipore system (Zug, Switzerland) and used in all aqueous solutions.

Silica TLC plates (20 cm × 20 cm, 200 μm layer thickness, PET foil base (0.4 mm thickness) with fluorescent indicator 254 nm) were purchased from Fluka (St. Gallen, Switzerland). HPRP C_{18} plates (10 cm × 10 cm, 200 μm layer thickness, glass plate (1.2 mm thickness) with fluorescent indicator 254 nm) were obtained from Merck (Zug, Switzerland).

2.2.2. Thin-layer chromatography

For the TLC-ESTASI-MS analyses of drugs (ENR, 4-Acetamidophenol, aspirin, caffeine, LOM or FLE), 1 μL of sample solution (0.5 mg/mL in methanol) was deposited on a silica TLC plate and developed under the mobile solution composed of methanol, 25% aqueous ammonia, ethyl acetate and acetonitrile (1:1:2:1 by volume). In the analysis of a drug mixture, an aqueous droplet (1 μL) containing ENR (1.4 nmole) and acetaminophen (3.3 nmole) was spotted on a silica TLC plate for the separation with the mobile solution as reported.[33]

For the TLC-ESTASI-MS analyses of dyes (fluorescein, rhodamine B, rhodamine 6G, sudan III, methylene blue or crystal violet), HPRP C_{18} plates were used. In the analysis of a dye mixture, a droplet (1 μL) of the dye mixture (1.7 nmole of methylene blue, 1 nmole of

rhodamine 6G and 1.5 nmole of fluorescein) was spotted on a HPRP C_{18} plate, and developed with the mobile phase composed of methanol, tetrahydrofuran (60: 40 by volume) and 100 mM ammonium acetate as reported.[21]

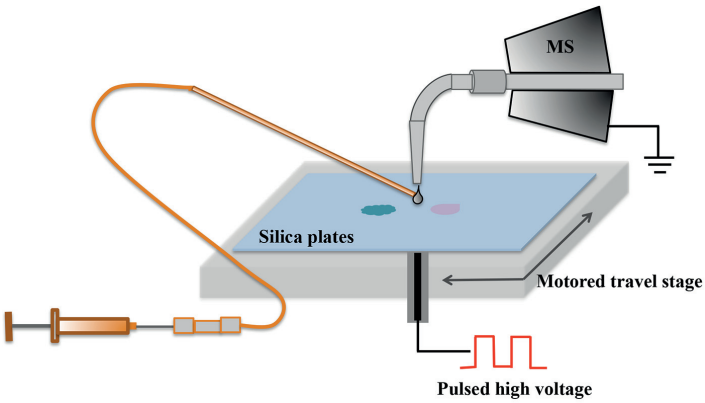

Figure 2.1. Schematic representation of the setup used for TLC-ESTASI-MS.

2.2.3. Modification and characterization of TLC plates

After sample separation, the silica gel TLC plates were coated by chlorotrimethylsilane to form hydrophobic surfaces. During the coating procedure, both a dry silica plate and a small bottle with 2 mL of chlorotrimethylsilane were placed inside a closed plastic box and all together in a fume hood overnight (~16 hours). The chlorotrimethylsilane was evaporated from the small bottle to react with silicon hydroxyl of the TLC plate. Afterwards, the modified plate was taken out of the box and placed in the fume hood for another 1h to let the excess chlorotrimethylsilane vapour evacuate.

Characterization of the modified and unmodified silica TLC and the HPRP C_{18} plate was performed by a Drop Shape Analysis System DSA100 from Krüss GmbH (Hamburg, Germany), where the contact angles of different solvents on the plates were tested.

2.2.4. ESTASI-MS

The mass spectrometer used to detect ions produced by ESTASI was a linear ion trap (Thermo LTQ Velos), where the MS inlet was always grounded and the positive ion-scanning mode was chosen. The ESI voltage of the internal power source of the MS instrument was always set as 0 during ESTASI-MS experiments. The enhanced ion trap scanning rate of 10000 mass-to-charge ratio (m/z) per second was used.

The ESTASI setup was illustrated in Figure 2.1. High voltage pulses (from 0 V up to 9 kV, 20 Hz) were generated by amplifying square wave voltage pulses with a high voltage amplifier (10HVA24-P1, HVP High Voltage Products GmbH, Martinsried/Planegg, Germany) to induce the ESTASI. A self-designed ion transfer capillary in "L" shape (2 mm of outer diameter (o.d.), 0.8 mm of inner diameter (i.d.)) replaced the original one for convenient scan of a horizontally placed surface. A TLC plate containing sample spots was supported on a thin insulating polymer substrate (PET, 0.2 mm thickness) and placed under the ion transfer capillary. The TLC plate was moved by two motored travel stages (MTS50-Z8, Thorlabs, Dachau/Munich, Germany) in x and y directions to bring the sample spots under the MS inlet for detection, linear scans or 2D MSI. A fused silica capillary (150 μm o.d., 50 μm i.d.) named wetting capillary was in contact with the TLC plate surface to deliver acidic solvent for sample extraction and ionization. Several parameters were adjusted precisely to obtain good MS signals, including the distance between the sample surface and the ion transfer capillary, the angle between the fused silica capillary and the sample surface, the flow rate of the acidic solvent and the solvent component.

ESTASI-MS selected reaction monitoring (SRM) was performed by collision induced dissociation (CID) with normalized collision energy of 25. The isolation width of precursor ion was set as 2 m/z and the scan range of SRM was set as ± 16 m/z. Data analysis was performed by Xcalibur Qual Browser (ThermoFisher Scientific, Reinach, Switzerland). The line-scan results and mass spectra were plotted by IGOR Pro (Version 6.00 for Macintosh, WaveMetrics, Lake Oswego, OR, USA). 2D MS image and 3D TLC-ESTASI-MS map were plotted by the data processing software MIRA (G. Wittstock, University of Oldenburg, http://www.uni-oldenburg.de/chemie/pc2/pc2forschung/secm-tools/mira/).

2.3. Results and discussion

2.3.1. ESTASI-MS analyses of samples from HPRP C_{18} plates

In TLC-ESTASI-MS, a wetting capillary was used to deliver extraction solution to a TLC plate locally, and extract samples from the plate. ESTASI-MS analysis[7] of the samples can be accomplished only when the extraction solvent can establish a droplet under the MS inlet and when the samples can be efficiently extracted into the droplet. Thus, the extracting solvent needs to be well chosen to combine a good solubility for the analytes and a good

wettability for the TLC plates. For different samples and TLC plates, the different solvent composition should be optimized accordingly.

One typical application of the TLC-ESTASI-MS system is based on reverse phase TLC plates. In this work, a HPRP C_{18} plate was selected, because of its excellent separation ability with respect to various organic molecules, and its highly hydrophobic surface property. Several identical sample droplets (1 μL, 0.3 mM fluorescein) were deposited on a HPRP C_{18} plate and then developed in parallel by the mobile solution of methanol and tetrahydrofuran (60: 40 v/v) with 100 mM ammonium acetate to obtain several sample spots with the size of ~5 mm in diameter each. Five extraction solvents, containing 0%, 25%, 50%, 75% and 99% H_2O respectively, in methanol with 1% acetic acid were tested. Sampling with each solvent lasted for 30 s on the centre of the fluorescein spot with continuous ESTASI-MS detection. Due to the different absorption of the HPRP C_{18} plate to different extraction solvents, the injection flow rate of each solvent was adjusted to obtain the best MS signals for the solvent.

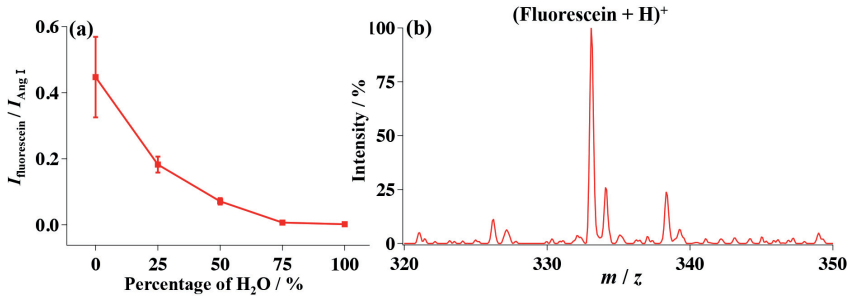

Figure 2.2. Extraction solvent optimization and detection limit of fluorescein on HPRP C_{18} plate. **(a)** Optimization of the extraction solvent (water and methanol mixture with 1% acetic acid). $I_{fluoresceine}$: intensity of singly protonated fluorescein at m/z = 333.3; $I_{Ang\ I}$: intensity of three-protonated angiotensin I at m/z = 432.9. **(b)** Mass spectrum of fluorescein detected by ESTASI-MS from the HPRP C_{18} plate with 1% acetic acid, 75% methanol and 24% H_2O as the extraction solvent under a flow rate of 1 μL/min. Sample on TLC: fluorescein (1 μL, 30 μM aqueous solution) developed by the mobile solution of methanol and tetrahydrofuran (60: 40 v/v) with 100 mM ammonium acetate.

From the recorded mass spectra, ratios between the peak intensities of the fluorescein ion and the internal standard (IS) ion, which was the triply protonated Ang I, were calculated, averaged and plotted versus the percentages of water in the extraction solvent, as shown in Figure 2.2(a). The MS intensity of fluorescein in comparison with the IS reduced greatly with the incremental change of water percentage. It is reasonable by considering that the less-polarized solvent with more methanol should have a better extraction capacity of samples

from the reverse phase TLC plates, where the affinity between the samples and the C_{18} modified plate is based on hydrophobic-hydrophobic interactions. In spite of the largest extraction efficiency, it was difficult to form a stable ESTASI MS signal with the solvent consisting of 99% methanol and 1% acetic acid. Because of the relatively strong absorption of the HPRP C_{18} plate to methanol, the extraction solvent with 99% methanol can also induce the development of the sample in the plate, which would especially influence the linear scan or 2D imaging of TLC spots by MS. Therefore, the solvent composed of 75% methanol, 24% water and 1% acetic acid was selected for the further experiments on the HPRP C_{18} plate to evaluate the detection limit of fluorescein by TLC-ESTASI-MS.

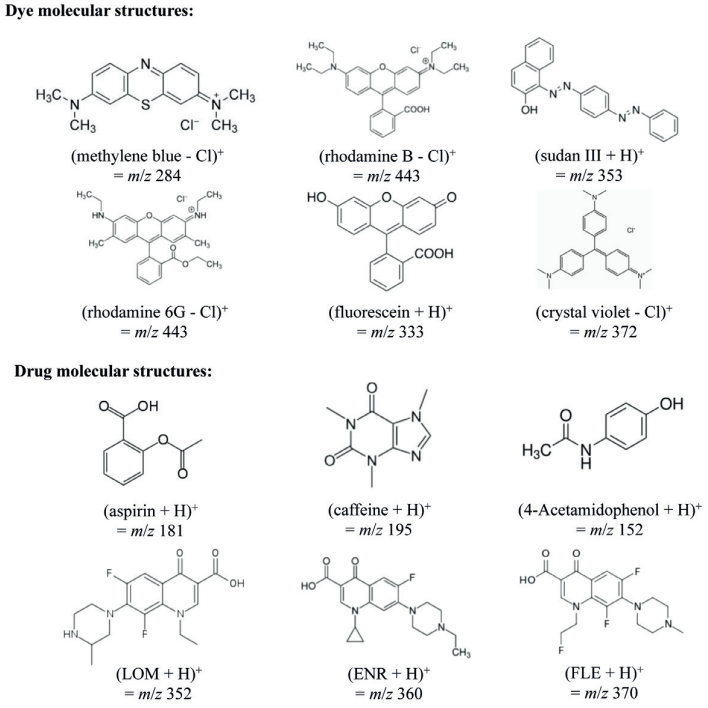

Figure 2.3. Molecular structures of the used six dyes and six drugs. LOM: lomefloxacin; ENR: enrofloxacin; FLE: fleroxacin.

Stock solutions with different concentrations of fluorescein were prepared. 1 μL of each was spotted on a HPRP C_{18} plate and then developed by the mobile phase described above to form final sample spots. The fluorescein spot dried from 1 μL of 30 μM solution could still be easily detected by ESTASI-MS with the signal-to-noise ratio (S/N) of about 12, Figure 2.2(b). The spot diameter was around 5 mm, while the extraction area was about 250 μm in diameter. Accordingly, the fluorescein consumption amount was estimated to be $\leq$75

fmole, indicating that the HPRP C_{18} TLC-ESTASI-MS system is suitable for the analyses of trace analytes.

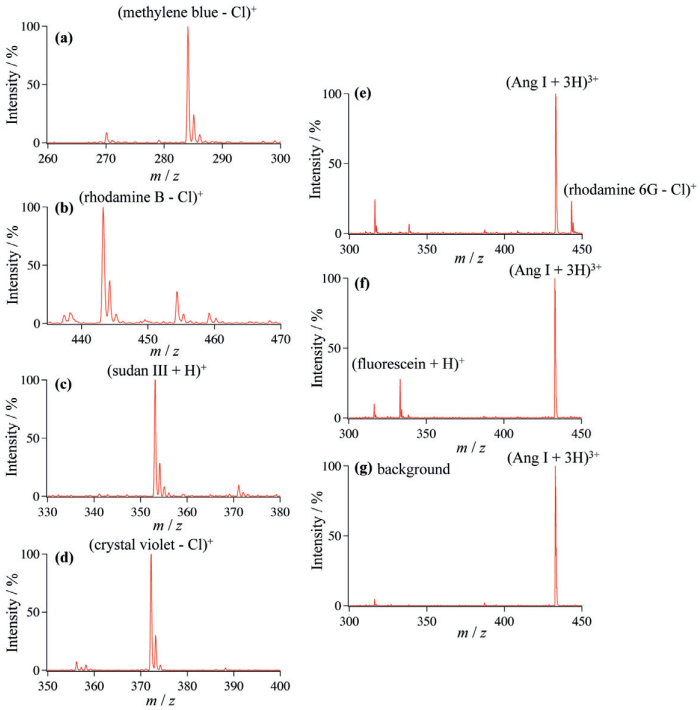

Figure 2.4. (a), **(b)**, **(c)** and **(d)** individual ESTASI-MS spectra of methylene blue (1.7 nmole), rhodamine B (1.1 nmole), sudan III (1.4 nmole) and crystal violet (1.3 nmole), respectively. **(e)**, **(f)** and **(g)** mass spectra obtained at x =7.5 mm and y =3 mm, x =4.5 mm and y =4 mm, x =5.5 mm and y =7 mm, respectively, of Figure 2.6. $(Dye + H)^+$: singly protonated dye; $(Dye - Cl)^+$: dechlorinated dye; $(Ang\ I + 3H)^{3+}$: triply protonated Ang I.

Rhodamine B, rhodamine 6G, sudan III, methylene blue and crystal violet can also be analyzed in the same way on the HPRP C_{18} plate by ESTASI-MS, as shown in Figure 2.3 and 2.4, indicating that the method is universal to a wide range of molecules with different chemical properties and polarities.

2.3.2. ESTASI line-scan and 2D imaging of sample spots separated by HPRP C_{18} plates

Based on the characterization of TLC spots by ESTASI-MS, line scan and 2D imaging of the spots were performed, which could be useful in discerning slightly overlapping spots or the analytes not readily visible on the plate. A dye mixture containing methylene blue (1.7 nmole), rhodamine 6G (1 nmole) and fluorescein (1.5 nmole) was

separated by a HPRP C_{18} plate. The obtained dye spots were subjected to line scan and 2D imaging by ESTASI-MS. The extraction solution of 3 μM Ang I in 1% acetic acid, 75% methanol and 24% water was delivered at 1 μL/min. In the line scan, the motored travel stage moved with the step size of 100 μm, the translation rate of 5 mm/s and the delay time of 1 s to bring different regions of the TLC plate to the wetting capillary for analyses. MS signals were recorded, and the ion current (IC) ratio between target molecule and internal standard was calculated and normalized as shown in Figure 2.5 for quantification.

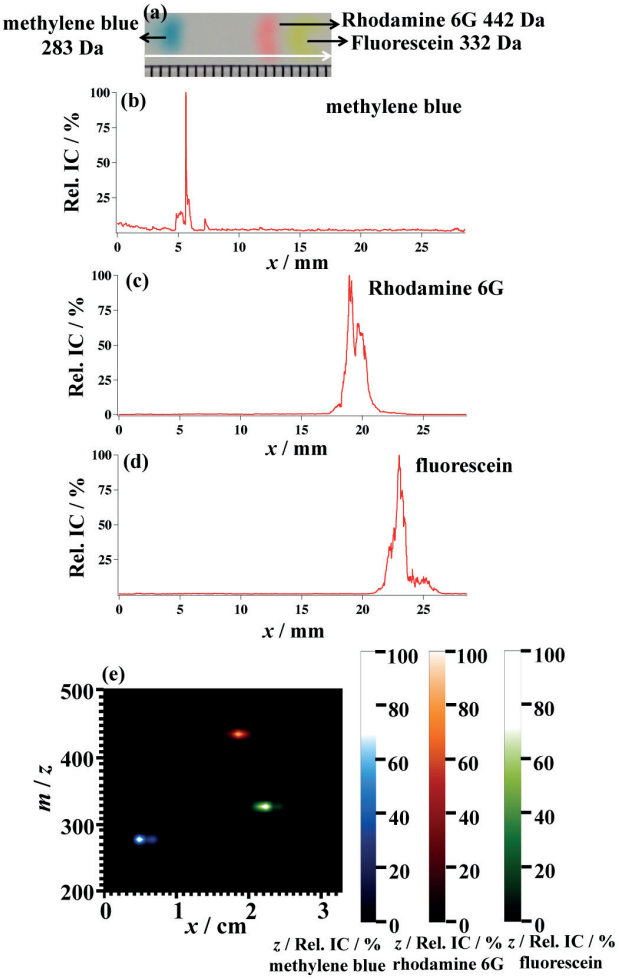

Figure 2.5. ESTASI-MS line scan of a dye mixture separated on a HPRP C_{18} plate. The dye mixture contains methylene blue (1.7 nmole), rhodamine 6G (1 nmole) and fluorescein (1.5 nmole). **(a)** Optical image of the dried samples. **(b)**, **(c)** and **(d)** normalized relative ion current (Rel. IC/%) chromatography of methylene blue, rhodamine 6G and fluorescein, respectively. **(e)** 3D TLC-ESTASI MS map of the three dyes. Rel. IC of each dye was calculated by dividing the IC of singly protonated sample molecule by that of the triply protonated Ang I, and then normalized, respectively.

Figure 2.5(a)-(d) showed the optical image of the development lane containing methylene blue, rhodamine 6G and fluorescein spots, and the IC chromatography of each dye from ESTASI-MS line-scan. The white arrow on the optical image indicated the TLC developing direction, which was also the line-scan direction. The line scan crossed the centre of the TLC spots. Although the amount of each dye was almost the same in the mixture, the mass spectra signals varied a lot because of the different extraction and ionization efficiencies of the samples. Comparing Figure 2.5(a) with Figure 2.5(b), (c) and (d), the ESTASI-MS line-scan showed the chromatography quite close to the optical image, but still with the following differences. The IC bandwidth of fluorescein in Figure 2.5(d) was larger than that of the visual fluorescein spot in Figure 2.5(a). From Figure 2.5(c) and (d), there was a small overlap between rhodamine 6G and fluorescein spots, which could not be discerned visually from the optical image. The resolution of chromatographic bands in TLC was further considered to evaluate the TLC-ESTASI-MS, which is defined as the distance between the band centres divided by the average width of the bands.[12] The calculated TLC resolutions were 5.52 and 5.38 for the separation of methylene blue and rhodamine 6G, and 1.60 and 1.20 for the separation of rhodamine 6G and fluorescein, based on the optical image and ESTASI-MS, respectively. On one hand, the difference between the IC chromatography and the optical image can stem from the limited spatial resolution of ESTASI-MS, which is regulated by the wetting capillary size, and the step size. On the other hand, the optical image could hinder some details of the sample spots when their surface concentration is too low to give a colour strong enough to see, which could still be revealed by ESTASI-MS.

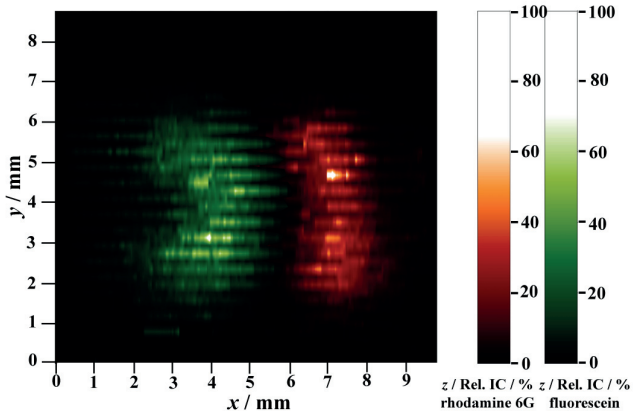

Figure 2.6. 2D TLC-ESTASI-MSI of rhodamine 6G and fluorescein spots in Figure 2.5(a). Rel. IC/% of each dye was plotted with respect to the position on the TLC plate and represented individually as the z-axis in a form of green (fluorescein) or red (rhodamine 6G) colour gradient.

The main advantages of MS scan of TLC plates compared with any spectroscopy detection method are the direct characterization of analytes and the possibility to differentiate in *m*/*z* the analytes not well separated by TLC. For this purpose, a concept of 3D TLC-ESTASI-MS map is shown here, with the *x*-axis representing the position of the sample spot on the scanned lane, the *y*-axis representing the *m*/*z* ratio and the *z*-axis in colour gradient representing the surface density. Figure 2.5(e) showed the 3D TLC-ESTASI-MS map reconstructed from the line scan MS data. There is a small degree of overlap on the *x*-axis between fluorescein and rhodamine 6G spots as already found in Figure 2.5(c) and (d), while the spots are well separated on the 3D map by *m*/*z* that brings a great value to the TLC analyses of mixtures.

2D ESTASI-MSI was further performed on the same rhodamine 6G and fluorescein bands on the TLC plate in Figure 2.5(a) with a protocol described in detail in a recent publication.[7] The same extraction solvent was used, and the motored travel stage was moved in both *x* and *y* directions with the step size of 200 μm, the translation rate of 5 mm/s and the delay time of 1s to accomplish the 2D scan. Normalized relative IC of each dye was calculated and plotted versus the position on the TLC plate to form a 2D MS image of the dye spots, where a more bright colour means a more intensive signal of the corresponding sample on mass spectrum, shown as Figure 2.6. The plotted image of the two dye spots by TLC-ESTASI-MSI was similar to the optical image. Before reaching the sample spots, only the 3 protonated Ang I was observed on the mass spectra in Figure 2.4(g) while both 3 protonated Ang I and dye ions were observed when ESTASI-MS was performed on the corresponding dye spot, in Figure 2.4(e) and (f). Considering that the spots had already been used for line scan before the 2D imaging, the ESTASI-MS consumed only small amount of samples for each analysis, making it possible to reanalyse the plate several times. The good correspondence between Figure 2.5(a) and 2.6 demonstrated that 2D ESTASI-MSI is a powerful method to reveal completely and accurately the spatial distribution of the analytes separated by TLC. Compared with the images obtained previously,[7] the image resolution and integrity have been improved significantly, which could be contributed to the hydrophobic-hydrophobic or hydrophilic-hydrophilic interactions between samples and TLC substrates leading to a reduced tailing effect.

2.3.3. Quantification of rhodamine 6G on HPRP C_{18} plates

Quantitative capability of TLC-ESTASI-MS was also explored by performing uniform ESTASI line-scans across the centre of five sample bands developed on a HPRP C_{18} plate, each band containing 1 μL 0.01 mg/mL, 0.05 mg/mL, 0.1 mg/mL, 0.15 mg/mL and 0.2 mg/mL rhodamine 6G respectively. 3 μM Ang I in 1% acetic acid, 75% methanol and 24% water was delivered at 1 μL/min to extract sample and act as internal standard for the quantitation. Three parallel tests were performed to determine the relative standard deviation (RSD). The integrated peak areas from the extracted relative ion current chromatography of rhodamine 6G to Ang I, as shown in Figure 2.7(b)-(f), were plotted with respect to rhodamine 6G solution concentrations to obtain the calibration curve as $y = 30.666\ x - 0.105$, in Figure 2.7(a).

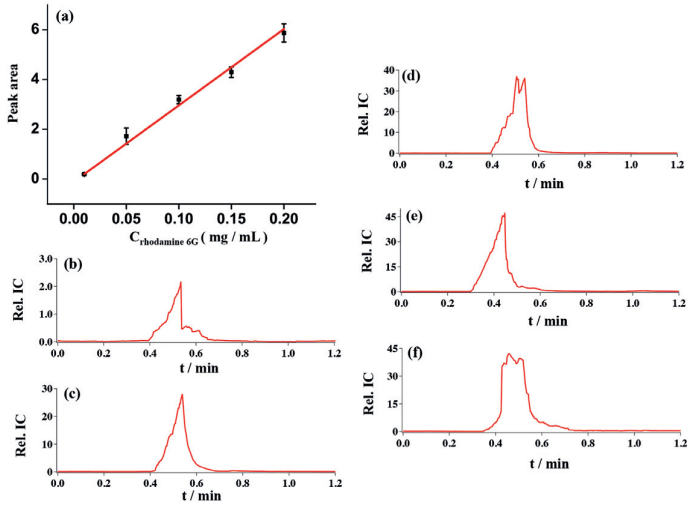

Figure 2.7. (a) Calibration plot of peak area of Rel. IC chromatography of sample spots versus the rhodamine solution concentration. The error bar was obtained from three parallel tests to show the standard deviation. **(b)**, **(c)**, **(d)**, **(e)** and **(f)** Rel. IC chromatography of dried spots on HPRP C_{18} plates from 1 μL rhodamine 6G solution at concentration of 0.01 mg/mL, 0.05 mg/mL, 0.1 mg/ml, 0.15 mg/mL and 0.2 mg/mL, respectively. Rel. IC was calculated by dividing the IC of singly protonated rhodamine 6G by that of triply protonated Ang I.

Two calibration curves employing different ranges, 0.01 μg/mL-0.1 μg/mL and 0.1 μg/mL-10 μg/mL, were used to determine the recovery rate of rhodamine 6G from the HPRP C_{18} plate. Rhodamine 6G solutions with different concentration were mixed with internal standard (3 μM Ang I) in 1% acetic acid, 75% methanol and 24% water and delivered by the wetting capillary at 1 μL/min for ESTASI-MS analyses. The MS signal was recorded for 3

min. The IC ratio between rhodamine 6G and Ang I was calculated, averaged and plotted with respect to rhodamine 6G solution concentration to make the two calibration curves with different ranges, respectively, as shown in Figure 2.7(a) and (b). The error bar was obtained from three parallel tests to show the relative standard deviation.

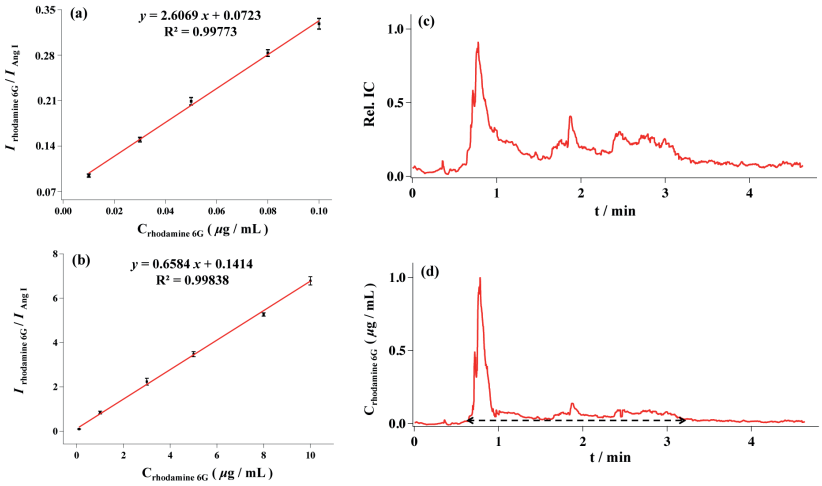

Figure 2.8. (a) and **(b)** calibration plot of Rel. IC intensity of rhodamine 6G to Ang I versus rhodamine 6G concentration in the wetting capillary among the 0.01 μg/mL-0.1 μg/mL and 0.1 μg/mL-10 μg/mL ranges, respectively. **(c)** Rel. IC chromatography of rhodamine 6G recovered from dried sample spot of 1 μL of 10 μg/mL rhodamine 6G on a HPRP C_{18} plate. **(d)** concentration chromatography of rhodamine 6G obtained by transforming the Rel. IC intensity into the concentration with the two calibration curves respectively.

Then, 3 μM Ang I in 1% acetic acid, 75% methanol and 24% water was delivered by the wetting capillary at 1 μL/min to extract sample continuously from the central point of a developed band of 1 μL, 10 μg/mL rhodamine 6G on a HPRP C_{18} plate for ESTASI analyses. The MS recording was kept until the signal of rhodamine 6G became rather weak to be around the background level. Rel. IC chromatography of rhodamine 6G, in Figure 2.8(c), was obtained by dividing the IC of singly protonated sample molecule by that of the triply protonated Ang I and transformed to be concentration chromatography with the two calibration curves, respectively, as in Figure 2.8(d). Considering the flow rate was at 1 μL/min, the integrated peak area of the concentration chromatography was calculated, which indicated the recovered amount of rhodamine 6G from the HPRP C_{18} plate. The theoretical amount of rhodamine 6G at the sampling point could be obtained by measuring the diameter of the sampling point, which was about 360 μm. By dividing the peak area of the

concentration chromatography by the theoretical amount of rhodamine 6G, the mean recovery rate was measured as 78 ± 3.5% based on three parallel tests.

2.3.4. Surface modification of normal phase silica TLC plates for ESTASI-MS analyses

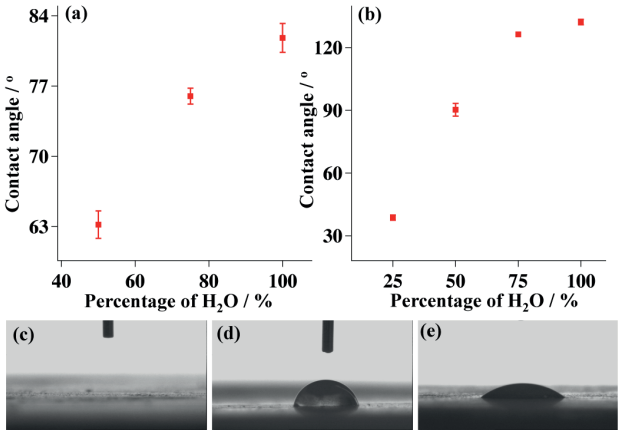

Figure 2.9. Contact angles of solvents on TLC plates. **(a)** Contact angles of the solvents containing 50%, 75% and 99% H_2O respectively on the silane-modified silica gel TLC plate. **(b)** Contact angles of the solvents containing 25%, 50%, 75% and 99% H_2O respectively on the HPTLC RP C_{18} plate. The error bar was obtained from three parallel tests to show the standard deviation. **(c)** Photograph of 75% H_2O on the silica plate. **(d)** Photograph of 75% H_2O on the silane-modified silica plate. **(e)** Photograph of 25% H_2O on the HPTLC RP C_{18} plate.

Solvent mixtures containing methanol, water and acetic acid are commonly used in most ESI-based MS systems. However, both water and methanol can be absorbed quickly by normal phase silica gel TLC plates without forming small droplets for the sample extraction of ESTASI-MS analysis. Furthermore, the absorbed liquid can induce sample developing inside the TLC plate. Therefore, normal phase and any water-wettable plates are very difficult to be directly analyzed by liquid-extraction based MS analysis methods. Surface modification of the plates is normally required before MS analysis. For example, silicone oil was sprayed onto the normal phase silica gel plates and HPTLC cellulose plates to form hydrophobic surfaces to enable the MS analysis by a liquid microjunction surface sampling probe.[34]

In this work, we use chlorotrimethylsilane vapour to modify silica gel TLC plates after sample separation to form highly hydrophobic surfaces for ESTASI-MS analyses. Chlorotrimethylsilane is volatile and reactive toward silicon hydroxyl groups, resulting in the

replacement of the hydrophilic hydroxyl groups by hydrophobic silane. Compared to other modification procedures, such as physical cover with paraffin or silicone oil,[35] the vapour reaction of chlorotrimethylsilane with silica gel can provide a surface homogeneously modified in a thin layer, and without the coverage of the sample molecules that can lead to lower sensitivity during MS analysis. In addition, the silane does not influence MS analysis as it is chemically immobilized on the stationary phase of TLC plates that cannot be removed during ESTASI.

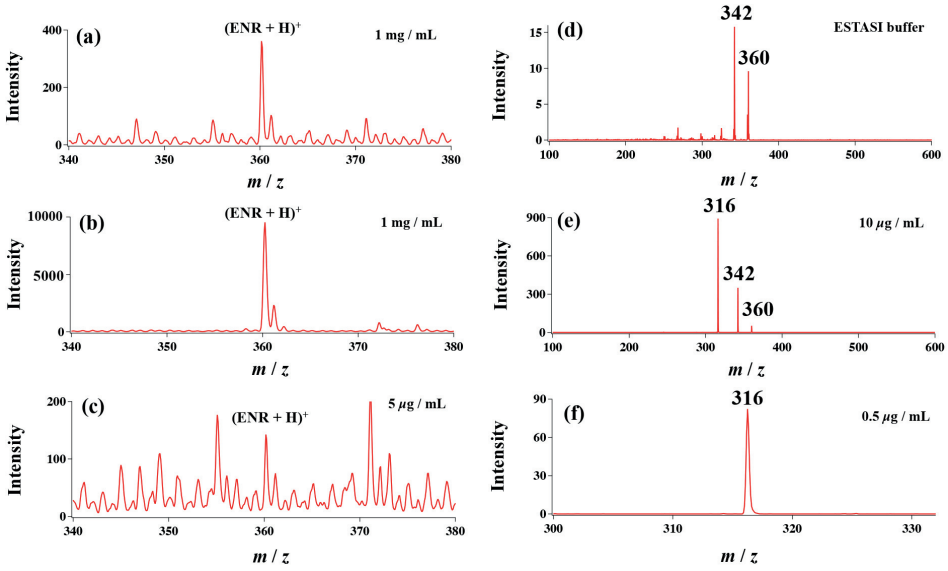

Figure 2.10. ESTASI-MS spectra of sample spots from: **(a)** 1 μL, 1 mg/mL ENR aqueous solution developed on a silica gel TLC plate, **(b)** 1 μL, 1 mg/mL ENR aqueous solution developed on a silica gel TLC plate with silane modification, and **(c)** 1 μL 5 μg/mL ENR solution developed on a silica gel TLC plate with silane modification. **(d)** ESTASI extraction solvent composed of 75% water, 24% methanol and 1% acetic acid, **(e)** 1 μL, 10 μg/mL ENR aqueous solution developed on a silica gel TLC plate with silane modification. **(f)** ESTASI-MS/MS SRM spectrum of a sample spot from 1 μL, 0.5 μg/mL ENR aqueous solution developed on a silica gel TLC plate with silane modification. The fragment at *m/z* 316 was selected as the diagnostic ion of ENR.

To evaluate the modification method, the contact angles of solvents containing different percentages of methanol and water were measured on the modified silica gel plate, the unmodified silica gel plate and the HPTLC RP C_{18} plate. As shown in Figure 2.9(a), the contact angles of the solvents composed of 99%, 75% and 50% water in methanol with 1% acetic acid on the silane modified silica gel plate was measured as 84°, 77° and 63°, respectively. When the water concentration was 25%, the solvent could no longer form a stable droplet. In contrast, on the silica gel plate without silane modifications, even the

solvent containing 75% of water cannot form a stable droplet, Figure 2.9(c). When the HPTLC RP C_{18} plate was employed, the contact angles for the solvents of 99%, 75%, 50% and 25% water in methanol with 1% acetic acid were measured as 135°, 126°, 90° and 39° respectively, in Figure 2.9(b). Therefore, although the silane-modified silica TLC plate is not as hydrophobic as the HPRP C_{18} plate, it is much more hydrophobic than the unmodified one and may be used in many liquid extraction based MS analysis methods. Because the affinity between the silica gel plate and samples is mainly based on hydrophilic-hydrophilic interactions, a higher concentration of water in the extraction solvent could benefit ESTASI-MS analysis. However, the surface tension of the solvent also increases with the amount of water, making the ESTASI itself more difficult.[6] Therefore, the solvent containing 75% water, 24% methanol and 1% acetic acid was used as the extraction solvent when analyzing the silica TLC plate.

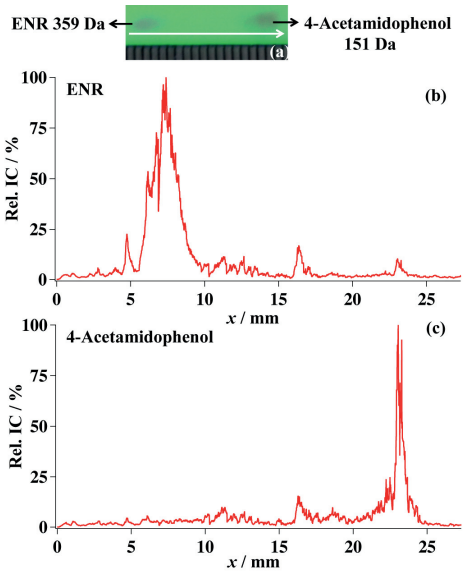

Figure 2.11. ESTASI-MS line-scan of a drug mixture containing ENR (1.4 nmole) and 4-acetamidophenol (3.3 nmole) on a silica gel TLC plate with silane modification. **(a)** an optical image of the dried sample spots on the TLC plate. **(b)** and **(c)** Rel. IC/% chromatography of ENR and 4-acetamidophenol, respectively.

To demonstrate the effect of the silane modification in ESTASI-MS analysis, enrofloxacin (ENR), an antibiotic, was developed in parallel on two silica TLC plates by the mobile solution of methanol, 25% aqueous ammonia, ethyl acetate and acetonitrile (1:1:2:1 by volume), and then analyzed by ESTASI-MS, one with silane modification and the other not. In Figure 2.10(a), only a weak MS peak with the S/N of about 10 was observed for ENR

at high amount (2.7 nmole) on the plate without modification under the extraction solvent flow rate of 2 μL/min. The high flow rate was used here to form temporarily a droplet for ESTASI-MS analysis under the strong absorption of the solvent by the TLC plate, which would induce quick diffusion of samples inside the TLC plate from the extraction droplet region. Therefore, only the spot of very high amount of ENR can be detected by ESTASI-MS. When the sample amount was lowered to 0.27 nmole, no signal of ENR was obtained from the silica gel TLC plate under optimized experimental conditions. In comparison, a much stronger MS peak of ENR with the S/N larger than 100 was obtained from the developed sample spot containing 2.7 nmole of ENR, when the silane modification was performed after TLC separation and before MS analysis, as shown in Figure 2.10(b). Even when the sample amount was lowered to 14 pmole, the ENR was still detectable from the TLC plate after silane modification with the S/N of about 3 in Figure 2.10(c). It should be mentioned that the flow rate was lowered to 1 μL/min during the analyses of the silane-modified silica gel TLC plate, since the plate cannot absorb the solvent any more. To confirm the signal at *m*/*z* 360 with quite low S/N comes from singly protonated ENR instead of noise signal, ESTASI-MS fragmentation of precursor ions at *m*/*z* 360 induced by CID was performed. A strong fragment ion at *m*/*z* 316 was obtained from a dried spot of 1 μL, 10 μg/mL ENR on a silica plate with silane modification, which was not observed for the extraction solvent composed of 75% water, 24% methanol and 1% acetic acid, in Figure 2.10(d) and (e). Therefore, fragment ion at *m*/*z* 316, which comes from the reduction of H_2O and CO_2 groups from ENR molecule, was selected as the diagnostic ion of ENR. ESTASI-MS/MS SRM of the diagnostic ion was further performed to evaluate the sensitivity of ENR analysis from the modified silica plate, in Figure 2.10(f). The diagnostic ion was still easily detectable with quite high S/N by ESTASI-MS/MS SRM even when the sample amount was lowed to 1.4 pmole in Figure 2.10(f). The sample amount could be further lowered until the S/N value of the diagnostic ion was around 3 (data not shown), indicating that ESTASI-MS/MS SRM can improve analysis specificity and sensitivity greatly from the modified silica plate. In the same way, we demonstrated that 4-acetamidophenol, aspirin, caffeine, lomefloxacin and fleroxacin can also been detected by ESTASI-MS from the silica gel TLC plate after silane modification, illustrating the universal applicability to a wide range of samples, in Figure 2.3 and 2.12. It is worth mentioning that ESTASI-MS under negative mode provides lower LOD for aspirin (0.42 μg/mL) compared with that (84 μg/mL) under positive mode (data not shown), which may be due to the susceptibility of aspirin molecule to

be negatively charged and further confirmed the alternative sprays of both cations and anions in ESTASI-MS and its advantage in the efficient analyses of samples with weak electronegativities.

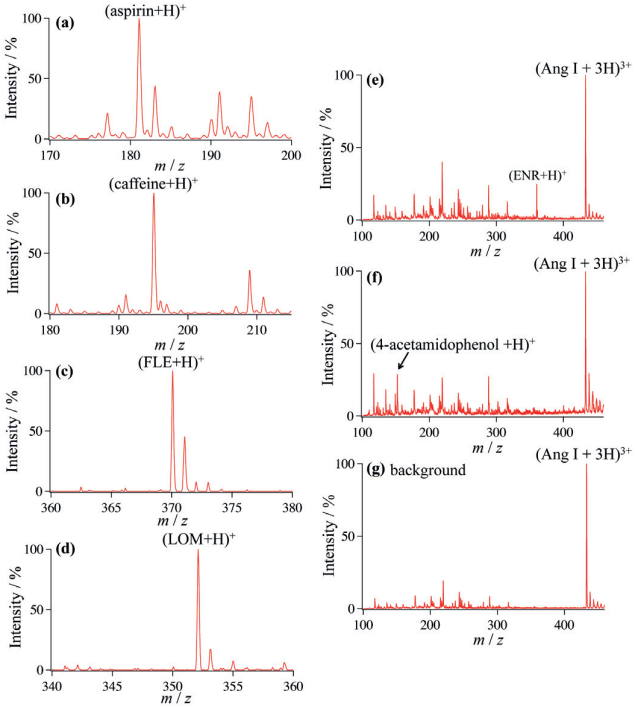

Figure 2.12. (a), **(b)**, **(c)** and **(d)** individual ESTASI-MS spectra of aspirin (2.7 nmole), caffeine (2.6 nmole), FLE (1.3 nmole) and LOM (1.4 nmole), respectively. **(e)**, **(f)** and **(g)** mass spectra obtained at x =7 mm, x =23 mm and x =14 mm, respectively, of Figure 2.11. (Drug + H)$^+$: singly protonated drug; (Ang I + 3H)$^{3+}$: triply protonated Ang I.

The line scan of sample spots on the silica gel TLC plate after silane modification can also be performed with ESTASI-MS. The drug mixture containing ENR (1.4 nmole) and 4-acetamidophenol (3.3 nmole) was separated by a silica plate. The obtained plate was then modified by silane before the ESTASI-MS line scan. The line scan was performed along the centre lane of the development bands in the developing direction indicated with a white arrow in Figure 2.11(a). The extraction solution was 3 μM Ang I in 1% acetic acid, 75% water and 24% methanol, injected at the flow rate of 1 μL/min. The motored travel stage moved with the step size of 100 μm, the translation rate of 5 mm/s and the delay time of 1 s. The normalized relative IC of ENR and 4-acetamidophenol was calculated and plotted to form the IC chromatography, as shown in Figure 2.11(b) and (c), which is in good correspondence with the optical TLC image. The TLC resolution for the separation of ENR and 4-

acetamidophenol was calculated as 4.0 from the optical image and 3.8 from the ESTASI-MS chromatography. Typical mass spectra in Figure 2.12(e), (f) and (g) presented the existence of the two drugs at different positions on the development band, or the background signal.

2.4. Conclusions

In this study, we have developed a direct coupling of TLC with ESTASI-MS for *in-situ* analyses under ambient conditions with no sample pretreatment. Dried samples separated by high performance reverse phase TLC plates can be analyzed directly by ESTASI-MS. We also proposed an effective, simple surface modification process using chlorotrimethylsilane to modify hydrophilic silica gel. In a line scan mode, both chemical identification and TLC separation information can be obtained from a number of mass spectra to generate a 3D TLC-MS map. The distribution image of compounds on TLC plates can also be accomplished with a good spatial resolution in the 2D scan mode. The method was found to be appropriate to the 12 tested samples. TLC-ESTASI-MS can be readily applied in many other chemical and biochemical analyses.

2.5. References

(1) Z. Takats, J. M. Wiseman, B. Gologan and R. G. Cooks, *Science*, 2004, 306, 471-473.

(2) J. Pol, V. Vidova, G. Kruppa, V. Kobliha, P. Novak, K. Lemr, T. Kotiaho, R. Kostiainen, V. Havlicek and M. Volny, *Anal. Chem.*, 2009, 81, 8479-8487.

(3) J. J. Coon, K. J. McHale and W. W. Harrison, *Rapid Commun. Mass Spectrom.*, 2002, 16, 681-685.

(4) Y. Y. Liu, X. X. Ma, Z. Q. Lin, M. J. He, G. J. Han, C. D. Yang, Z. Xing, S. C. Zhang and X. R. Zhang, *Angew Chem Int Edit*, 2010, 49, 4435-4437.

(5) G. J. Van Berkel, V. Kertesz, K. A. Koeplinger, M. Vavrek and A. N. T. Kong, *J. Mass Spectrom.*, 2008, 43, 500-508.

(6) L. Qiao, R. Sartor, N. Gasilova, Y. Lu, E. Tobolkina, B. Liu and H. H. Girault, *Anal. Chem.*, 2012, 84, 7422-7430.

(7) L. Qiao, E. Tobolkina, A. Lesch, A. Bondarenko, X. Q. Zhong, B. H. Liu, H. Pick, H. Vogel and H. H. Girault, *Anal. Chem.*, 2014, 86, 2033-2041.

(8) J. Sherma, *Anal. Chem.*, 2000, 72, 9R-25R.

(9) J. Sherma, *Anal. Chem.*, 2002, 74, 2653-2662.

(10) H. York, W. Funk, W. Fischer and H. Wimmer, eds., *Thin-Layer Chromatography*, VCH, New York, 1990.

(11) F. Geiss, ed., *Fundamentals of Thin Layer Chromatography (Planar Chromatography)*, Huethig, Heidelberg, 1987.

(12) B. Fried and J. Sherma, eds., *Thin-Layer Chromatography*, Marcel Dekker, New York, 1999.

(13) S. C. Cheng, M. Z. Huang and J. Shiea, *J. Chromatogr. A*, 2011, 1218, 2700-2711.

(14) G. Morlock and W. Schwack, *Trac-Trends Anal. Chem.*, 2010, 29, 1157-1171.

(15) G. C. Didonato and K. L. Busch, *Anal. Chem.*, 1986, 58, 3231-3232.

(16) T. T. Chang, J. O. Lay and R. J. Francel, *Anal. Chem.*, 1984, 56, 109-111.

(17) A. J. Kubis, K. V. Somayajula, A. G. Sharkey and D. M. Hercules, *Anal. Chem.*, 1989, 61, 2516-2523.

(18) A. I. Gusev, A. Proctor, Y. I. Rabinovich and D. M. Hercules, *Anal. Chem.*, 1995, 67, 1805-1814.

(19) Y. C. Chen, J. Shiea and J. Sunner, *J. Chromatogr. A*, 1998, 826, 77-86.

(20) C. C. Chen, Y. L. Yang, C. L. Ou, C. H. Chou, C. C. Liaw and P. C. Lin, *Analyst*, 2013, 138, 1379-1385.

(21) G. J. Van Berkel, A. D. Sanchez and J. M. E. Quirke, *Anal. Chem.*, 2002, 74, 6216-6223.

(22) H. Luftmann, *Anal. Bioanal. Chem.*, 2004, 378, 964-968.

(23) S. Y. Lin, M. Z. Huang, H. C. Chang and J. Shiea, *Anal. Chem.*, 2007, 79, 8789-8795.

(24) G. J. Van Berkel, M. J. Ford and M. A. Deibel, *Anal. Chem.*, 2005, 77, 1207-1215.

(25) R. Haddad, R. Sparrapan and M. N. Eberlin, *Rapid Commun. Mass Spectrom.*, 2006, 20, 2901-2905.

(26) M. Himmelsbach, M. Waser and C. Klampfl, *Anal. Bioanal. Chem.*, 2014, 406, 3647-3656.

(27) P. J. Roach, J. Laskin and A. Laskin, *Analyst*, 2010, 135, 2233-2236.

(28) K. G. Asano, M. J. Ford, B. A. Tomkins and G. J. Van Berkel, *Rapid Commun. Mass Spectrom.*, 2005, 19, 2305-2312.

(29) J. L. Zhang, Z. G. Zhou, J. W. Yang, W. Zhang, Y. Bai and H. W. Liu, *Anal. Chem.*, 2012, 84, 1496-1503.

(30) M. Resano, E. G. Ruiz, V. G. Mihucz, A. M. Moricz, G. Zaray and F. Vanhaecke, *J. Anal. At. Spectrom.*, 2007, 22, 1158-1162.

(31) J. Chirinos, D. Oropeza, J. Gonzalez, M. Ranaudo and R. E. Russo, *Energy Fuels*, 2013, 27, 2431-2436.

(32) J. Laskin, B. S. Heath, P. J. Roach, L. Cazares and O. J. Semmes, *Anal. Chem.*, 2012, 84, 141-148.

(33) V. L. Dorofeev, A. A. Konovalov, V. Y. Kochin and A. P. Arzamastsev, *Pharm. Chem. J.*, 2004, 38, 510-512.

(34) M. J. Walworth, J. J. Stankovich, G. J. Van Berkel, M. Schulz, S. Minarik, J. Nichols and E. Reich, *Anal. Chem.*, 2011, 83, 591-597.

(35) J. Gasparic, *Adv. Chromatogr. (Boca Raton, FL, U. S.)*, 1992, 31, 153-252.

CHAPTER III.

Electrostatic spray ionization from 384-well microtiter plates for mass spectrometry analysis based enzyme assay and drug metabolism screening

*Based on L. Qiao and X. Zhong et al. Anal. Chem., **2017**, 89, 5983-5990.*

Abstract

We have realized the direct ionization of samples from wells of microtiter plates under atmospheric conditions for mass spectrometry analysis without any liquid delivery system or any additional interface. The microtiter plate is a commercially available 384-well plate without any modification, working as a container and an emitter for electrostatic spray ionization of analytes. The approach provides high throughput for the large batches of reactions and both the qualitative and quantitative analysis of a single compound or mixture. The limits of detection in small drug molecules, peptides and proteins are similar in comparison with standard direct infusion electrospray ionization. The analysis time per well is only seconds. These analytical merits benefit many microtiter plate-based studies such as combinatorial chemistry and high throughput screening in enzyme assay or drug metabolism. Herein, we illustrate the application in enzyme assay using tyrosine oxidation catalyzed by tyrosinase in the presence or absence of inhibitors. The potential application in drug development is also demonstrated with cytochrome P450-catalyzed metabolic reactions of two drugs in microtiter plates followed with direct ESTASI-MS/MS based characterization of the metabolism products.

3.1. Introduction

Microtiter plates are used as a standard tool in analytical chemistry, clinical assay, and life science study. Because of the large number of wells per plate, it is widely used for combinatorial chemistry and high throughput screening. Coupled with various chemical analysis techniques, such as ultraviolet-visible spectroscopy, fluorescence spectroscopy, liquid chromatography, capillary electrophoresis, and mass spectrometry, it is extensively used for enzyme-linked immunosorbent assays,[1] enzyme activity or inhibition assays,[2,3] and drug metabolism studies.[4,5] Compared to spectroscopy techniques, MS can offer direct qualification and quantification of a wide range of analytes, providing accurate and specific characterization to avoid false positive or negative results, thereby is highly suitable for the studies of enzymatic assays, inhibitor screening assays, and drug metabolism assays.[6-10]

MS is normally coupled with microtiter plates with the help of liquid delivery robots or autosamplers from various suppliers. To improve analysis throughput and speed, a multi-probe autosampler was developed by Kassel *et al.*[11] and thereafter modified by Morand *et al.* to finish the analysis of a 96-well plate in 5 minutes.[12] The 96-well plate could also be modified with disposable micropipette tips as emitters for solvent assisted inlet ionization (SAII).[13] More details could be found in § 1.2.2.

Herein, we have realized direct ionization of liquid samples from an unmodified microtiter plate, where the plate itself works as both containers and emitters for ionization. It is the first method of direct ionization from a microtiter plate without any liquid delivery interface and any modification to the plate. The ionization is achieved using the recently developed electrostatic spray ionization (ESTASI) method.[14-16] The microtiter plate is simply placed between the ion transfer capillary of a mass spectrometer and the electrode connected to a pulsed high voltage (HV) power source. When the pulsed HV is applied, ESTASI occurs to generate alternative spray of cations and anions for MS analysis, as shown in § 1.1.4.[14]

The performance of the ionization for qualification and quantification was evaluated. Different types of samples, including small drug molecules, amino acids, peptides and proteins could be detected with limits of detection (LOD) similar as standard direct infusion ESI. Quantitative analysis was also realized by adding a proper internal standard into the tested sample. Because the microtiter plate is disposable and no liquid delivery is needed, washing steps can be avoided to shorten analysis time and eliminate cross contamination between samples. The analysis time per well is only seconds. With the advantages, the

technique is highly suitable for fast analysis of a single compound or mixture. In addition, it holds potential applications in high throughput assays, such as enzyme inhibition screening and drug metabolism studies. To illustrate these, tyrosinase-catalyzed oxidation of tyrosine with or without inhibitors and the *in-vitro* drug metabolism by cytochrome P450 in microtiter plates were directly read by ESTASI-MS.

3.2. Experimental section

3.2.1. Chemicals and materials

Ciprofloxacin (CIP), enrofloxacin (ENR), lomefloxacin (LOM) and fleroxacin (FLE) of analytical reagent grade were purchased from TCI Deutschland GmbH (Eschborn, Germany). Angiotensin I (Ang I, 98%) was obtained from Bachem (Bubendorf, Switzerland). Cytochrome c (Cyt c, horse heart, 95%), magnesium chloride hexahydrate (98%), sodium phosphate dibasic dodecahydrate (99%), sodium phosphate monobasic (99%) and sodium chloride (99.5%) were obtained from Fluka (St. Gallen, Switzerland). Methanol (99.9%, HPLC grade) was purchased from Applichem GmbH (Darmstadt, Germany). Acetic acid (HAc, 99%) was obtained from Merck (Zug, Switzerland). Ammonium bicarbonate (NH_4HCO_3, 99%,), calcium chloride (93%), tyrosinase (from mushroom, lyophilized powder, ≥1000 unit/mg solid), L-tyrosine (99%), reduced nicotinamide adenine dinucleotide phosphate (NADPH), nifedipine (≥98%, powder), testosterone (≥98%, powder) and cytochrome P450 CYP3A4 isozyme microsomes expressed in baculovirus-infected cells were purchased from Sigma-Aldrich (St. Gallen, Switzerland). Potassium chloride (99%) was obtained from Roth AG (Arlesheim, Switzerland). Cupferron (for analysis) was purchased from Fisher Scientific (Waltham, MA, USA). All these reagents and materials were used as received without further purification. Deionized water (18.2 MΩ cm) was obtained from an ultra-pure water system (Milli-Q 185 Plus, Millipore) and used for all experiments. MicroAmp® optical 384-well reaction plate with barcode was purchased from life technologies (Carlsbad, CA, USA).

3.2.2. Tyrosine oxidation and drug metabolism

Wells of a 384-well microtiter plate were filled with 8 μL of phosphate buffered saline (PBS, 2 mM, pH 7.4), 1 μL of tyrosinase (0.2 mg/mL in 2 mM PBS) and 1 μL of tyrosine (0.5 mg/mL in 2 mM PBS). The detection by ESTASI-MS was directly performed from the

wells at different time intervals to monitor the oxidation results. When enzyme inhibition was studied, 1 μL of ascorbic acid (AA, 1 mg/mL or 0.1 mg/mL in 2 mM PBS) or 1 μL of cupferron (20 mM in 2 mM PBS) was added, followed by the addition of 7 μL of PBS (2 mM), 1 μL of tyrosinase (0.2 mg/mL in 2 mM PBS), and 1 μL of tyrosine (0.5 mg/mL in 2 mM PBS).

For drug metabolism, 80 μg/mL of nifedipine or 40 μg/mL of testosterone was prepared in 10 mM NH_4HCO_3 (pH 7.4), respectively. 1 μL of NADPH (50 mg/mL in 10 mM NH_4HCO_3), 1 μL of CYP3A4 (1 μM in 100 mM KH_2PO_4, pH 7.4) and 8 μL of the drug solution were added in multiple wells of a 38-well plate. After being incubated for different periods under room temperature, 9 μL of the reaction solution was discarded and 9 μL of 50% MeOH/49% H_2O/1% acetic acid was added for ESTASI-MS analysis.

3.2.3. ESTASI-MS

ESTASI-MS was performed as described in previous publications,[14,17] and illustrated by Figure 3.1. A 384-well plate was placed on a PET substrate (120 μm thickness), and all together between an electrode and the ion transfer capillary of a linear ion trap mass spectrometer (LTQ Velos, Thermo scientific). The ion transfer capillary was a self-designed "L-shaped" ion transfer capillary instead of the original linear one of the MS instrument in order to place the microtiter plate horizontally for MS analysis. The plate was moved in x, y, z directions by travel translation stages to bring different wells under the ion transfer capillary. A pulsed high voltage (HV, from 0 V to 8 kV, frequency 20 Hz) was generated by amplifying voltage square wave pulses (0 to 8 V) with a high voltage amplifier (10HVA24-P1, HVP High Voltage Products GmbH, Martinsried/Planegg, Germany), and applied on the electrode to induce ESTASI against the ion transfer capillary that was set at 275 °C and always grounded. The ESI voltage of the internal power of the MS instrument was always set as 0 and all the source gas flow rates were set at 0. Enhanced ion trap scanning rate of 10,000 m/z per second was used. The other parameters of the MS instrument were optimized for the selected analytes. All MS analyses were performed under positive scanning mode. For the collision-induced dissociation (CID), full scan mode was performed with normalized collision energy of 30 and isolation width of 1 m/z.

For the sensitivity comparison, the samples were also applied *via* a direct infusion mode with a syringe at the flow rate of 3 μL/min and analyzed with the standard ESI. The

sample spray with the commercial ESI source is from a needle of 500 μm in diameter and assisted with a sheath gas flow of 10 arbitrary units and aux gas flow of 5 arbitrary units. The ESI voltage of the internal power of the MS instrument was always set as 3.7 kV. The temperatures of the heater and the MS inlet capillary were set at 42 °C and 275 °C, respectively. All other parameters of the MS instrument were the same as those for ESTASI analysis.

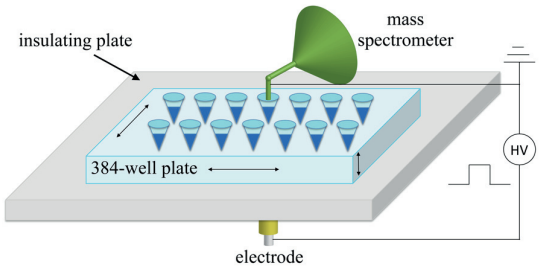

Figure 3.1. Schematic representation of the setup used for ESTASI-MS from a 384-well plate. HV: high voltage, which is a square wave pulsed HV here.

3.3. Results and discussion

3.3.1. 384-well plate ESTASI-MS

According to the previous studies, ESTASI occurs during electrostatic charging/discharging of the capacitors formed by (i) electrode-insulator-electrolyte solution and (ii) electrolyte solution-gas-ion transfer capillary.[14] Charge separation happens inside the electrolyte solution during charging of the capacitors, *e.g.* anions to the part close to the electrode and cations to the part close to the ion transfer capillary when a positive HV is applied on the electrode. When the charge density on the part close to the ion transfer capillary is large enough, electrospray of cations occurs. Afterwards, spray of anions can be induced by simply grounding the electrode to make the electrolyte solution neutral. According to this ionization principle, it is crucial to reach a large charge density to start ESTASI that can be realized either by increasing the charge amount accumulated on the part of the electrolyte solution close to the ion transfer capillary or by reducing the surface area of the region. The charge amount can be increased by increasing the HV, increasing the surface area of the electrode, decreasing the thickness of the insulator, and decreasing the distance from the electrolyte solution to the ion transfer capillary.[14]

When the solution is inside the wells of a microtiter plate, its surface area exposed to the ion transfer capillary is determined by the shape of the well. A typical 96-well plate has normally quasi-cylindrical wells (about 8 mm Ø) with the volume up to 1 mL each, resulting in a large area of sample solution inside exposed to the ion transfer capillary during ESTASI. Indeed, it is very difficult to perform direct ESTASI of samples from a normal 96-well plate. Herein, we chose a commercially available 384-well plate with cone-shaped wells that had the volume of 40 μL each with the diameter of 3 mm at the base of the cone. When 10 μL of sample solution was filled in a well for ESTASI-MS analysis, the liquid exposed to the ion transfer capillary was a disc with a diameter less than 2 mm. The ion transfer capillary probed into the well and kept the distance of 1-2 mm from the sample to avoid sucking the sample solution. As soon as the pulsed HV was applied on the electrode, ESTASI happened to produce ions for MS analysis. During ESTASI, the sample was consumed, resulting in enlarging the distance between the ion transfer capillary and the sample solution. This would decrease the charge amount on the liquid surface, and finally stop ESTASI. Therefore, the 384-well plate should be lifted up during ESTASI until all the sample solution in the well was exhausted. The analysis of many wells was performed with the help of an *x, y, z* translation system.

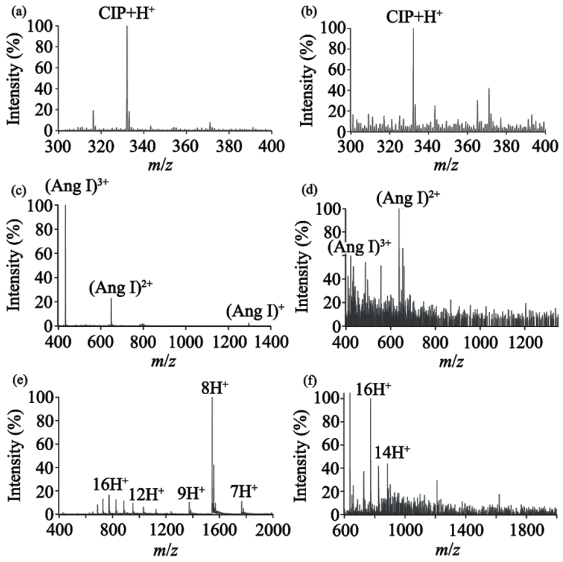

Figure 3.2. Mass spectra obtained by the 384-well plate ESTASI-MS of **(a)** 1.5 μM of CIP, **(b)** 15 nM of CIP, **(c)** 15 μM of Ang I, **(d)** 15 nM of Ang I, **(e)** 10 μM of Cyt c and **(f)** 100 nM of Cyt c. Solution: 50% MeOH/49% H_2O/1% acetic acid. $CIP+H^+$: singly protonated CIP; $(Ang\ I)^{x+}$: Ang I ion with *x* proton(s); XH^+: Cyt c ion with *x* proton(s).

The 384-well plate ESTASI-MS was tested with different samples, including small organic molecules, peptides and proteins. A group of synthetic antibiotics derived from quinolone nalidixic acid, including ciprofloxacin (CIP), enrofloxacin (ENR), lomefloxacin (LOM) and fleroxacin (FLE), were selected as examples of small organic drug molecules. These antibiotics were introduced for the therapeutic treatment of respiratory and urinary infections since the mid-1990s.[18] The extensive use of the antibiotics has led to their accumulation in food, which have potential health hazard for humans.[19] Therefore, it is highly important to develop analytical techniques in the detection of trace amount of the antibiotics. As shown in Figure 3.2(a), an intense peak of the single protonated CIP was obtained from 1.5 μM CIP in 50% MeOH/49% H_2O/1% acetic acid by the 384-well plate ESTASI-MS. When the concentration of CIP was lowered to 15 nM, the peak was still clearly observed with the signal-to-noise (S/N) ratio >10, Figure 3.2(b) and Table 3.1. Detection of other antibiotics was also performed. When 1.4 μM LOM, FLE and ENR were used, peaks for the single protonated antibiotics were easily observed. When the concentration was lowered to 140 nM, the peaks could still be observed but with the S/N of only 4, 2, and 3 for LOM, FLE and ENR, respectively, Table 3.1. The results were compared with standard direct infusion ESI-MS analysis of the same samples by the same linear ion trap mass spectrometer (Thermo, LTQ Velos). Similar LOD was demonstrated under the optimized instrumental conditions, Table 3.1.

Peptide (angiotensin I (Ang I), 1295 Da) was also tested by the 384-well plate ESTASI-MS. As illustrated in Figure 3.2(c), a mass spectrum similar to that from the standard direct infusion ESI-MS was obtained from 15 μM Ang I in 50% MeOH/49% H_2O/1% acetic acid. The LOD of Ang I by the 384-well plate ESTASI-MS was found about 15 nM, where a peak at m/z 649 for the doubly protonated Ang I was observed with the S/N of 5, Figure 3.2(d). In contrast, standard infusion mode ESI-MS needs at least 50 nM of Ang I to generate a clear peak (S/N=10) of the peptide at m/z 433 for the triply protonated ion, Table 3.1.

The analysis of proteins by the 384-well plate ESTASI-MS was demonstrated using cytochrome c from horse heart (Cyt c, 12 kDa). When the concentration of Cyt c was high (10 μM in 50% MeOH/49% H_2O/1% acetic acid), the obtained mass spectrum showed the strongest peak at m/z 1546 for the protein ions with 8 protons, Figure 3.2(e). The LOD was found at 100 nM of Cyt c, with the strongest peak (S/N=10) at m/z 773 for the protein ions with 16 protons. The shift of proton's number from 8 to 16 may originate from the change of

pH value caused by different concentrations of Cyt c, as previously reported.[20] Direct infusion mode ESI-MS provides the LOD of Cyt c (70 nM) slightly better than the 384-well plate ESTASI-MS, with also the strongest peak (S/N=10) at *m*/*z* 773, Table 3.1.

Table 3.1. Comparison of the detection of antibiotics, Ang I and Cyt c by 384-well plate ESTASI-MS and standard direct infusion ESI-MS.

Compound	Method	m/z	LOD	S/N
CIP	ESTASI-MS	332	15 nM	>10
CIP	ESI-MS	332	15 nM	3
LOM	ESTASI-MS	352	140 nM	4
LOM	ESI-MS	352	140 nM	4
FLE	ESTASI-MS	370	140 nM	2
FLE	ESI-MS	370	140 nM	3
ENR	ESTASI-MS	360	140 nM	3
ENR	ESI-MS	360	140 nM	5
Ang I	ESTASI-MS	649[a]	15 nM	5
Ang I	ESI-MS	433[b]	50 nM	10
Cyt c	ESTASI-MS	773[c]	100 nM	10
Cyt c	ESI-MS	773[c]	70 nM	10

a: doubly protonated angiotensin I; b: triply protonated angiotensin I; c: Cyt c with 16 protons

Besides the sample characteristics, mainly including the molecule size, the amount, exposure and pK_a values of the easily protonated sites in the structure, the analysis sensitivity is also determined by the ionization technique used. According to the results, the 384-well plate ESTASI-MS is as sensitive as standard direct infusion ESI-MS in the analysis of small organic molecules and peptides. For proteins, the slightly better sensitivity of standard ESI-MS than 384-well plate ESTASI-MS may be mainly contributed to the smaller commercial emitter size of 500 μm in diameter, which could facilitate the multi-protonation of proteins for efficient detection by the ion trap. The easy multi-protonation also explains the dominant ions of triply protonated angiotensin I in ESI-MS detection. However, different from the standard ESI-MS, the 384-well plate ESTASI-MS can provide much higher throughput and lower sample consumption in analysis. During 384-well plate ESTASI-MS, the sample volume in each well is normally from 2 to 10 μL. The ionization device is simply a disposable microtiter plate, where washing procedures are not required from one analysis to the next. The analysis time per well is seconds. In contrast, direct infusion ESI-MS requires

either a LC autoinjector or continuous syringe injection. In the both cases of direct infusion ESI-MS, washing of the liquid delivery part is required after each analysis, which is time-consuming especially when the analytes are strongly adsorbed by the tubing system.

3.3.2. Enzyme inhibition assay by 384-well plate ESTASI-MS

One of the potential applications of the 384-well plate ESTASI-MS is the enzyme assay study. MS has drawn increasing interests in enzyme activity assays and enzyme inhibition assays during the last years.[6] Compared to spectroscopy-based methods, MS strategy does not need expensive labelling reagents, and provides highly accurate identification to avoid false positive results. Both laser desorption/ionization and electrospray ionization based MS techniques are used for enzyme assay study.[8,21] The former holds the advantage of high throughput, but difficulty in quantification. The later provides better quantification, but is limited by throughput. ESTASI was demonstrated as a concentration-dependent ionization technique, similar to ESI, suitable for quantification.[16] Therefore, the 384-well plate ESTASI-MS can hold both the advantages of quantitative analysis like ESI-MS and high throughput like LDI-MS. By avoiding the washing procedure, the time to analyze a sample is only seconds.

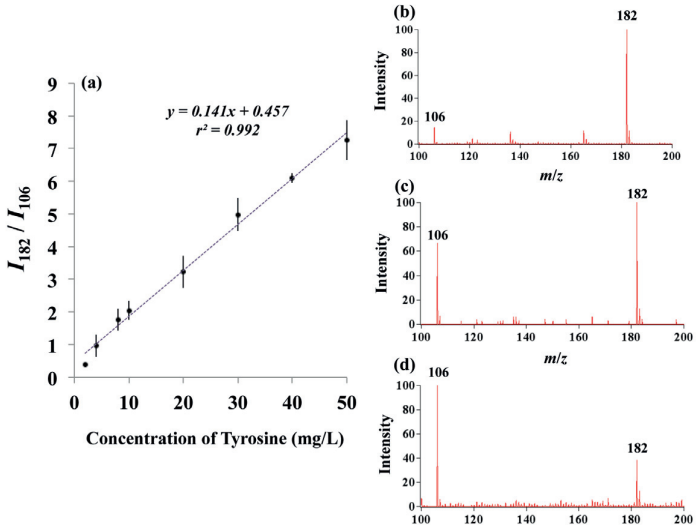

Figure 3.3. (a) Liner curve fitted for tyrosine quantification with internal standard calibration method. I_{182}/I_{106} : relative ion intensities between tyrosine (I_{182}) and serine (I_{106}). **(b)**, **(c)** and **(d)** Mass spectra for 50 mg/L, 8 mg/L and 2 mg/L of tyrosine, respectively. The analyses were performed with direct ESTASI-MS from a 384-well plate, each well containing 10 μL of analyte solution in 50%

MeOH/49% H_2O/1% acetic acid. The internal standard of serine was always kept at 10 mg/L. Error bar shows standard deviation (n=3).

The quantitative capability of 384-well plate ESTASI-MS was demonstrated by detecting tyrosine of different concentrations. The classical method of internal standard calibration was used for tyrosine quantification, where serine was chosen as the internal standard. The high correlation coefficient value (R^2 = 0.992) obtained from the fitted curve in Figure 3.3 indicates the good linear response of the relative ion intensities to the tyrosine concentrations within the range of 2 to 50 mg/L, demonstrating the concentration-dependent ionization performance of the 384-well plate ESTASI-MS.

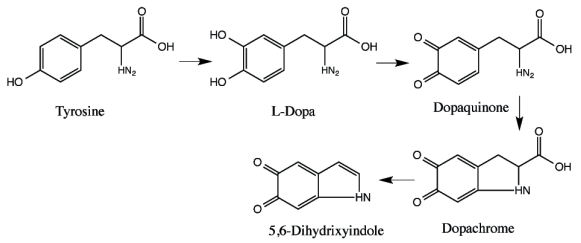

Scheme 3.1. Oxidation of tyrosine catalyzed by tyrosinase.

To demonstrate the application in enzyme assay, we performed the oxidation of tyrosine in the presence of tyrosinase without and with inhibitors, followed by ESTASI-MS analysis. Oxidation of tyrosine catalyzed by tyrosinase, peroxidases or haem-containing proteins can form DOPA, 5,6-dihydroxyindole (5,6-DHI), and finally melanin,[22] as show in Scheme 3.1. It is also involved in browning reactions in damaged fruits.[23] A number of wells were prepared containing tyrosine (0.05 mg/mL) and tyrosinase (0.02 mg/mL) in 2 mM PBS (pH 7.4), and incubated at room temperature for various periods before ESTASI-MS analysis. After 3 min of reaction, a clear peak for single protonated 5,6-DHI at *m*/*z* 150 was observed in Figure 3.4(a), together with a peak for singly protonated tyrosine at *m*/*z* 182. The other oxidation products were hardly observed, indicating that they were quickly consumed after formation to produce 5,6-DHI or hardly ionized for MS analysis. During ESTASI-MS analysis, the buffer was 2 mM PBS at pH 7.4. Prolonging the reaction time, the tyrosine concentration continued to decrease slowly. After 20 min of reaction, only a very weak peak of tyrosine was obtained in Figure 3.4(b), indicating that most of the reactant was consumed. The reaction kinetics was analyzed based on the classic Michaelis-Menten kinetic process[24] and followed pseudo-first-order reaction with the reaction rate constant of 0.069 min^{-1},

indicating that the Michaelis constant K_M is much larger than the substrate (tyrosine) concentration (0.05 mg/mL) in the case, Figure 3.4(c) and (d).

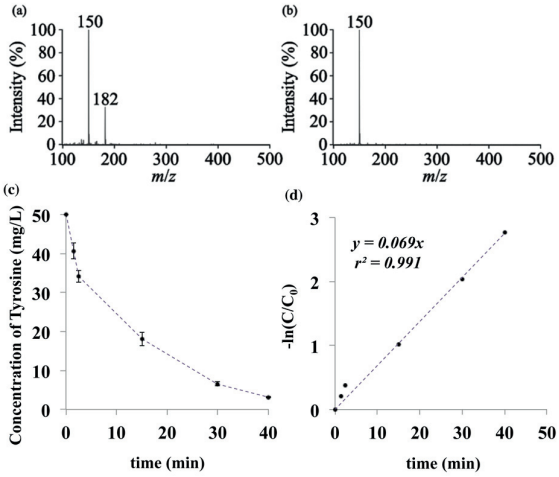

Figure 3.4. Mass spectra of the products of tyrosine (0.05 mg/mL) oxidation catalyzed by tyrosinase (0.02 mg/mL) after **(a)** 3min and **(b)** 20 min of reaction. **(c)** Concentration variation of tyrosine during the enzyme-catalytic oxidization within 40 min. **(d)** Reaction kinetics of tyrosine oxidation. The reaction was performed in the wells of a 384-well plate followed with direct ESTASI-MS analysis in a buffer condition of 2 mM PBS at pH 7.4. Error bar shows standard deviation (n=3).

The inhibition of tyrosinase-catalyzed tyrosine oxidation is an important topic in food and cosmetic chemistry to avoid hyperpigmentation in human skin and enzymatic browning in fruits or fungi. Recently developed inhibitors have been summarized in several reviews.[23,25,26] In this work, we used two inhibitors, ascorbic acid and cupferron, to illustrate the feasibility of applying the 384-well plate ESTASI-MS in enzyme inhibition assays. Ascorbic acid is an antioxidant, working as an inhibitor of many enzymatic oxidative reactions. The enzyme inhibition assay was performed by preparing a number of wells containing ascorbic acid at different concentrations (0.1 mg/mL and 0.01 mg/mL) with tyrosine (0.05 mg/mL) and tyrosinase (0.02 mg/mL) in 2 mM PBS, followed by ESTASI-MS analysis after different time of incubation. As shown in Figure 3.4(a), tyrosine oxidation was efficiently inhibited by 0.01 mg/mL ascorbic acid within 20 min of incubation but the tyrosine concentration started to decrease sharply when prolonging the incubation time and was almost completely consumed after 40 min. It suggests that ascorbic acid works as a competitive inhibitor, continuously consumed during the enzymatic reaction. In contrast, with a higher concentration of ascorbic acid (0.1 mg/mL), the inhibition can last effectively for at

least 40 min, in Figure 3.4(b). Therefore, a successful and continuous inhibition requires proper amount of ascorbic acid or the addition of ascorbic acid round-the-clock.

Cupferron is a metal-chelating agent that can coordinate the copper ion of mushroom tyrosinase to inhibit completely its activity.[27] Replacing ascorbic acid by cupferron, the inhibition was studied by 384-well plate ESTASI-MS. As a competitive inhibitor, the concentration of cupferron should be sufficiently higher than that of tyrosine for the efficient inhibition of tyrosinase (0.15 μM). Theoretically, at least 1 mM of cupferron is required for complete inhibition of tyrosinase when existing 0.3 mM of tyrosine.[27] Here, 2 mM of cupferron was applied to ensure maximum inhibition of tyrosinase. As shown in Figure 3.5(c), no oxidation product was observed after 10 min of reaction. With longer incubation time, the oxidation was still not observed by ESTASI-MS, in consistent with the proposed inhibition mechanism that cupferron deactivates completely tyrosinase. The strong peak on Figure 3.5(c) at *m*/*z* 157 was from cupferron, which was also observed by standard direct infusion ESI-MS of pure cupferron in 50% MeOH/49% H_2O/1% acetic acid (data not shown).

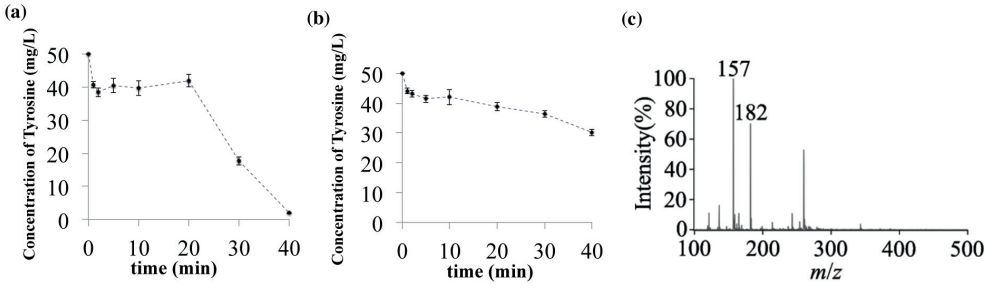

Figure 3.5. Tyrosinase inhibition assay with different amounts of ascorbic acid as the inhibitor. **(a)** 0.01 mg/mL of ascorbic acid **(b)** 0.1 mg/mL of ascorbic acid. **(c)** Mass spectrum obtained after 10 min of reaction inhibited by 2 mM of cupferron. The reactions were performed in 10 μL solutions containing 0.05 mg/mL of tyrosine, 0.02 mg/mL of tyrosinase and different amounts of inhibitors in a buffer of 2 mM PBS at pH 7.4 in the wells of a 384-well plate followed by direct ESTASI-MS analysis.

3.3.3. Drug metabolites screening by the 384-well plate ESTASI-MS.

Another important application of 384-well plate is drug candidate screening. *In-vitro* studies of drug candidate metabolism could predict its potential toxicity, which is crucial in early-stage drug discovery.[28] The rapid development of combinatorial chemistry and advances in bioinformatics, genomics and proteomics have driven the potential targets for new drug development increase dramatically in the past decade.[29]

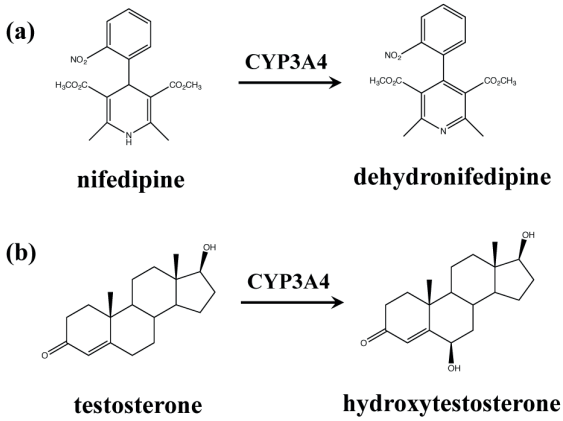

Scheme 3.2. Oxidative metabolisms of **(a)** nifedipine and **(b)** testosterone catalyzed by cytochrome P450 CYP3A4.

Therefore, low-cost, rapid and high throughput drug candidates screening methods are urgently needed. 384-well plate combined with ESTASI-MS or ESTASI-MS/MS can be applied in drug candidates screening by characterizing the metabolites of drug candidates in a high throughput manner.

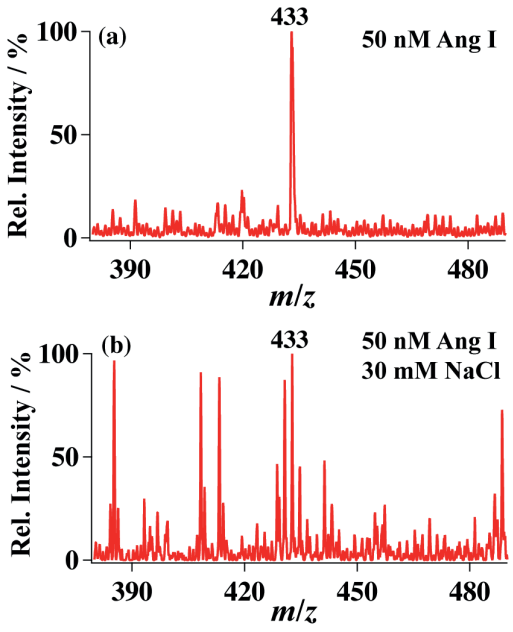

Figure 3.6. The test of ESTASI tolerance to salt by the analysis of 10 μL 50 nM Ang I in the well of a 384-well plate. The buffer of 50% methanol, 49% H_2O and 1% acetic acid contains **(a)** no salt or **(b)** 30 mM NaCl.

To demonstrate this application, cytochrome P450, one major family of human liver microsome enzymes widely used for in vitro metabolism and toxicity studies,[30] was chosen to induce drug metabolism in the wells of microtiter plates, while nifedipine and testosterone were used as substrates. Nifedipine is a prototype of the dihydropyridine class of calcium channel blockers that is widely used in the treatment of hypertension, prinzmtal's angina pectoris and other vascular disorders,[31] while testosterone is a male sex hormone that is important for sexual and reproductive development and plays a vital role in carbohydrate, fat, and protein metabolism.[32]

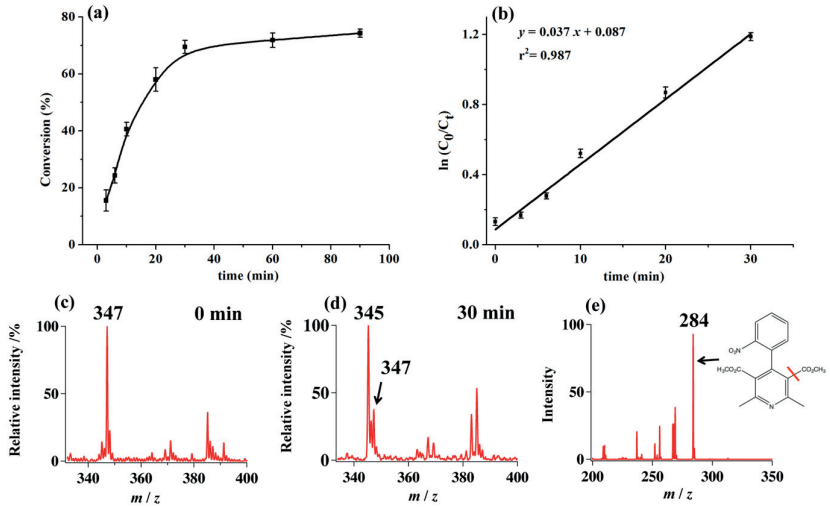

Figure 3.7. Fitted curves and mass spectra for CYP3A4-catalyzed metabolism of nifedipine. **(a)** Conversion ratio of nifedipine as a function of time. **(b)** Reaction kinetics of nifedipine metabolism. **(c)** and **(d)** Mass spectra of nifedipine and its metabolites before reaction and after 30 min of reaction, respectively. **(e)** CID spectrum of the precursor ion at *m*/*z* 345 with normalized collision energy of 30 and isolation width of 1 *m*/*z*. The reactions were performed with 64 μg/mL of nifedipine, 1 mg/mL of NADPH and 0.1 μM of CYP3A4 in 10 μL of 10 mM NH_4HCO_3 (pH 7.4) in a 384-well plate. 9 μL of the reaction solution was discarded and replaced with 9 μL of the ionization buffer (50% MeOH/49% H_2O/1% acetic acid) prior to ESTASI-MS analysis.

The CYP3A4-catalyzed metabolisms of both nifedipine and testosterone were simultaneously studied by the 384-well plate ESTASI-MS during a single run analysis. In both cases, NADPH was added as an electron donor. Multiple wells in a 384-well plate were filled with 10 μL of solutions, each containing 64 μg/mL of nifedipine or 32 μg/mL of testosterone, 1 mg/mL of NADPH and 0.1 μM CYP3A4 in 10 mM NH_4HCO_3 (pH 7.4). The solutions were incubated for a certain time under room temperature and then directly analyzed by ESTASI-MS at different time intervals. The tolerance to salty solution of the

384-well plate ESTASI-MS was estimated be around 30 mM NaCl for the analysis of 50 nM Ang I, in Figure 3.6. Considering that the high concentration of salts (around 30 mM) in the reaction solution could hinder the efficient detection of the drugs and their metabolic products, 9 μL of the reaction mixture was discarded and replaced by 9 μL of the ionization buffer (50% MeOH/49% H_2O/1% acetic acid) for ESTASI-MS analysis.

The primary product of nifedipine metabolism catalyzed by CYP3A4 is dehydronifedipine with the *m*/*z* at 345, as shown in Scheme 3.2(a) and Figure 3.7(d), in consistent with the literature report.[31] After 30 min of incubation, the majority of nifedipine were oxidized and the conversion ratio reached around 70%, as shown in Figure 3.7(a). When prolonging the reaction time to 90 min, little nifedipine was further oxidized. A linear regression was obtained in Figure 3.7(b) and the nifedipine oxidation could be considered as the pseudo-first-order reaction. Within 30 min, the reaction rate constant was determined as 0.037 min^{-1}, in Figure 3.7(b).

Structural elucidation of drug candidates metabolic products could facilitate the prediction of its toxicity based on the regression model of quantitative structure-toxicity relationship (QSTR), which relates the structure variables to the potency of toxicity variables.[33] For this purpose, tandem MS with collision-induced dissociation (CID) was further applied to characterize the structure of the oxidized nifedipine. With normalized collision energy of 30, the precursor ion of *m*/*z* 345 generated a predominant fragment ion with *m*/*z* 284, corresponding to the loss of CH_3COOH from the metabolic product, in Figure 3.7(e). Both the precursor ion and the fragments indicated the generation of dehydronifedipine.

Metabolic oxidation of testosterone was also monitored in the same 384-well plate together with nifedipine during a single run of analysis. From Scheme 3.2(b) and Figure 3.8(d), the testosterone metabolism generated hydroxytestosterone and 6β-hydroxytestosterone is the primary structure, according to the literature report.[32] Figure 3.8(a) and (b) presented the oxidation process and only 40 % of conversion ratio was obtained until 90 min of incubation. A reaction rate constant was obtained as 0.0072 min^{-1} for the metabolism of testosterone, Figure 3.8(b). Corresponding mass spectra of the testosterone and its oxidation product are shown in Figure 3.8(c) and (d). The metabolic product ion with *m*/*z* 305 was selected for the CID process and generated the primary fragments by the detachment of two -OH groups, confirming the formation of hydroxytestosterone, Figure 3.8(e).

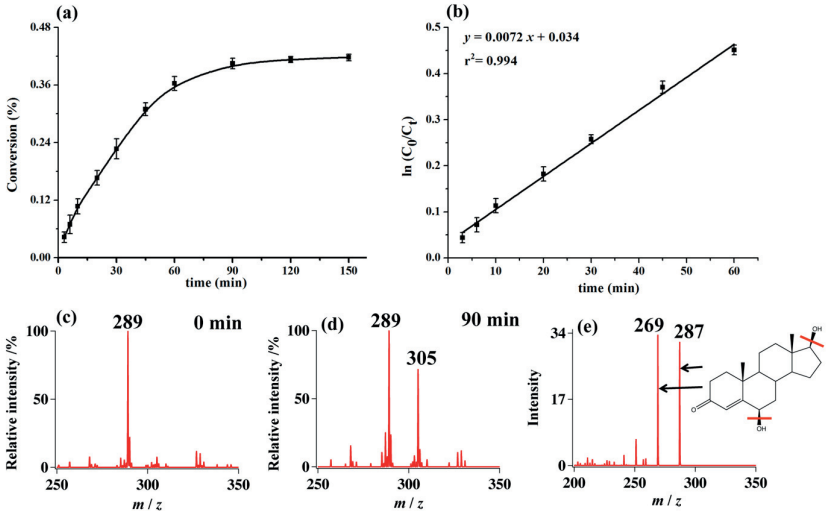

Figure 3.8. Fitted curves and mass spectra for CYP3A4-catalyzed metabolism of testosterone. **(a)** Conversion ratio of testosterone as a function of time. **(b)** Reaction kinetics of testosterone metabolism. **(c)** and **(d)** Mass spectra of testosterone and its metabolites before reaction and after 90 min reaction, respectively. **(e)** CID spectrum of the precursor ion at *m/z* 305 with normalized collision energy of 30 and isolation width of 1 *m/z*. The reactions were performed with 32 μg/mL of nifedipine, 1 mg/mL of NADPH and 0.1 μM of CYP3A4 in 10 μL of 10 mM NH_4HCO_3 (pH 7.4) in a 384-well plate. 9 μL of the reaction solution was discarded replaced with 9 μL of the ionization buffer (50% MeOH/49% H_2O/1% acetic acid) prior to ESTASI-MS analysis.

These results show that the 384-well plate ESTASI-MS/MS provides the possibility to directly characterize metabolic products in a high speed and throughput way without any solution purification or delivery interface. The 384-well plate ESTASI-MS and ESTASI MS/MS will be of great value in rapid and accurate in-vitro drug metabolism study and toxicity prediction.

3.4. Conclusion

In conclusion, we have realized direct ionization of liquid samples inside a microtiter plate by electrostatic spray ionization. Analytical characters, including sensitivity and quantification capability, were evaluated. The method can be universally applied for a wide range of samples, from organic molecules with molecular weight of ~150 Da to proteins of >10 kDa. The ionization device is demonstrated as efficient as standard ESI in the view of sensitivity to trace amount of analytes, while holds advantages in analysis throughput. Two applications were further explored, enzyme assay and drug metabolism screening. We would expect the current ionization method a powerful tool in high throughput MS-based enzyme activity assays, enzyme inhibition assays, immunoassays and drug candidate screenings.

3.5. References

(1) Cho, Y. A.; Kim, Y. J.; Hammock, B. D.; Lee, Y. T.; Lee, H. S. J. Agric. Food Chem. 2003, 51, 7854-7860.

(2) Palamanda, J. R.; Favreau, L.; Lin, C. C.; Nomeir, A. A. Drug Discov Today 1998, 3, 466-470.

(3) Brik, A.; Wu, C. Y.; Wong, C. H. Org. Biomol. Chem. 2006, 4, 1446-1457.

(4) Kariv, I.; Fereshteh, M. P.; Oldenburg, K. R. J Biomol Screen 2001, 6, 91-99.

(5) Barros, A.; Ly, V.; Chando, T. J.; Ruan, Q. A.; Donenfeld, S. L.; Holub, D. P.; Christopher, L. J. J. Pharm. Biomed. Anal. 2011, 54, 979-986.

(6) Greis, K. D. Mass Spectrom. Rev. 2007, 26, 324-339.

(7) Liesener, A.; Karst, U. Anal. Bioanal. Chem. 2005, 382, 1451-1464.

(8) Hsieh, F.; Keshishian, H.; Muir, C. J Biomol Screen 1998, 3, 189-198.

(9) Xu, R. N. X.; Fan, L. M.; Rieser, M. J.; El-Shourbagy, T. A. J. Pharm. Biomed. Anal. 2007, 44, 342-355.

(10) Lahoz, A.; Donato, M. T.; Picazo, L.; Gomez-Lechon, M. J.; Castell, J. V. Toxicol. in Vitro 2007, 21, 1247-1252.

(11) Wang, T.; Zeng, L.; Strader, T.; Burton, L.; Kassel, D. B. Rapid Commun. Mass Spectrom. 1998, 12, 1123-1129.

(12) Morand, K. L.; Burt, T. M.; Regg, B. T.; Chester, T. L. Anal. Chem. 2001, 73, 247-252.

(13) Wang, B.; Trimpin, S. Anal. Chem. 2014, 86, 1000-1006.

(14) Qiao, L.; Sartor, R.; Gasilova, N.; Lu, Y.; Tobolkina, E.; Liu, B.; Girault, H. Anal. Chem. 2012, 84, 7422-7430.

(15) Qiao, L.; Tobolkina, E.; Liu, B.; Girault, H. H. Anal. Chem. 2013, 85, 4745-4752.

(16) Qiao, L.; Tobolkina, E.; Lesch, A.; Bondarenko, A.; Zhong, X.; Liu, B.; Pick, H.; Vogel, H.; Girault, H. H. Anal. Chem. 2014, 86, 2033-2041.

(17) Tobolkina, E.; Qiao, L.; Xu, G.; Girault, H. H. Rapid Commun. Mass Spectrom. 2013, 27, 2310-2316.

(18) Golet, E. M.; Strehler, A.; Alder, A. C.; Giger, W. Anal. Chem. 2002, 74, 5455-5462.

(19) Hermo, M. P.; Nemutlu, E.; Kir, S.; Barron, D.; Barbosa, J. Anal. Chim. Acta. 2008, 613, 98-107.

(20) Konermann, L.; Douglas, D. J. Biochemistry, 1997, 36, 12296-12302.

(21) Cancilla, M. T.; Leavell, M. D.; Chow, J.; Leary, J. A. Proc. Natl. Acad. Sci. U. S. A. 2000, 97, 12008-12013.

(22) Bertazzo, A.; Costa, C. V. L.; Allegri, G.; Favretto, D.; Traldi, P. J. Mass Spectrom. 1999, 34, 922-929.

(23) Chang, T.-S. Int. J. Mol. Sci. 2009, 10, 2440-2475.

(24) Michaelis, L.; Menten, M. L. Biochem Z 1913, 49, 333-369.

(25) Parvez, S.; Kang, M.; Chung, H.-S.; Bae, H. Phytother. Res. 2007, 21, 805-816.

(26) Kim, Y. J.; Uyama, H. Cell. Mol. Life Sci. 2005, 62, 1707-1723.

(27) Xie, L. P.; Chen, Q. X.; Huang, H. A.; Liu, X. D.; Chen, H. T.; Zhang, R. Q. Int. J. Biochem. Cell Biol. 2003, 35, 1658-1666.

(28) Lee, M. Y.; Park, C. B.; Dordick, J. S.; Clark, D. S. Proc. Natl. Acad. Sci. U. S. A. 2005, 102, 983-987.

(29) Ma, S. G.; Chowdhury, S. K. Anal. Chem. 2011, 83, 5028-5036.

(30) Bajrami, B.; Zhao, L. L.; Schenkman, J. B.; Rusling, J. F. Anal. Chem. 2009, 81, 9921-9929.

(31) Wang, X. D.; Li, J. L.; Lu, Y.; Chen, X.; Huang, M.; Chowbay, B.; Zhou, S. F. J Chromatogr B 2007, 852, 534-544.

(32) Choi, M. H.; Skipper, P. L.; Wishnok, J. S.; Tannenbaum, S. R. Drug Metab. Dispos. 2005, 33, 714-718.

(33) Tropsha, A. Mol Inform 2010, 29, 476-488.

CHAPTER IV.

Mass barcode signal amplification for multiplex allergy diagnosis by MALDI-MS

*Based on X. Zhong et al., Anal. Chem., **2016**, 88, 6184-6189.*

Abstract

A highly sensitive method based on mass-barcoded gold nanoparticles (AuNPs) and immunomagnetic separation has been developed for multiplex allergy diagnosis by MALDI mass spectrometry in a component-resolved manner. Different analytical probes were prepared by coating AuNPs with individual allergenic proteins and mass barcode, represented by polyethylene glycol molecules of various chain lengths. Magnetic beads (MBs) functionalized with anti-human IgE antibodies (Abs) were used as immunomagnetic capture probes. IgE Abs were extracted from a patient's blood serum by the formation of a sandwich structure between the AuNPs and MBs. Multiple specific IgE Abs were simultaneously identified by mass spectrometry detection of the mass barcodes, providing an efficient component-resolved allergy diagnosis. Because of the signal amplification provided by the mass barcodes, the developed diagnosis method is very sensitive with a limit of detection down to picograms per milliliter level for specific IgE Abs. The method can be potentially useful when the sample amount is highly limited and a multiplex diagnostic procedure is required.

4.1. Introduction

Mass barcode-based mass spectrometry signal amplification is a technique widely utilized in DNA assays,[1,2] immunoassays[3,4] and tissue imaging, as shown in § 1.1.2.3.[5,6] Mass barcodes, which are small tag molecules and easily detectable by MS, are grafted on nano-/micro-particles in large excess together with the large target biomolecules. The detection of these tag molecules results in an amplified signal of the targets. For immunoassays,[3,4,7] the mass barcodes have been utilized to probe the IgG antibodies (Abs)-involved immune binding events on a biochip or a gold plate, which acted as a flat surface to capture and separate the antigens from bulk solutions. This surface-based separation approach requires a multiple-step procedure, which is rather cumbersome and time-consuming. Besides, the full accessibility of antigens to the Abs, which are pre-immobilized on a 2D surface, is also limited.

Meanwhile, commercially available micro-magnetic beads (MBs) with immunoaffinity coating are more advantageous for fast and convenient isolation of the target molecules. They possess large active surface area and are easy in manipulation. The immunoreactions can be performed in a homogenous way through gentle mixing of MBs with other reagents and may result in a faster target-binding process. Optimization of the target enrichment for sensitive analysis can also be easily realized by adjusting the MBs amount and the final sample volume applied for analysis. Therefore, the combination of MBs-based immunoassays with mass barcode signal amplification protocol can be promising for MS detection of large biomolecules such as allergens.

Allergies, especially the ones caused by food products and plant pollen, are a constantly growing health problem worldwide.[8] As pollen and foodstuff often contain multiple allergenic proteins that can provoke allergic reactions for a patient, component resolved diagnosis (CRD) should be performed.[8] Allergy CRD is typically performed with individual purified allergenic proteins to detect the level of specific IgE Abs in human blood serum by enzyme-linked immunosorbent assay (ELISA).[9] Commercially available ELISA-based kits[10] or automated platforms for allergy CRD usually require 20-50 μL of blood serum and provide the limit of detection (LOD) for specific IgE Abs as low as 0.24 ng/mL (0.1 IU/mL) level.[11] Fluorophore-labeled immunoassay,[12] magnetophoretic immunoassay,[13] interferometric reflectance imaging sensors,[14] microfluidic ELISA coupled with electrochemical detection,[15] and immunoaffinity capillary electrophoresis (IACE) coupled

with fluorescence[16] or MS detection,[17] were also developed. However, in the listed analytical methods, the allergy diagnosis usually relies on expensive enzyme or fluorescent labels. Special devices, such as the antigen array immobilized on a 2D surface, the microfluidic chip or the separation capillary preloaded with affinity probes, are also required for these techniques, making them quite complex and laborious. Regarding these factors above, the simplification of the device, improvement of sensitivity and reduction of sample consumption are still needed and under development for the analysis of specific IgE Abs in the allergic patient's blood serum.

Here, we employ a mass barcode amplification strategy combined with commercial protein A/G coated-MBs (protein A/G@MBs) to enhance the simplicity and sensitivity of the multiplex allergy CRD with MS detection as displayed in Figure 4.3. Polyethylene glycol molecules with different chain lengths were chosen as mass barcodes and grafted onto gold nanoparticles (AuNPs) that were further modified with specific allergenic proteins to form AuNPs probes. At the same time, protein A/G@MBs were modified with anti-human IgE Abs and formed a sandwich structure with specific IgE Abs from patient's blood serum and AuNPs probes. The MS detection of the mass barcodes from AuNPs indicated the presence of respective specific IgE Abs and allowed allergy CRD in a highly sensitive manner. LOD of 18 pg/mL (7.5 mIU/mL) for specific IgE Abs was achieved for the analysis of anti-beta-lactoglobulin Abs in model experiments, allowing using afterwards only 1 μL of blood serum from allergic patient for CRD diagnosis.

4.2. Experimental section

4.2.1. Materials and reagents

Pierce protein A/G@MBs (1 μm diameter) were purchased from Thermo Fisher Scientific (Reinach, Switzerland). Estapor tosyl-activated MBs (1.29 μm diameter) were kindly offered by Merck Chimie (France). Three kinds of mass barcodes, $[S(CH_2)_{11}(OCH_2CH_2)_xOH]_2$), x=3 for Mbc1 (670 Da), x=4 for Mbc2 (758 Da), x=6 for Mbc3 (934 Da), were bought from Sigma-Aldrich (Buchs, Switzerland). Protein linker 1 (PL1, 98%), HS-$(CH_2)_{10}$-COOH, was purchased from Sigma-Aldrich (Buchs, Switzerland). PL2 (HS-$(PEG)_n$-CH_2CH_2-COOH, MW 2000) and PL3 (HS-$(PEG)_n$-NHS, MW 2000) were bought from Nanocs (NY, USA). PL4 (HS-$(CH_2)_{11}(OCH_2CH_2)_6$-OCH_2COOH) was obtained from SensoPath technologies (MT, USA). *N*-hydroxysuccinimide (NHS, 98%), 1-ethyl-3(3-

dimethylaminopropyl) carbodiimide hydrochloride (EDC, >98%), 2-(N-morpholino)ethanesulfonic acid (MES), gold(III) chloride trihydrate (>99.9%), sodium citrate dehydrate (>99%), sodium phosphate dibasic dehydrate (>99%), sodium phosphate monobasic dehydrate (>99%) and polyoxyethylene-sorbitan monolaurate (Tween 20) were obtained from Sigma-Aldrich (Buchs, switzerland). Acetic acid (99.5%), acetonitrile (99.8%), trifluoroacetic acid (TFA, >99%), sinapinic acid (≥ 99%), and 2,5-dihydroxybenzoic acid (DHB) (>99%) were purchased from Fluka (Buchs, Switzerland). Purified bovine milk proteins, including *β*-lactoglobulin B (*β*-lac B), bovine serum albumin (BSA), lactoferrin, *α*-casein, *β*-casein, and *κ*-casein were obtained from Sigma-Aldrich (Buchs, Switzerland). Polyclonal anti-bovine *β*-lac B antibodies (Abs) and monoclonal anti-human IgE Abs were purchased from AbD Serotec (Oxford, U.K.). Blood serum of patient allergic to cow's milk was purchased from Bioreclamation LLC (Westbury, NY, USA). Deionized water (18.2 MΩ cm) was purified by an alpha Q Millipore system (Zug, Switzerland) and used in all aqueous solutions.

4.2.2. Synthesis and characterization of AuNPs

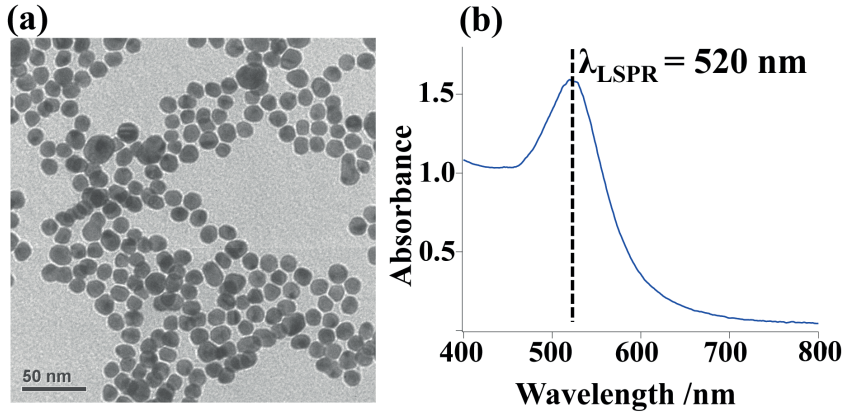

Figure 4.1. (a) TEM image of synthesized AuNPs. **(b)** UV-Vis spectrum of the synthesized AuNPs.

The citrate stabilized AuNPs were synthesized following a protocol reported previously.[18] Briefly, 250 mL of 1 mM $HAuCl_4$ in water was brought to the boil with vigorous stirring, and then rapidly mixed with 25 mL of 38.8 mM sodium citrate. Boiling was continued for 10 min. The heating source was then removed and stirring was continued for another 15 min.

The mean diameter of the synthesized AuNPs was defined as ~12 nm by the transmission electron microscopy (TEM) image recorded by a FEI CM12 (Phillips,

Eindhoven, Netherlands) transmission electron microscope, operating with a LaB6 electron source at 120 kV, as shown in Figure 4.1(a). An alternative method to determine the mean diameter and approximate concentration of the colloidal AuNPs solution is UV-Vis spectroscopy analysis on a PerkinElmer Lambda XLS+ spectrophotometer (Waltham, MA, USA) with a 10 mm polystyrene cell, as detailed by Haiss *et al.*[19] Based on this method, the concentration was calculated as 4.5×10^{12} particles/mL, and the mean diameter was defined as 13 nm, in Figure 4.1(b). Considering that the AuNPs solutions were diluted twice for UV-Vis absorption measurement, the original concentration of AuNPs was 9×10^{12} particles/mL (~15 nM).

4.2.3. Preparation of mass-barcoded AuNPs probes.

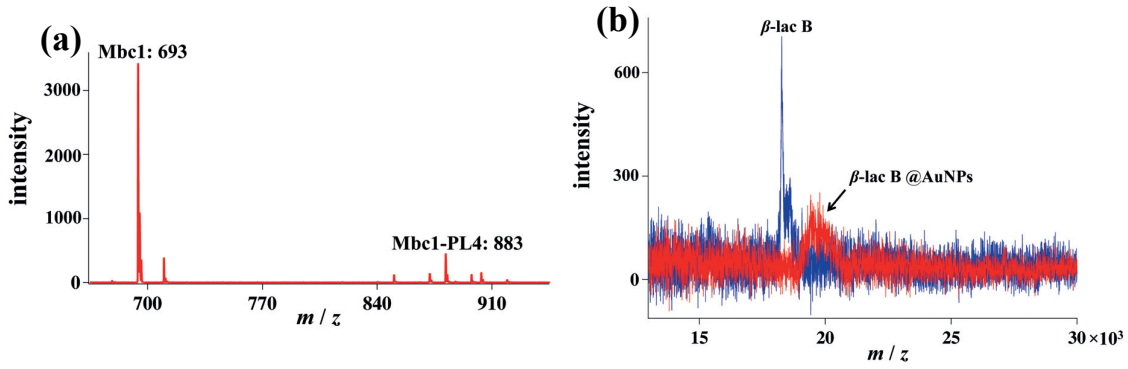

Figure 4.2. (a) MALDI-MS analysis of mass barcode Mbc1 and chosen protein linker PL4 present on modified AuNPs. The Mbc1 corresponded to a peak at *m/z* 693 $(M+Na)^+$. The PL4 formed disulfide bonds with Mbc1 ($(HO(OCH_2CH_2)_3(CH_2)_{11}S\text{-}S(CH_2)_{11}(OCH_2CH_2)_6\text{-}OCH_2COOH$) and presented as a major peak at *m/z* 883 $(M+Na)^+$, indicating the successful immobilization of PL4 to the AuNPs. PL: protein linker. **(b)** MALDI-MS analysis of *β*-lac B (1 *μ*g/mL, blue spectrum) and *β*-lac B@AuNPs (15 nM, red spectrum) with 5 mg/mL sinapinic acid as the matrix. There is a mass shift of around 900 Da for *β*-lac B covalently conjugated on Mbc1-coded AuNPs, which may origin from the Mbc1-PL4 modification (+860 Da) to *β*-lac B.

To prepare the AuNPs probes, the obtained AuNPs were firstly derivatized with mass barcodes and protein linkers through the formation of stable Au-S bonds on particle surfaces. The saturation amount of thiol-terminated oligomers that can replace citrates and fully wrap the AuNPs in a brush shape was estimated to be around 15 nmol for 500 *μ*L of AuNPs by considering that each thiol-PEG molecule occupied a footprint area of 0.35 nm^2 on the AuNPs surface.[20] It is necessary to ensure complete surface functionalization for efficient protection of AuNPs from the salt-induced aggregation and nonspecific adsorption during the following protein conjugation and immunobinding steps. Therefore, in a typical experiment,

five times higher amount (75 nmol) of thiol-containing oligomer mixture of mass barcodes (64 nmol) and protein linkers (11 nmol) in ethanol was mixed with 500 μL of AuNPs in water and incubated for 12 h with moderate vortexing. Excessive reagents were removed by centrifugation for 20 min at 13000 rpm. The precipitate was washed with pure water (1 mL each) for three times by successive centrifugation and redispersion. For semi-quantification purposes, similar protocol was applied for the preparation of internal standard conjugated AuNPs (IS@AuNPs), just by replacing the polymer mixture with pure IS (75 nmol), which was Mbc2, when Mbc1 was used for AuNPs probe in the analysis of a model analyte, anti-bovine β-lac B Abs. The successful modification of AuNPs by the mass barcode, *e.g.* Mbc1, and the chosen protein linker PL4 was demonstrated by MALDI-MS analysis in Figure 4.2(a).

In a second step, proteins were immobilized on the mass-barcoded AuNPs *via* EDC-NHS coupling protocol. Before protein conjugation, 500 μL of AuNPs probes were concentrated to 10 μL by centrifugation. Then, they were activated with 50 μL of freshly prepared EDC (15 mg/mL) and NHS (15 mg/mL) in 15 mM MES buffer (pH 5) for 30 min at room temperature (RT). After washing with MES buffer for 3 times (1 mL each), the NHS-activated AuNPs were immediately incubated with sufficient amount of appropriate allergenic proteins (30 μL, 1 mg/mL) in 10 mM phosphate buffer (PB, pH 7.4) for 3h at RT. Then, after washing with 10 mM PB for 3 times to remove unbound proteins, obtained proteins@AuNPs were finally resuspended in 500 μL of 10 mM PB to a final concentration of 15 nM and stored at 4 °C. The successful immobilization of proteins, *e.g.* β-lac B, was also demonstrated by MALDI-MS analysis in Figure 4.2(b), providing β-lac B@AuNPs.

4.2.4. Semi-quantification of anti-bovine β-lac B Abs.

The experimental procedure was shown in Figure 4.3(a). 300 μL of anti-bovine β-lac B Abs at different concentrations in 10 mM PB were incubated with 10 μL of 10 mg/mL protein A/G@MBs for 30 min at RT. After magnetic separation, the captured anti-bovine β-lac B Abs on the MBs were mixed with 300 μL of β-lac B@AuNPs (1 nM AuNPs)[21] for another 30 min. After rinsing with 10 mM PB for 3 times (300 μL each), the β-lac B@AuNPs captured on MBs surface were eluted with 5 μL of 10% acetic acid and then concentrated to ~1 μL with a weak stream of nitrogen. The concentrated sample was deposited together with 0.5 μL of 10 mg/mL DHB (dissolved in 70% acetonitrile, 29.9% water, 0.1% TFA) and 0.5 μL of IS@AuNPs (0.1 nM AuNPs) on a MALDI target plate for MS detection by a Microflex

LRF MALDI TOF instrument (Brüker Daltonics, Bremen, Germany). The instrument was operated in a positive reflectron mode. An average spectrum from 800 laser shots at different positions was collected for each sample spot. Instrumental parameters were optimized to achieve highest sensitivity and resolution for the detection of mass barcode molecules.

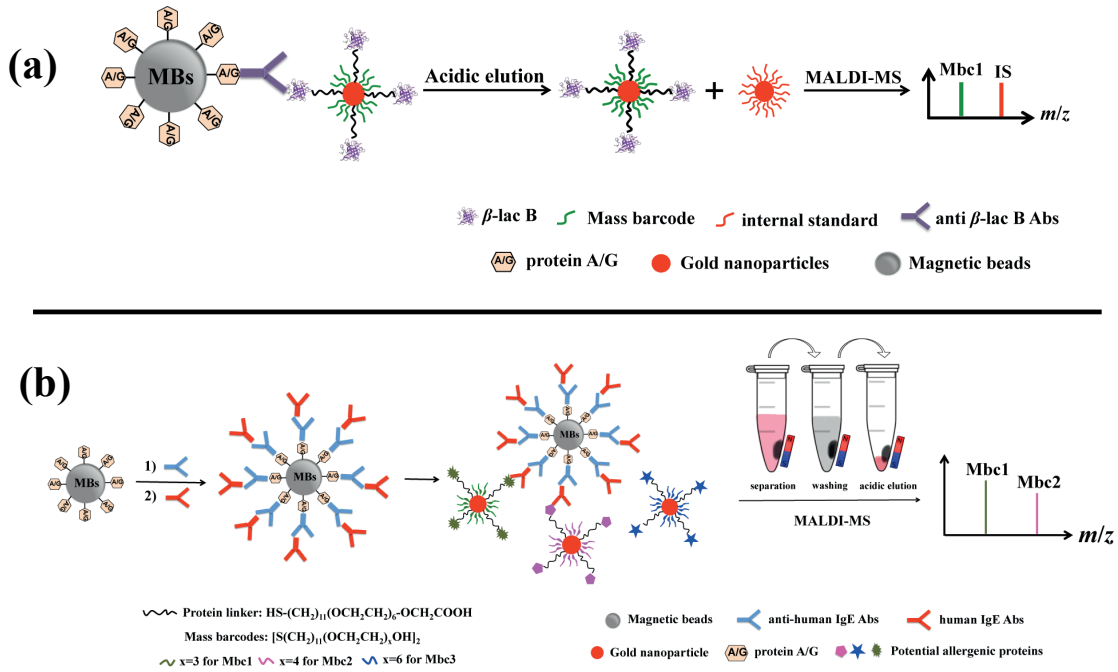

Figure 4.3. Schematic representation of **(a)** *β*-lac B Abs semi-quantification and **(b)** simultaneous diagnosis of multiple allergic reactions *via* detection of specific IgE Abs with mass barcoded AuNPs and MBs. MALDI-MS: matrix–assisted laser desorption/ionization mass spectrometry; MBs: magnetic beads; Mbc: mass barcode; IS: internal standard; Abs: antibodies.

4.2.5. Allergy CRD with the patient's blood serum

Firstly, the citrate-stabilized AuNPs were derivatized with the mixed thiol-containing oligomers of mass barcodes and protein linkers. Various allergenic proteins-conjugated AuNPs probes were then produced by immobilizing individual purified cow's milk proteins, including lactoferrin, bovine serum albumin (BSA), *β*-lactoglobulin B (*β*-lac B), *α*-casein, *β*-casein, and *κ*-casein, onto the AuNPs with distinct mass barcodes covalently, with synthesis procedures as described in experimental parts of 4.2.2 and 4.2.3.

The anti-human IgE Abs-modified MBs were prepared by incubating 10 *μ*L of 10 mg/mL protein A/G@MBs with 5 *μ*L of 1 mg/mL anti-human IgE Abs for 30 min at room temperature (RT). Blood serum of a milk allergic patient was always diluted with 10 mM phosphate buffer (PB, pH 7.4) prior to the diagnosis. Initial required volume of the serum

varied from 50 to 1 μL depending on the dilution factor changing from 10 up to 100000 times. The modified MBs were then added to 300 μL of the diluted blood serum to extract human IgE Abs through 30 min of incubation at RT. The supernatant was discarded and the protein A/G-anti-human IgE Abs-human IgE Abs immunocomplex formed on MBs was resuspended into 10 μL of 10 mM PB, pH 7.4 for subsequent use.

Allergy diagnosis was firstly performed with each type of the allergen-conjugated AuNPs separately. 20 μL of appropriate protein-conjugated AuNPs (15 nM AuNPs) were mixed with 10 μL of the prepared human IgE-based immunocomplex on MBs. The mixture was diluted to 300 μL with 10 mM PB and incubated for 30 min at RT. After magnetic separation step, acidic elution and MALDI-MS detection of captured allergen-coated AuNPs were carried out as described in Figure 4.3(b). Multiplex allergy diagnosis was realized by adding simultaneously various AuNPs probes (20 μL and 15 nM, each) into 10 μL of the human IgE-captured MBs. The mixture was diluted to 300 μL with 10 mM PB and incubated for 30 min at RT, followed by magnetic separation step, AuNPs elution and MALDI-MS detection.

4.3. Results and discussion

4.3.1. Immunoaffinity MBs and protein linker

In the preliminary feasibility test, two kinds of MBs, tosyl-activated MBs and protein A/G@MBs, were compared. The immunoaffinity reaction between β-lac B Abs captured on MBs and β-lac B on AuNPs was studied as the model system. To simplify the process, 2.5 μg of β-lac B were nonspecifically adsorbed onto 500 μL of 15 nM AuNPs that were further blocked with 1 μL of Tween 20 prior to the washing step. The β-lac B-coated AuNPs through nonspecific adsorption (β-lac B_NA@AuNPs) were finally dissolved in 500 μL of 10 mM PB containing 0.1% Tween 20.

Anti-bovine β-lac B Abs can be covalently immobilized onto tosyl-activated MBs following a commercially available protocol.[22] 20 μL of the formed β-lac B Abs@MBs (5 mg/mL) were then treated with 20 μL of β-lac B_NA@AuNPs for 30 min at RT in 300 μL 10 mM PB. No obvious red colour was observed in the supernatant after acidic elution and MALDI-MS analysis of the supernatant gave weak signal of β-lac B. The low immunobinding efficiency of β-lac B Abs@MBs with β-lac B_NA@AuNPs may come from

the steric hindrance between the two kinds of particles and the random orientation of the Abs and antigens on particles.

Instead, we adopted commercial recombinant protein A/G@MBs, where each protein A/G holds four Fc binding domains toward anti-bovine *β*-lac B Abs and thus can capture more Abs on MBs. Moreover, the Abs are highly oriented on MBs, exposing Fab-binding domains outside properly for efficient binding with antigens. A high concentration of anti-bovine *β*-lac B Abs (10 nM in 300 *μ*L of 10 mM PB) were analyzed with 10 *μ*L protein A/G@MBs (10 mg/mL) and 20 *μ*L *β*-lac B_NA@AuNPs (15 nM). The collected and concentrated supernatant had a red colour and gave a strong peak of *β*-lac B in MALDI mass spectra (data not shown). Therefore, protein A/G@MBs were employed as the immunomagnetic support in this work.

Four protein linkers (PLs) were compared for the protein conjugation on AuNPs. Their structures were as shown below: PL1: HS-$(CH_2)_{10}$-COOH, MW 218 Da; PL2: HS-$(PEG)_n$-CH_2CH_2-COOH, MW 2000 Da; PL3: HS-$(PEG)_n$-NHS, MW 2000 Da; PL4: HS-$(CH_2)_{11}(OCH_2CH_2)_6$-OCH_2COOH, MW 526 Da.

The carboxyl-based PLs, including PL1, PL2 and PL4, were modified onto AuNPs together with Mbc1 at an amount ratio of 10:90. The total amount of the oligomer mixture was 75 nmol per 500 *μ*L of AuNPs. Then, three kinds of *β*-lac B@AuNPs probes were prepared *via* EDC-NHS reaction with the three PLs. *K*-casein@AuNPs were also prepared with the PLs and used for control experiments. These AuNPs probes were utilized with protein A/G@MBs to detect 10 nM of anti-bovine *β*-lac B Abs in 300 *μ*L 10 mM PB. For PL1, serious nonspecific adsorption was observed from control experiments, which may come from the strong hydrophobicity of the PL1. For PL2, the obtained AuNPs could not be stabilized in salt-rich solution during the NHS activation-based protein conjugation process.

To prepare proteins@AuNPs *via* PL3, 50 *μ*L of protein solution (1 mg/mL) in 10 mM PB firstly reacted with excess amount of PL3 (3 *μ*L, 10 mg/mL) for 3h at RT. Then, the formed protein-PL3 complex was purified by ultrafiltration with Amicon Ultra-2mL centrifugal filter to remove excess PL3. The purification procedure was repeated for 3 times. 2.5 *μ*g of the protein-PL3 complex was added into 500 *μ*L of 15 nM AuNPs solution for 20 min reaction. The protein-conjugated AuNPs were further treated with excess amount of Mbc1 (75 nmol) for 12h at RT. The obtained *β*-lac B@AuNPs probes were then used with protein A/G@MBs to detect 10 nM anti-bovine *β*-lac B Abs in 300 *μ*L 10 mM PB. However, the captured AuNPs gave only weak MS signal of Mbc1.

Finally, PL4 was chosen as the protein linker for the allergy CRD application. The resulting AuNPs co-modified with Mbc1 and PL4 were stable throughout the NHS activation-based protein conjugation process, showed low level of nonspecific adsorption during the immunoassay, and higher signal intensity of Mbc1 than the AuNPs probes prepared with PL3.

4.3.2. Combining MALDI-MS signal amplification by mass barcoded AuNPs with immunomagnetic separation: optimization and validation

With the optimal immunomagnetic support and protein linker, analysis of anti-bovine *β*-lac B IgG Abs was chosen as a model system for the protocol optimization. Anti-bovine *β*-lac B Abs could bind with both protein A/G@MBs and *β*-lac B-coated AuNPs (*β*-lac B @AuNPs) probe forming a sandwich structure and then be detected through MALDI-MS analysis of corresponding mass barcode, as shown in Figure 4.3(a). The validity and sensitivity of the method were also evaluated based on this model.

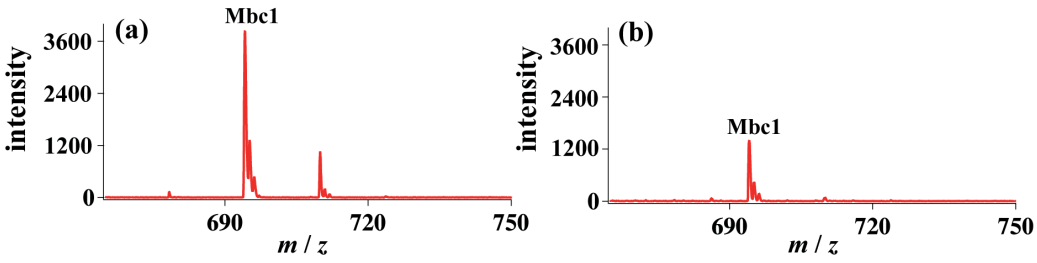

Figure 4.4. (a) and **(b)** MALDI mass spectra of 1 nM Mbc1-coded AuNPs with and without DHB as matrix, respectively. The spectra were acquired under positive mode with an accelerating voltage of 19 kV, a 20 Hz repetition rate, the laser intensity of ~ 40% (instrumental value) and an average of 800 shots.

First of all, the amount ratio between mass barcode and protein linker for AuNPs surface modification needed the optimization. Excessive mass barcode amount in comparison to the protein linker could negatively affect the protein conjugation efficiency. In contrast, insufficient amount of mass barcode would lead to limited signal amplification effect. To find an optimal mass barcode/protein linker ratio, several identical solutions containing 1 nM of anti-bovine *β*-lac B IgG Abs in 300 *μ*L of 10 mM PB were analyzed separately with the fixed amount of protein A/G@MBs (100 *μ*g) and 20 *μ*L of *β*-lac B@AuNPs prepared with various mass barcode-to-protein linker amount ratios (n : m) ranging from 95:5 to 75:25. The amount of MBs was much more excessive in comparison to the amount of IgG Abs. According to the

protocol,[25] provided by the manufacturer of protein A/G@MBs, the chosen amount was enough to fix 4 μg of IgG Abs. Therefore, most of the anti-bovine β-lac B IgG Abs should be immobilized on the MBs. The amount of β-lac B@AuNPs was chosen to match the amount of IgG Abs.

For semi-quantitative comparison, internal standard-coated AuNPs (IS@AuNPs) and proper matrix were deposited together with the concentrated sample on a MALDI target plate for MS detection. AuNPs were previously demonstrated to facilitate MS analysis and used as desorption/ionization matrices.[26,27] In the current work, we have compared the MS analysis of mass barcodes with and without organic matrices. The results showed that mass barcode was detectable with only AuNPs-assisted LDI. However, the Mbc1 signal could be highly enhanced in the presence of 2,5-dihydroxybenzoic acid (DHB) as a matrix, in Figure 4.4. It is worth to mention that DHB was used as the matrix due to its low interference to the MS signal of the chosen mass barcodes. Therefore, all the mass spectra presented in the paper were obtained with DHB matrix.

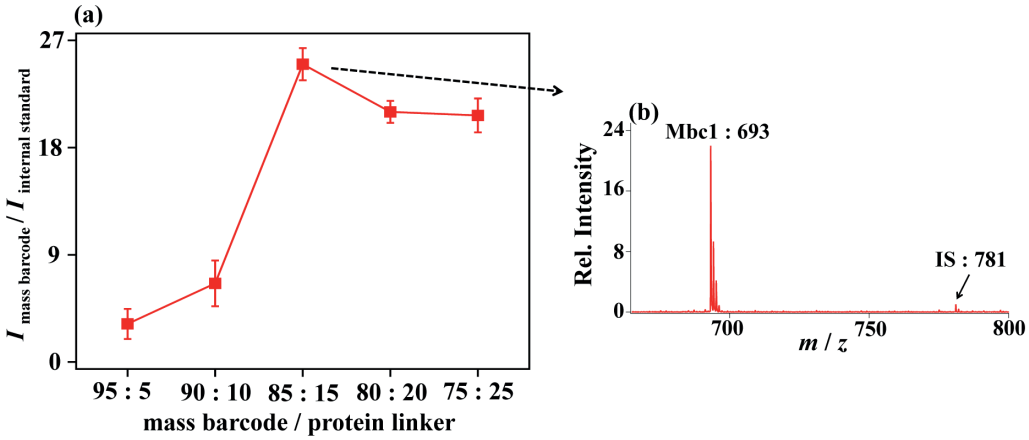

Figure 4.5. Detection of 1 nM anti-bovine β-lac B IgG Abs by the mass-barcoded AuNPs MALDI-MS signal amplification method combined with immunomagnetic separation. **(a)** Optimization of the amount ratio between mass barcode Mbc1 and protein linker PL4 on AuNPs. **(b)** Mass spectrum of the Mbc1 (M + Na^+ = 693 m/z) under the optimized condition for AuNPs functionalization. Conditions: 1 nM anti-bovine β-lac B Abs in 300 μL 10 mM PB, 100 μg of protein A/G@MBs, and 300 fmol β-lac B@AuNPs.

Mass barcode 2 (Mbc2) was used as the IS, which has similar molecular structure as the signal reporter, Mbc1, coated on AuNPs to ensure similar ionization efficiency during MALDI-MS analysis. The relative intensity of the mass barcode to IS was considered for the evaluation of the signal amplification effect during the detection of anti-bovine β-lac B Abs.

From the recorded MALDI mass spectra, Mbc1 relative intensity reached the highest value, when the mass barcode-to-protein linker ratio was 85:15, in Figure 4.5. Therefore, the oligomer mixture composed of 85% mass barcode and 15% protein linker was selected to functionalize AuNPs for all the following immunoassays.

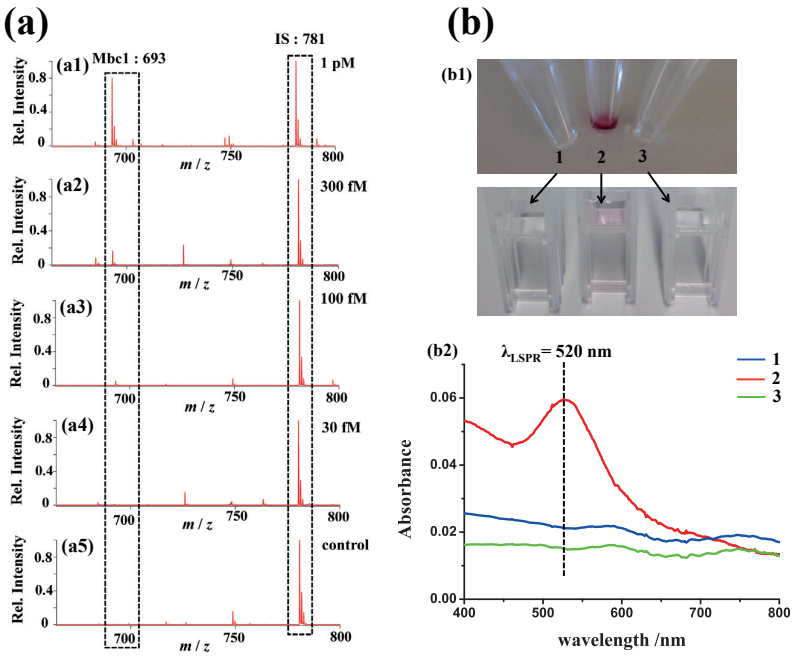

Figure 4.6. (a) Detection of anti-bovine *β*-lac B IgG Abs by mass barcoded AuNPs-based MALDI-MS signal amplification method combined with immunomagnetic separation. MALDI mass spectra obtained for the analyses of **(a1)** 1 pM, **(a2)** 300 fM, **(a3)** 100 fM and **(a4)** 30 fM of anti-bovine *β*-lac B Abs. **(a5)** 1 pM of anti-bovine *β*-lac B Abs analyzed with *κ*-casein conjugated AuNPs as a negative control. **(b)** Optical image **(b1)** and UV-Vis spectra **(b2)** of 5 *μ*L eluents from 100 *μ*g of protein A/G@MBs and diluted in 500 *μ*L H_2O for the analysis of **(1)** blank sample and 1 nM anti-bovine *β*-lac B Abs in 300 *μ*L 10 mM PB with 300 fmol **(2)** *β*-lac B@AuNPs, and **(3)** *κ*-casein@AuNPs, respectively. Rel.: relative. Conditions: Abs in 300 *μ*L of 10 mM PB, 100 *μ*g of protein A/G@MBs, 300 fmol AuNPs, 85:15 of Mbc1: protein linker ratio.

With the proposed strategy, the semi-quantification of anti-bovine *β*-lac B IgG Abs was further performed. The method sensitivity was accessed by determining the LOD of anti-bovine *β*-lac B IgG Abs. Following the optimized conditions, both the amounts of the *β*-lac B@AuNPs probes and protein A/G@MBs were kept constant at 300 fmol and 100 *μ*g respectively, while the concentration of target Abs were decreased from 1 pM to 30 fM. Figure 4.6(a) shows the obtained mass spectra of Mbc1 and IS with intensities normalized to the intensity of IS. As expected, the relative intensity of Mbc1 gradually decreased, as the concentration of Abs decreased, from Figure 4.6(a1) to (a4). Due to the signal amplification

effect, the lowest concentration of anti-bovine *β*-lac B IgG Abs that can be analyzed with a good reproducibility was around 100 fM (18 pg/mL). Once the concentration was lowered to 70 fM, the signal of Mbc1 was hardly detected with S/N around or less than 3 (data not shown).

In the negative control experiment using *κ*-casein@AuNPs and anti-bovine *β*-lac B Abs, only IS signal was observed in Figure 4.6(a5). Thanks to the oligomer coating of AuNPs and washing step applied, the obtained spectrum demonstrated clearly the high specificity of the system. Successful suppression of nonspecific interactions by the ethylene glycol oligomers[26] was also confirmed by the optical estimation of the colour difference and UV-Vis absorption measurement of the supernatant eluted from the MBs by acidic solution when analyzing anti-bovine *β*-lac B Abs at high concentration (1 nM) or blank sample with *β*-lac B@AuNPs and *κ*-casein@AuNPs, as shown in Figure 4.6(b1) and (b2).

4.3.3. Multiplex allergy CRD

The mass barcode-based MALDI-MS signal amplification strategy was further applied to cow's milk allergy CRD. In this case, the immunoaffinity reactions between specific IgE Abs from the patient's blood serum and allergenic proteins were detected *via* the observation of amplified mass barcodes signals. Anti-human IgE Abs were immobilized onto protein A/G@MBs to selectively extract human IgE Abs from the blood serum of the patient. A large amount of magnetic immunosupport carrying anti-human IgE Abs could be prepared at once with the commercial protocol[23] and divided into equal portions for all the following diagnostic steps, 100 *μ*g per each analysis. This amount of anti-human IgE-protein A/G@MBs was chosen to be largely in excess in comparison to the total IgE Abs in patient's blood serum. The total IgE Abs concentration in the original blood serum of the milk allergic patient was detected as 2150 ± 160 ng/mL (10 nM, or 900 ± 70 IU/mL, n=3) by classical commercial ELISA.[17] Initial volume of the blood serum was diluted continuously with 10 mM PB and, therefore varied depending on the dilution factor: for example, 50 *μ*L were for 10 times dilution, 10 *μ*L for 50 times dilution and 1 *μ*L for the dilution 500 times and higher. Then, 300 *μ*L of the samples diluted were analyzed separately to evaluate the diagnosis sensitivity as described below.

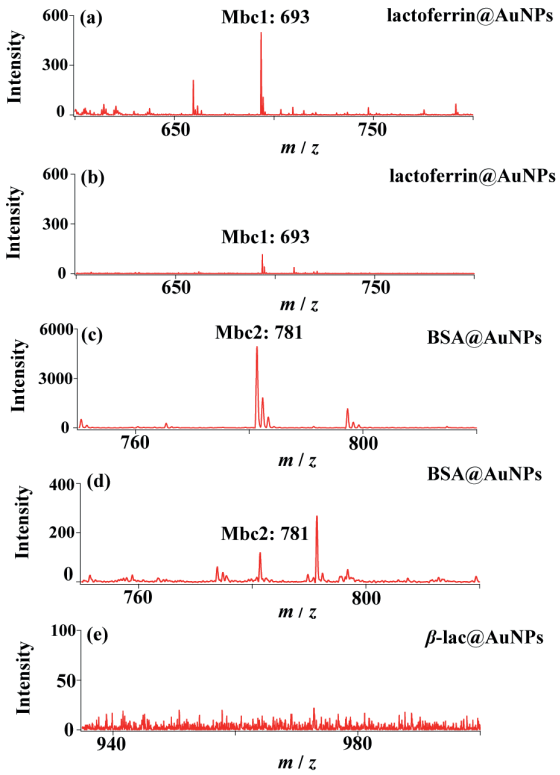

Figure 4.7. Diagnosis of cow's milk allergy with individual AuNPs probes combined with immunomagnetic separation. MALDI mass spectra of Mbc1 for lactoferrin allergy diagnosis with the patient's serum diluted **(a)** 30,000 and **(b)** 100,000 times. MALDI mass spectra of Mbc2 for BSA allergy diagnosis with the patient's blood serum diluted **(c)** 10,000 and **(d)** 30,000 times. **(e)** Mass spectrum obtained using the Mbc3 coded β-lac@AuNPs and 10 times diluted patient's serum. Conditions: diluted sample volume of 300 μL, 100 μg of anti-human IgE-protein A/G@MBs and 300 fmol AuNPs probes.

Firstly, diagnosis was performed with individual AuNPs probes, Mbc1-coded lactoferrin@AuNPs, Mbc2-coded BSA@AuNPs or Mbc3-coded β-lac B@AuNPs using the protocol, illustrated in Figure 4.3(b). Among the three whey proteins, BSA@AuNPs and lactoferrin@AuNPs displayed the binding with the patient's IgE Abs on MBs based on the corresponding observation of Mbc1 and Mbc2 peaks in MS spectra (Figure 4.7). The Mbc1 and Mbc2 signals were still detectable even when the blood serum was diluted 100,000 and 30,000 times, as shown in Figure 4.7(b) and (d), respectively. Considering that the original total concentration of the IgE Abs in the blood serum was around 10 nM (900 IU/mL), lactoferrin- and BSA-specific IgE Abs were still detectable with the total IgE Abs concentrations of 100 and 300 fM (18 and 54 pg/mL or 7.5 and 22.5 mIU/mL), respectively. Owing to such sensitivity, less than 1 μL of original patient's blood serum could be enough for the allergy CRD based on MS signal amplification.

In contrast, no signal of Mbc3 at *m*/*z* 957 was observed for *β*-lac B@AuNPs even with the 10 times diluted patient's blood serum, (Figure 4.7(e)), indicating that the patient should not be allergic to bovine *β*-lac, while he may have an allergy to BSA and lactoferrin.

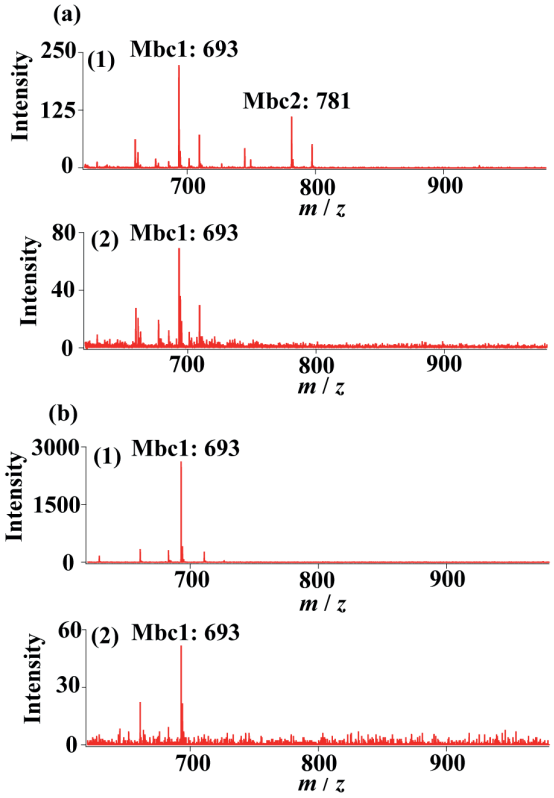

Figure 4.8. (a) Multiplex diagnosis of lactoferrin allergy (Mbc1), BSA allergy (Mbc2) and *β*-lac B allergy (Mb3) by AuNPs probes combined with immunomagnetic separation. MALDI mass spectra obtained with the patient's blood serum diluted **(1)** 30,000 and **(2)** 100,000 times. **(b)** Multiplex diagnosis of *α*-casein (Mbc1 coded), *β*-casein (Mbc2 coded) and *κ*-casein (Mbc3 coded) allergies. MALDI mass spectra obtained with the patient's blood serum diluted **(1)** 50 and **(2)** 1000 times. Conditions: diluted sample volume of 300 *μ*L, 100 *μ*g of anti-human IgE coated MBs and 300 fmol of each kind of AuNPs probes.

To check the feasibility of the present strategy for multiplex analysis, the CRD of cow's milk allergy was performed with various AuNPs probes simultaneously in a single run. For this purpose, same amounts of the three kinds of AuNPs probes (300 fmol each) were mixed together to react with the patient's IgE Abs extracted on the MBs. As each kind of AuNPs probe binds with its specific IgE Abs from the patient's serum without competition, the experimental parameters, *e.g.* amount of individual AuNPs probes, were kept the same as those in individual allergen identification. As expected, for patient's blood serum diluted 30,000 times, both signals of Mbc1 for lactoferrin specific IgE Abs and Mbc2 for BSA

specific IgE Abs were detected, but without Mbc3 signal for *β*-lac B specific IgE Abs, as shown in Figure 4.8(a1). When the serum was diluted by 100,000 times, the Mbc2 signal could not be observed any more, while Mbc1 was still detectable (Figure 4.8(a2)), in accordance with the results obtained using individual AuNPs probes. These results demonstrate that the multiplex diagnosis would not sacrifice detection sensitivity, but could provide a gain in time and reagent consumption.

The same protocol was further applied for the multiplex diagnosis of allergy to caseins. Mbc1 mass barcode was used for *α*-casein@AuNPs, while Mbc2 and Mbc3 mass barcodes were utilized for *β*- and *κ*-casein@AuNPs probes. With 50 times and 1,000 times diluted patient's serum, only Mbc1 was observed, demonstrating that the patient is solely allergic to *α*-casein. In comparison with lactoferrin and BSA, the Mbc1 signal from *α*-casein conjugated AuNPs probes was observed at LOD level with 1000 times diluted serum, as shown in Figure 4.8(b2). These data reveal that the amount of *α*-casein specific IgE Abs existing in the blood serum is approximately 30 and 100 times lower than the amount of BSA and lactoferrin specific IgE Abs, respectively.

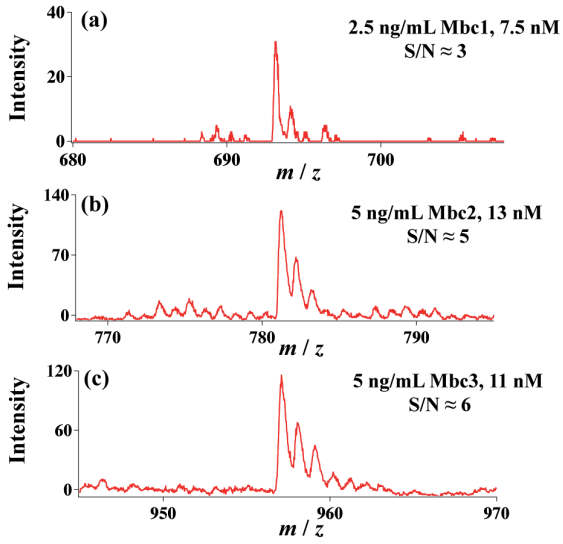

Figure 4.9. MALDI mass spectra of the mass barcodes: 1 *μ*L of **(a)** 2.5 ng/mL Mbc1, **(b)** 5 ng/mL Mbc2, and **(c)** 5 ng/mL Mbc3. 0.5 *μ*L of 10 mg/mL DHB was used as the matrix.

These results are in good accordance with those, previously obtained by IACE-UV/MS strategy and classical ELISA protocol,[17] confirming the reliability of the present procedure. This diagnostic approach is qualitative, but provides the possibility to make a conclusion about the relative abundance of individual allergen specific IgE Abs coexisting in

the patient's blood serum: specific IgE Abs to lactoferrin > IgE Abs to BSA > IgE Abs to α-casein. Such a comparison is feasible, since the diagnosis is only based on the observation of mass barcode molecules, which have similar molecular structures and comparable sensitivities during MALDI-MS analysis, as shown in Figure 4.9.

4.3.4. Comparison with existing approaches for allergy diagnosis

Different from the previous work based on IACE-UV/-MS, this strategy aims at sensitively detecting specific IgE Abs in the allergic patient's blood serum with a set of known allergenic proteins. With the three mass-barcoded and allergen-conjugated AuNPs, we have demonstrated the proof-of-concept of this strategy for qualitative multiplex allergy CRD. A high throughput multiplex diagnosis can be potentially realized by preparing more AuNPs modified with different mass barcode molecules and allergenic proteins. The high resolution of MS detection affords a wide choice of PEG based mass barcodes to perform the analysis of specific IgE Abs against various allergens within a single assay.

The arbitrarily selected mass barcodes, easily controllable MBs in tube and sensitive MS detection allow performing multiplexed allergy diagnosis in a simple manner, avoiding the use of spatially resolved architectures, such as microarray systems,[11,12] costly fluorescent[27] or enzyme labels,[28] and capillary electrophoresis that needs laborious preloading of immunoaffinity MBs and coupling with MS detection of the collected CE fractions for simultaneous antigen identification instead of UV analysis.[17] Owing to the signal amplification procedure, the allergy diagnosis sensitivity has been enhanced to a level, which is 13 times better than that obtained with IACE-UV analysis,[17] and comparable to previously reported results employing nanocrystal clusters[29] or nanoparticle hybrid probes.[30] In another case, surface plasmon resonance signals from AuNPs have been shown to provide ultrasensitive total IgE quantification with LOD of only 0.18 pg/mL (0.075 mIU/mL).[31] However, the method only provided quantification of the standard IgE solution instead of allergy CRD using patient's blood serum. Due to the high sensitivity, our method requires extremely low amount (3-30 nL in theory) of patient's blood serum in contrast to 20-100 μL of blood serum consumption by commercial ELISA or other developed methods and 2 μL by microarray chip with DLC solid support[32] or IACE-UV/MS approach.[17]

In addition, another three specific features distinguish this analysis platform from previously developed Au particle-based MS signal amplification for immunoassay performed on gold chips.[3,4] First, MBs as the immunosupport with large surface area are commercially

available with a wide variety of surface functionalization. They provide great flexibility for immunoassay design in effective and simple manner without complex and time-consuming surface conjugation processes for the gold chip. Second, the immune reactions may be faster in bulk solution with stirring in comparison with one on a fixed gold surface, facilitating sample handling and accelerating the immunobinding process. Third, deposition of concentrated AuNPs together with IS on the MALDI plate can provide more homogeneous MS analysis and allow avoiding spot-to-spot variation during the direct detection on the gold chip or complicated concentration process of AuNPs by centrifugation after their detachment from the gold chip.

All in all, due to the simplicity, tiny sample consumption and high sensitivity, the present technique can be a helpful tool for ultratrace analysis during clinical allergy diagnosis.

4.4. Conclusions

In this study, we have constructed a MALDI-MS signal amplification system based on mass-barcoded AuNPs and immunomagnetic separation. We have applied this system to enhance the sensitivity of allergy CRD. For diagnostic purpose, the patient's IgE Abs were firstly extracted from the blood serum by anti-human IgE Abs modified MBs, and then probed by different mass-barcoded and allergenic proteins-conjugated AuNPs. The immunobinding events between the patient's IgE Abs and allergens were reported by the corresponding mass barcodes. High sensitivity and potential for multiplexing allergy CRD were successfully demonstrated with down to 1 μL of the initial patient's blood serum, that could be diluted up to 100000 times prior to the analysis. Besides the food allergen diagnosis, we believe that this system can be easily modified and applied to many other immunoassays with a vast range of target analytes.

4.5. References

(1) Qiu, F.; Jiang, D. W.; Ding, Y. B.; Zhu, J.; Huang, L. L. *Angew Chem Int Edit* **2008**, *47*, 5009-5012.

(2) Qiu, F.; Gu, K.; Yang, B.; Ding, Y. B.; Jiang, D. W.; Wu, Y.; Huang, L. Q. L. *Talanta* **2011**, *85*, 1698-1702.

(3) Lee, J. R.; Lee, A.; Kim, S. K.; Kim, K. P.; Park, H. S.; Yeo, W. S. *Angew Chem Int Edit* **2008**, *47*, 9518-9521.

(4) Hong, S. H.; Kim, J. I.; Kang, H.; Yoon, S.; Kim, D. E.; Jung, W.; Yeo, W. S. *Chem. Commun. (Cambridge, U. K.)* **2014**, *50*, 4831-4834.

(5) Yan, B.; Kim, S. T.; Kim, C. S.; Saha, K.; Moyano, D. F.; Xing, Y. Q.; Jiang, Y.; Roberts, A. L.; Alfonso, F. S.; Rotello, V. M.; Vachet, R. W. *J. Am. Chem. Soc.* **2013**, *135*, 12564-12567.

(6) Yang, J. H.; Chaurand, P.; Norris, J. L.; Porter, N. A.; Caprioli, R. M. *Anal. Chem.* **2012**, *84*, 3689-3695.

(7) Nam, J.; Yoo, M.; Yeo, W. S. *Biochip J* **2015**, *9*, 124-130.

(8) Hochwallner, H.; Schulmeister, U.; Swoboda, I.; Spitzauer, S.; Valenta, R. *Methods* **2014**, *66*, 22-33.

(9) Fiocchi, A.; Schunemann, H. J.; Brozek, J.; Restani, P.; Beyer, K.; Troncone, R.; Martelli, A.; Terracciano, L.; Bahna, S. L.; Rance, F.; Ebisawa, M.; Heine, R. G.; Assa'ad, A.; Sampson, H.; Verduci, E.; Bouygue, G. R.; Baena-Cagnani, C.; Canonica, W.; Lockey, R. F. *J Allergy Clin Immun*, **2010**, *126*, 1119-1128.

(10) http://www.abnova.com.

(11) http://www.phadia.com/en/Products/Allergy-testing-products/ImmunoCAP-ISAC/.

(12) Monroe, M. R.; Reddington, A. P.; Collins, A. D.; LaBoda, C.; Cretich, M.; Chiari, M.; Little, F. F.; Unlu, M. S. *Anal. Chem.* **2011**, *83*, 9485-9491.

(13) Hahn, Y. K.; Jin, Z.; Kang, J. H.; Oh, E.; Han, M. K.; Kim, H. S.; Jang, J. T.; Lee, J. H.; Cheon, J.; Kim, S. H.; Park, H. S.; Park, J. K. *Anal. Chem.* **2007**, *79*, 2214-2220.

(14) Monroe, M. R.; Daaboul, G. G.; Tuysuzoglu, A.; Lopez, C. A.; Little, F. F.; Unlu, M. S. *Anal. Chem.* **2013**, *85*, 3698-3706.

(15) Proczek, G.; & Gassner, A. L.; Busnel, JM.; Girault, H. H. *Anal. Bioanal. Chem.,* **2012**, *402*, 2645-2653.

(16) Chen, H.; Busnel, JM.; Peltre, G.; Zhang, X.; Girault H. H. *Anal. Chem.*, **2008**, *80*, 9583-9588.

(17) Gasilova, N.; Girault, H. H. *Anal. Chem.,* **2014**, *86*, 6337-6345.

(18) Grabar, K. C.; Freeman, R. G.; Hommer, M. B.; Natan, M. J. *Anal. Chem.*, **1995**, *67*, 735-743.

(19) Haiss, W.; Thanh, N. T. K.; Aveyard, J.; Fernig, D. G. *Anal. Chem.*, **2007**, *79*, 4215-4221.

(20) Wuelfing, W. P.; Gross, S. M.; Miles, D. T.; Murray, R. W. *J. Am. Chem. Soc.*, **1998**, *120*, 12696-12697

(21) Zhou, X.; Cao, P.; Tian, Y.; Zhu, J. *J. Am. Chem. Soc.*, **2010**, *132*, 4161-4168.

(22) http://www.diagnoswiss.com/web_new/technote_tosylactivated_beads_merck_estapor.pdf.

(23) https://tools.thermofisher.com/content/sfs/manuals/MAN0011761_Pierce_Protein_AG_Mag_Bead_UG.pdf.

(24) McLean, J. A.; Stumpo, K. A.; Russell, D. H. *J. Am. Chem. Soc.*, **2005**, *127*, 5304-5305.

(25) Hua, L.; Chen, J. R.; Ge, L.; Tan, S. N. *J Nanopart Res*, **2007**, *9*, 1133-1138.

(26) Prime, K. L.; Whitesides, G. M. *Science* **1991**, *252*, 1164-1167.

(27) Cerecedo, I.; Zamora, J.; Shreffler, W. G.; Lin, J.; Bardina, L.; Dieguez, M. C.; Wang, J.; Muriel, A.; de la Hoz, B.; Sampson, H. A. *J Allergy Clin Immun* **2008**, *122*, 589-594.

(28) Fall, B. I.; Eberlein-Konig, B.; Behrendt, H.; Niessner, R.; Ring, J.; Weller, M. G. *Anal. Chem.* **2003**, *75*, 556-562.

(29) Yao, J. J.; Han, X. G.; Zeng, S.; Zhong, W. W. *Anal. Chem.* **2012**, *84*, 1645-1652.

(30) Li, H.; Qiang, W. B.; Vuki, M.; Xu, D. K.; Chen, H. Y. *Anal. Chem.* **2011**, *83*, 8945-8952.

(31) Kim, S.; Lee, J.; Lee, S. J.; Lee, H. J. *Talanta* **2010**, *81*, 1755-1759.

(32) Suzuki, K.; Hiyoshi, M.; Tada, H.; Bando, M.; Ichioka, T.; Kamemura, N.; Kido, H. *Anal. Chim. Acta* **2011**, *706*, 321-327.

CHAPTER V.

On-chip spyhole nanoelectrospray ionization mass spectrometry for sensitive biomarker detection in small volumes

Based on the manuscript submitted to JASMS.

Abstract

A polyimide microfluidic chip with a microhole emitter (Ø 10-12 μm) on top of a microchannel has been designed for nanoelectrospray ionization (spyhole-nanoESI) to couple microfluidics with mass spectrometry. The spyhole-nanoESI showed higher sensitivity compared to standard ESI and microESI from the end of the microchannel. The limits of detection (LOD) for peptide with the spyhole-nanoESI MS reached 50 pM, which was 600 times lower than that with standard ESI. The present microchip emitter allows the analysis of small volumes of samples. As an example, a small cell lung cancer biomarker, neuron-specific enolase (NSE), was detected by monitoring the transition of its unique peptide with the spyhole-nanoESI MS/MS. NSE at 0.2 nM could be well identified with a signal to noise ratio (S/N) of 50 and thereby its LOD was estimated to be 12 pM. The potential application of the spyhole-nanoESI MS/MS in cancer diagnosis was further demonstrated with the successful detection of 2 nM NSE from 1 μL of human serum without any complicated sample preparation steps. The concentration matched the real condition of clinical samples. In addition, the microchips can be disposable to avoid any cross contamination. The present technique provides a highly efficient way to couple microfluidics with MS, which brings additional values to various microfluidics and MS based analysis.

5.1. Introduction

Biosensors and clinical diagnostic tools based on microfluidics are now commercially available for point-of-care diagnosis.[1,2] These devices usually rely on three major detection methods: spectroscopic, electrochemical and mass spectrometry (MS) methods.[3] Despite their simplicity and high sensitivity, optical and electrochemical methods often require labeling procedures using tags with optical or electrochemical properties. The indirect sensing process can cause false positive signals and cannot provide exact information about the analyte itself.[4,5] In contrast, MS provides direct, highly specific and accurate characterization and quantification of target analytes and thereby has gained increasing importance as a detection method for microfluidic chips.[6] However, compared to optical and electrochemical methods, which can be integrated in chips, a key difficulty in coupling microfluidics with MS is the design of the emitter.[7]

Compatible with the small volumes of samples used in microfluidic chips, nanoelectrospray ionization (nanoESI) is one of the most suitable interfaces for integrating microfluidics with MS, as it provides good detection sensitivity at sub microliter/min flow rates.[8] NanoESI interfaces between MS and microfluidic chips can be classified in three types: i) spraying from the microchannel outlet;[9,10] ii) spraying from an externally coupled emitter;[11] iii) spraying from an emitter integrated on chip.[12,13] Electrospray directly from a microfluidic channel is the most straightforward interfacing approach used in early days, but the performance is limited by the solution spreading at the nontapered and hydrophilic flat edge of the channel.[9,10] Many approaches have been followed to address this problem. For example, Bedair *et al.* constructed a polymeric monolith at the edge of an open channel to spray samples from the pores.[14] Another option is to integrate the microfluidic chip with an external nanoESI emitter, which is normally obtained from a conventional pulled glass capillary with a diameter of several micrometers to several hundred nanometers.[15,16] However, the dead volume originating from the external connection is inevitable. Clogging of the emitter tip is also a disturbing aspect for stable performance.[17] As a result, on-chip integrated emitters have become popular and a wide range of fabrication methods have been employed to build them.[18-21] Microchannel created by laser ablation as an ESI emitter is perhaps the easiest approach,[22-24] where a channel outlet could also be cut into a sharp-tip shape to assist stable electrospray ionization, as described in §1.2.3.[25,26] Lower sample consumption and higher detection sensitivity could be obtained by decreasing the size of

sample infusion channel or delivering sample solution into another dedicated nanoESI emitter channel. However, the continuous sample infusion will be impeded in both cases due to the large backpressure caused by the small emitter channel with a length of several millimeters. An on-chip microhole as an emitter for electrostatic spray ionization was created for coupling MS with droplet-based microfluidics previously (spyhole-ESTASI), as shown in §1.2.3. However, it was difficult to align the contactless electrode with the spyhole and MS inlet, and the spray performance was limited by the electrical field spreading due to the much larger size of the electrode compared with the spyhole.

To alleviate these problems, I present here a novel interface (spyhole-nanoESI) to couple microfluidic chips with MS by drilling a microhole with a diameter of 10-12 μm directly on top of a microchannel. Different from spyhole-ESTASI, an internal electrode contacting the sample channel was integrated on the chip to induce nanoESI for higher sensitivity and better spray performance. Under optimal conditions, the flow rate could be lowered to 100 nL/min for nanoESI. The dead volume of the microchip emitter is about 100 nL and an easy way to reduce the sample consumption is to use an 8-way valve to split the flow and pressure. Limits of detections (LODs) could be obtained at attomole per microliter levels for small organic molecules and peptides, which is 600 times lower than that usually obtained with standard ESI and microESI. To take advantages of the high sensitivity and low dead volume, the spyhole-nanoESI was used to detect a small cell lung cancer (SCLC) biomarker protein of neuron-specific enolase (NSE). By monitoring the transition of the unique peptide of NSE, LOD for the biomarker by the spyhole-nanoESI was at 12 pM. Its potential application in cancer diagnosis was further demonstrated with 1 μL of human serum containing 2 nM NSE, which is in accordance with the real abundance of the biomarker in blood at the extensive stage of the lung cancer,[27] without any complicated sample preparation steps, such as immunoaffinity extraction and liquid chromatography separation. In addition, the microchips can be disposable to avoid any cross contamination.

5.2. Experimental Section

5.2.1. Chemicals and materials

Angiotensin I (Ang I, trifluoroacetate salt, 98%) was obtained from Bachem (Dübendorf, Switzerland). Cytochrome c (from horse heart), acetic acid (99.5%), trifluoroacetic acid (TFA), 1,4-dithiothreitol (DTT, ≥99%), and ammonium bicarbonate

(NH_4HCO_3, 99.5%) were purchased from Fluka (Buchs, Switzerland). Methanol (99.9%), isopropanol (≥99.5%), reserpine (≥99%), iodoacetamide (IAA, 97%), insulin (from bovine pancreas, HPLC) and recombinant human neuron-specific enolase (NSE, ≥95%) were obtained from Sigma-Aldrich (Buchs, Switzerland). Trypsin (from bovine pancreas) was obtained from Applichem (Darmstadt, Germany). Human plasma was purchased from Bioreclamation LLC (Westbury, NY, USA). Deionized water produced by an alpha Q-Millipore System (Zug, Switzerland) was used for all experiments. Pierce Top 12 abundant protein depletion Spin Columns were purchased from Thermo Scientific (Switzerland). Amicon Ultra-2 centrifugal filters were ordered from Merck Millipore (Schaffhausen, Switzerland). Aquapel® solution was obtained from Aquapel Glass Treatment (Pittsburgh, USA).

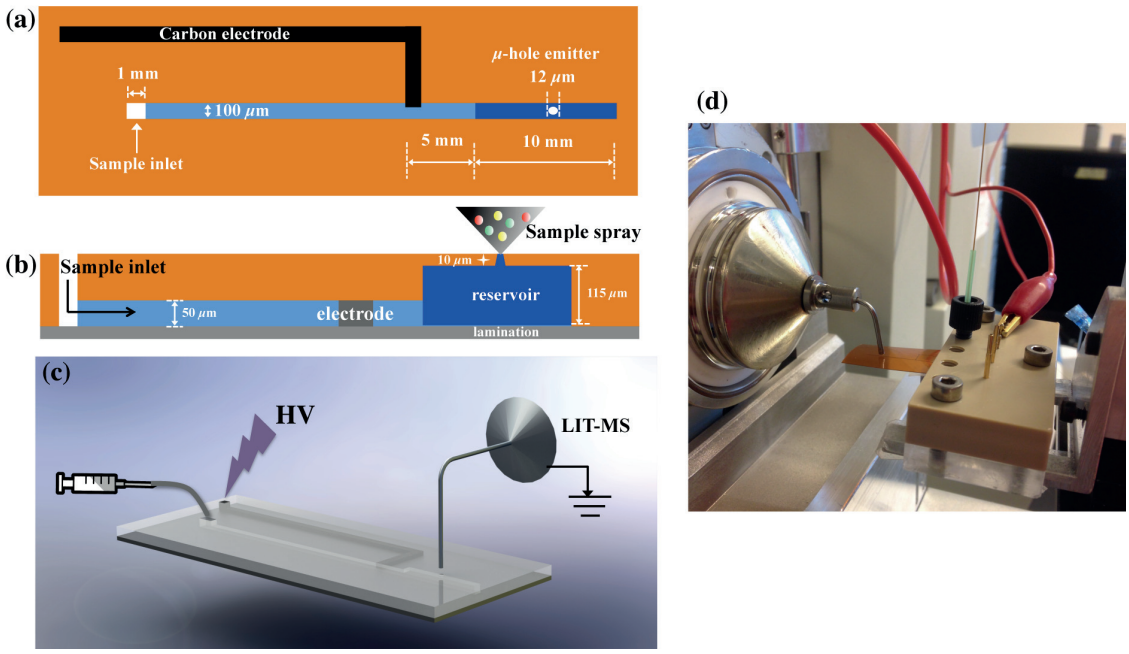

Figure 5.1. Schematic representation of the spyhole-nanoESI device: **(a)** top-view image, **(b)** side-view image, **(c)** 3D image, and **(d)** real picture on a plastic holder. The holder was fixed onto an *x*, *y*, *z* positioning stage and placed horizontally under an "L-shaped" MS ion transfer capillary. HV: high voltage. LIT-MS: linear ion trap mass spectrometry.

5.2.2. Spyhole-nanoESI fabrication, treatment and MS experiment

A spyhole-nanoESI device was designed as shown in Figure 5.1 and fabricated from a polyimide (PI) substrate (125 μm thick, Dupont, Switzerland) by scanning laser ablation as

previously reported.[28] The photoablation was performed with an ArgonFluoride excimer laser (Lambda Physics LPX 210I, Göttingen, Germany) at 193 nm with a pulse width about 20 ns, fluence of 0.35 J and frequency of 50 Hz. With these parameters, the microchannels for sample infusion and electrode strip were made around 50 μm in depth and 100 μm in width through the inspection under a laser-scanning microscope VK-8710 (Keyence Corporation, Osaka, Japan). A deeper short channel called reservoir was created with a depth around 115 μm and length of 10 mm at the end of the sample channel (30 mm length) to facilitate continuous sample delivery and avoid easy clogging of the spyhole. On top of this reservoir, a spyhole with a diameter of ~10 μm was drilled from the same side of the channels using a proper mask for the laser ablation in a static shot mode. The constructed spyhole was cleaned by the consecutive sonication in isopropanol and pure water for 10 min, respectively. The electrode microchannel was filled with conductive carbon ink (Electrador, Electra Polymer & Chemicals Ltd., UK) and the substrate was cured for 30 min at 80 ºC in the oven. Finally, the channel side of the spyhole-nanoESI was laminated with a 25/10 μm thick polyethylene/polyethylene terephthalate (PE/PET) layer using a lamination apparatus (Morane Senator, Oxon, UK) at 135 ºC and 3 bars and further cured for 1 h at 85 °C in the oven. The spyhole remained open for the sample spray on the opposite side of channel after the lamination.

A water-repellent commercial solution called Aquapel®, was flown through the sample channel for about 2 minutes and dipped around the spyhole outlet for the hydrophobic modification. To avoid the clogging of the channel and spyhole, the spyhole was immediately washed with water and ready to use. During the experiments, the solutions were injected into the fused silica capillary (75 μm i.d, 360 μm o.d., BGB analytik AG, Böckten, Switzerland) *via* a glass syringe (Hamilton, Bonaduz, Switzerland) by a syringe pump (KD Scientific, Holliston, MA, USA) and delivered to the spyhole *via* a homemade plastic holder with tight fittings (IDEX Health and Science LLC, Oak Harbor, WA, USA).

For the MS analysis, the spyhole-nanoESI assembled on a homemade holder was fixed onto an *x*, *y*, *z* positioning stage (Thorlabs, Dachau/Munich, Germany) and placed horizontally under a self-designed "L-shaped" ion transfer capillary instead of the original linear one of the Thermo LTQ Velo instrument (Thermo Scientific, San Jose, USA), as shown in Figure 5.1(d). The vertical distance between the spyhole and the ion transfer capillary was adjusted accurately with the positioning stage and kept always at around 1 mm. The sample was infused at 100 nL/min with a syringe pump. The nanoESI was induced by

applying an optimized voltage of 3 kV to the electrode on the spyhole against the MS inlet and the MS detection was performed under positive mode with a normal scan rate and an optimal automatic gain control (AGC) target value of 10'000. The maximum ion injection time for a single MS microscan was 500 ms. The ion transfer capillary was always set at 275 °C and all the source gases were set at 0. During tandem MS analysis, the AGC target values for MS and MS2 were set at 30'000 and 10'000, respectively. Collision-induced dissociation (CID) was used for the fragmentation of the isolated precursor ion with an isolation width of 1 *m*/*z* and optimized collision energy of 20 under a single reaction monitoring (SRM) scan mode. The maximum ion injection time of MS and MS^n were all set as 500 ms for a single microscan.

5.2.3. Chiptip-ESI, spyhole-nanoESTASI and standard ESI

For sensitivity comparisons, three other setups, called chiptip-ESI,[25] spyhole-nanoelectrostatic spray ionization (nanoESTASI)[28] and standard ESI, were also used, as described below.

Chiptip-ESI. Besides the spyhole-nanoESI, another two similar microchips, chiptip-ESI and spyhole-nanoESTASI, were designed and fabricated with the same laser ablation process in spyhole-nanoESI. In chiptip-ESI, the sample channel and electrode were same as those in spyhole-nanoESI but the reservoir and spyhole were removed. Instead, the sample channel exit was cut into a V-shape and acted as a spray emitter, as shown in Figure 5.2(a). The V-shaped emitter was measured exactly as 110 μm in length and 50 μm in width. The hydrophobic modification of chiptip-ESI was also performed with a same procedure as for spyhole-nanoESI.

The commercial linear ion transfer capillary of LTQ Velos was used for the chiptip-ESI. The lamination in chiptip-ESI could resist the flow rate up to 8 μL/min. To obtain a stable spray from chiptip-ESI, 5 nM Ang I in ESI buffer (50% MeOH, 49% H_2O and 1% acetic acid) was infused at 1 μL/min and 2.3 kV was found to be optimal when the V-shape tip of chiptip-ESI was placed 1 mm away from and in line with MS inlet. Therefore, 2.3 kV was applied for all the following analyses with chiptip-ESI. The parameters of the MS instrument for MS and tandem MS analyses were the same as those for spyhole-nanoESI.

Spyhole-nanoESTASI. Similarly, the sample spray with a spyhole-nanoelectrostatic spray ionization (spyhole-nanoESTASI) was from a spyhole but through a different

ionization process of ESTASI recently developed in our group. In spyhole-nanoESTASI, the sample channel and spyhole were the same as those in spyhole-nanoESI but the electrode strip was removed. Instead, a disk electrode (Ø 1 mm) was placed below the microchip and in line with the spyhole and the "L-shaped" ion transfer capillary inlet, as shown in Figure 5.2(b). A pulsed high voltage (HV, from 0 V to 10 kV, frequency 40 Hz) was generated by amplifying voltage square wave pulses (0 to 10 V) with a high voltage amplifier (10HVA24-P1, HVP High Voltage Products GmbH, Martinsried/Planegg, Germany), and applied on the disk electrode to induce ESTASI against MS inlet that was set at 275 °C and always grounded. The ESI voltage of the internal power of the MS instrument was always set as 0 and all the source gas flow rates were set at 0. Other MS parameters were set the same as those in spyhole-nanoESI. The flow rate was adjusted in each case to obtain a stable signal.

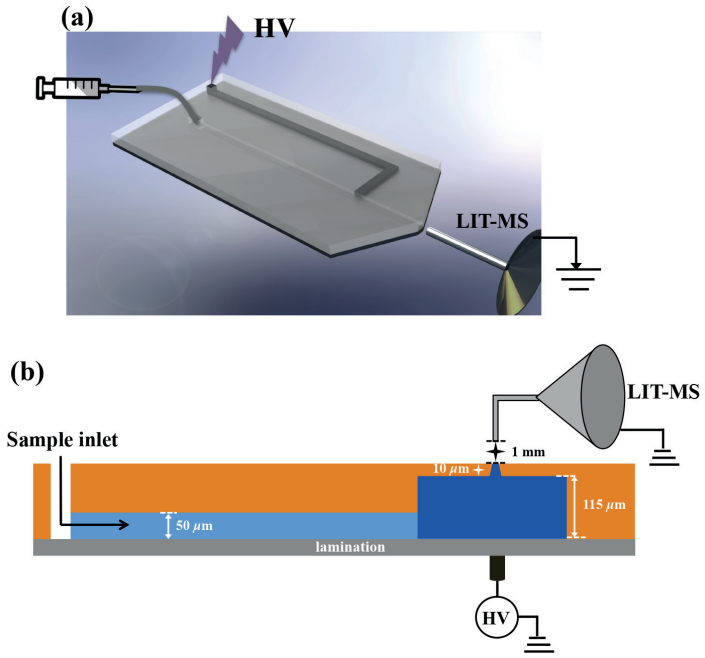

Figure 5.2. Schematic representation of different devices: **(a)** 3D image of chiptip-ESI and **(b)** side-view image of spyhole-nanoESTASI. HV: high voltage. LIT-MS: linear ion trap mass spectrometry.

Standard ESI. The samples were also applied *via* a direct infusion mode with a syringe at the flow rate of 3 μL/min and analyzed with the standard ESI. The sample spray with the commercial ESI source is from a needle of 500 μm in diameter and assisted with a sheath gas flow of 10 arbitrary units and aux gas flow of 5 arbitrary units. The ESI voltage of the internal power of the MS instrument was always set as 3.7 kV. The temperatures of the

heater and the MS inlet capillary were set at 42 °C and 275 °C, respectively. All other parameters of the MS instrument were the same as those in spyhole-nanoESI.

5.2.4. NSE tryptic digestion, *in silico* digestion and unique peptide determination

Enzymatic digestion of NSE was performed with a commonly used procedure, including reduction, alkylation and tryptic digestion. First, 30 μL NSE at 10 μg/mL and 100 ng/mL in 10 mM NH_4HCO_3 buffer (pH 8) were denatured at 95 °C for 5 min and then incubated with 0.5 μL of freshly prepared 60 mM DTT in H_2O at 57 °C for 30 min, respectively. After being cooled to room temperature (RT), 0.5 μL of freshly prepared 30 mM IAA in H_2O were added into the sample solutions and placed in dark for another 30 min at RT. For the tryptic digestion, 0.5 μL trypsin solutions at 12 μg/mL and 0.6 μg/mL in 10 mM NH_4HCO_3 buffer (pH 8) were added into these two samples containing 10 μg/mL and 100 ng/mL NSE respectively, and incubated overnight at 37 °C with moderate shaking. The digestions were quenched by adding 0.5 μL TFA and the diluted digests in ESI buffer (50% MeOH, 49% H_2O and 1% acetic acid) were ready to be directly analyzed by spyhole-ESI MS/MS under the optimized conditions as described above without any additional procedure.

The NSE sequence was acquired through the UniprotKB database with the accession number of P09104. MS-digest program from protein prospector version 5.19.1 (University of California, San Francisco, CA, USA) was used to perform an *in silico* digest of NSE. The results allowed the selection of possible unique peptide candidates by matching with the experimental data. To investigate if the candidate peptides solely originate from NSE, peptide search with Uniprot was performed to find all proteins in UniProtKB that contain the query peptide sequence. The search was limited to homo sapiens and bos taurus because trypsin was derived from bovine pancreas.

5.2.5. Detection of NSE in human serum

The serum was derived from the human plasma by overnight clotting and centrifugation, and certain amounts of NSE were fortified into 30 μL serum to reach a final concentration of 200 ng/mL, 100 ng/mL and 50 ng/mL respectively. Firstly, the depletion of high abundant proteins in the serum was performed to reduce the sample complexity. 30 μL of the serum sample was pooled into a Pierce Top 12 abundant protein depletion spin column

and incubated for 1 h at RT. Centrifugation at 1000 × *g* was then performed with the spin column for 2 min to collect the depleted serum sample in 500 μL 10 mM phosphate-buffered saline (PBS) buffer (0.15 M NaCl, 0.02% azide, pH 7.4). Before tryptic digestion, 500 μL of the protein solution collected from the 30 μL depleted serum sample was desalted by an Amicon Ultra-2 centrifugal filter device with the nominal molecular weight limit of 10K and finally concentrated in 30 μL 10 mM NH_4HCO_3 buffer (pH 8). After denaturation at 95 °C for 5 min, 1 μL of freshly prepared DTT (150 mM) was added and incubated at 57 °C for 30 min. Then, the sample solution was alkylated by 1 μL of freshly prepared IAA (75 mM) in dark for 30 min at RT, followed by digestion with 0.5 μL of 600 μg/mL trypsin (freshly prepared in 10 mM NH_4HCO_3) overnight at 37 °C with moderate shaking. After the digestion quenched by 0.5 μL TFA, the serum digests with or without fortified NSE were diluted 10 times with ESI buffer (50% MeOH, 49% H_2O and 1% acetic acid) and then analyzed directly with different methods, including the spyhole-nanoESI MS/MS, chiptip-ESI MS/MS and standard ESI MS/MS without additional desalting, concentration or fractionation procedures. The MS parameters were described in experimental part of 5.2.2.

5.3. Results and discussion

5.3.1. Spyhole-nanoESI MS: microchip design and setup optimization

Two parameters of the spyhole, depth and width, were optimized. The spyhole depth was the distance between the spyhole outlet and the sample channel, and should be as small as possible to facilitate the continuous sample delivery and avoid being susceptible to clogging. Instead of making the whole sample channel deeper, a short reservoir was created on the bottom of the sample channel to keep the total chip volume as small as possible to minimize dead volumes and sample consumption. Using a test sample of angiotensin I (Ang I) in ESI buffer (50% MeOH, 49 % H_2O and 1% acetic acid), the optimal spyhole depth was found to be 10 μm. A smaller depth of spyhole was not considered, because the short reservoir would then be easily penetrated during the laser ablation or the following treatment of the microchip. For nanoESI, the spyhole size plays a critical impact on the ionization efficiency and should be fabricated as small as possible. A spyhole with the diameter of 10-12 μm could be made reproducibly by laser ablation, as shown in Figure 5.3(a). In addition, the surface of the polyimide microchip was further modified to be hydrophobic by a commercial water-repellent Aquapel® solution, in order to form a stable and small droplet

for nanoESI. Under optimal conditions, 0.15 nM of Ang I could be detected at 433 *m*/*z* with a signal-to-noise ratio (S/N) of 10 by the spyhole-nanoESI with an ion trap mass spectrometer (Thermo LTQ Velos), Figure 5.3 (c).

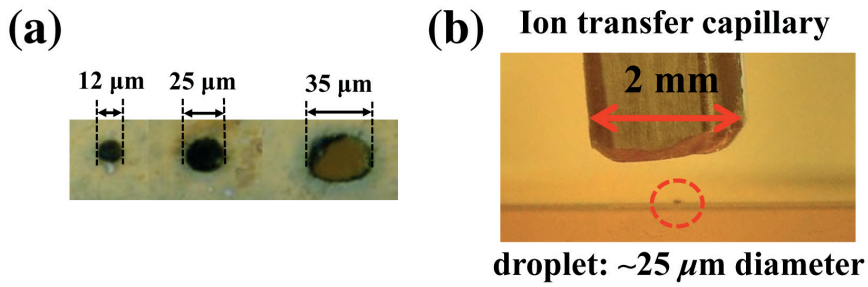

(c)

microchip No.	spyhole size	spyhole depth	Ang I Con.	S/N@433	Flow rate
Ⅰ	12 μm	10 μm	0.15 nM	10	100 nL/min
Ⅱ	25 μm	9 μm	0.5 nM	7	100 nL/min
Ⅲ	35 μm	11 μm	1 nM	5	100 nL/min

Figure 5.3. Optimization of the spyhole width and depth of the spyhole-nanoESI microchip: **(a)** microscopic images of spyholes with diameters of 12 μm, 25 μm and 35 μm. **(b)** microscopic image of the charged droplet generated at the spyhole of 12 μm in diameter. **(c)** LODs of Ang I in ESI buffer (50% MeOH, 49% H_2O and 1% acetic acid) by three spyhole-nanoESI microchips with different spyhole dimensions. The MS detection conditions were optimized as given in experimental part of 5.2.2.

The optimization of the spyhole-nanoESI MS with respect to hydrophobic modification, ESI voltage, the automatic gain control (AGC) target value of the ion trap instrument, and the vertical distance between the spyhole and the ion transfer capillary were performed with 0.15 nM Ang I in ESI buffer (50% MeOH, 49% H_2O and 1% acetic acid). The other analysis parameters were the same as those described in experimental part of 5.2.2.

The AGC value was initially set as 10'000. Five voltage values, 2.6, 2.8, 3, 3.2 and 3.4 kV, were tested individually and 3 kV was found to give the highest S/N of 10 for the triply charged Ang I ions at *m*/*z* 433 in Figure 5.4(c). Increasing the voltage to 3.2 kV did not make the S/N better because the analyte ions were overwhelmed by noisy background ions. When the voltage was increased to a point of 3.4 kV, the Taylor cone would break down instantly before ejecting the analyte ions into MS and no significant signal was observed, as shown in Figure 5.4(e). In contrast, fewer analyte ions were generated under a lower voltage of 2.8 kV comparing to 3 kV. When the voltage was decreased to 2.6 kV, the sample solution accumulated extensively at the spyhole instead of forming a Taylor cone and thereby no ions

were measured, in Figure 5.4(a). In summary, a stable nanoelectrospray could be induced by a voltage ranging from 2.8 kV to 3.2 kV and 3 kV was chosen for all the following tests under the detection conditions given in experimental part of 5.2.2.

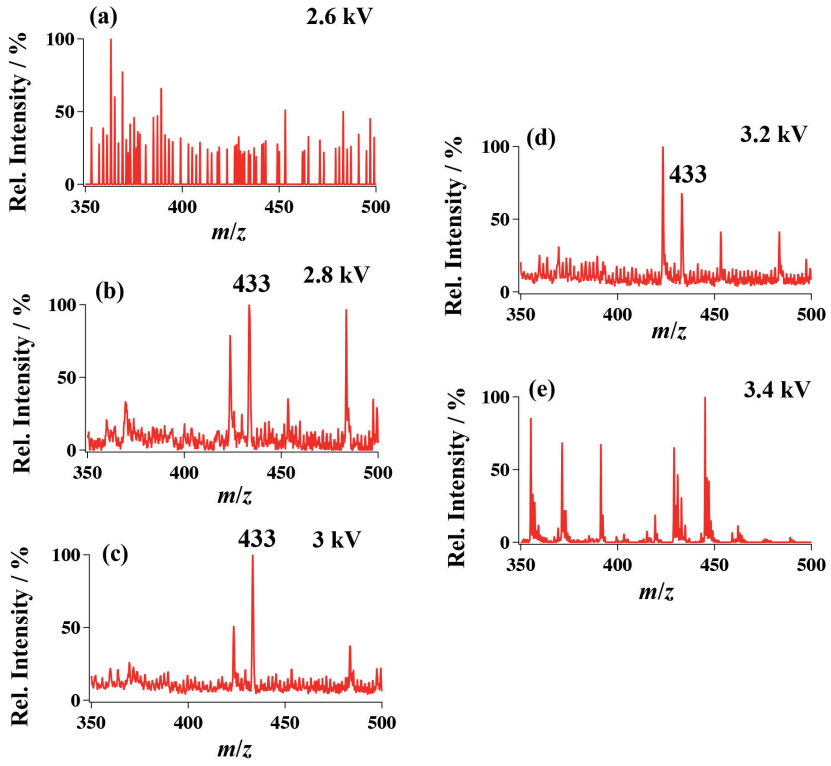

Figure 5.4. Analyses of 0.15 nM Ang I in ESI buffer by spyhole-nanoESI MS with voltages of: **(a)** 2.6 kV, **(b)** 2.8 kV, **(c)** 3 kV, **(d)** 3.2 kV and **(e)** 3.4 kV. AGC target value was set as 10'000. The other detection conditions were the same as those given in experimental part of 5.2.2.

Besides voltage, the signal quality is also greatly dependent on AGC target value. With LTQ Velos, the AGC value refers to the maximum quantity of total ions injected into the first ion trap during the defined maximum ion injection time of 500 ms. With an improper AGC value, the collected analyte ions are either not abundant enough or suppressed by coexisting background ions, resulting in a low S/N. Different AGC values were set for the analyses of 0.15 nM Ang I at a flow rate of 100 nL/min and with a voltage of 3 kV. In Figure 5.5, the AGC value of 10'000 gave the best S/N and was applied for all the following MS analyses.

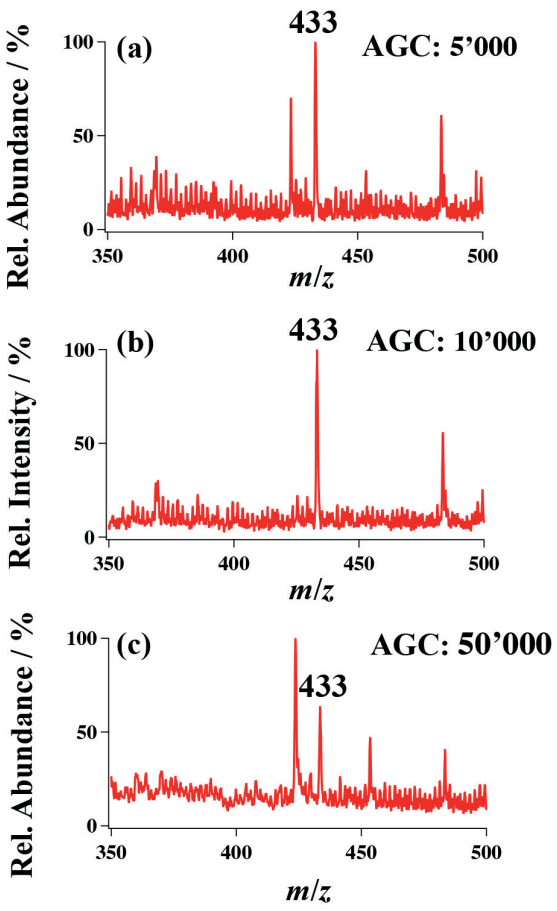

Figure 5.5. Analyses of 0.15 nM Ang I in ESI buffer by spyhole-nanoESI MS with AGC values of: **(a)** 5'000, **(b)** 10'000 and **(c)** 50'000. Voltage: 3 kV. The other detection conditions were the same as those given in experimental part of 5.2.2.

It is worth mentioning that the spyhole distance to the "L-shaped" ion transfer capillary inlet should be adjusted to obtain an optimal signal. The improper distance of either being too small or too big will hinder the continuous formation of a small and stable Taylor cone. In the present work, the optimal distance was found to be around 1 mm with the voltage of 3 kV. When the distance was smaller than 1 mm, the sample solution would be sucked into the ion transfer capillary under vacuum. On the contrary, with the distance larger than 1 mm, a higher voltage than 3 kV would be required to prevent the sample solution aggregation at the spyhole. However, the efficient ion transmission could be deteriorated by the enlarged distance and a higher voltage would also be a problem for the safety consideration. Therefore, a stable electrospray process could be obtained by applying a voltage of 3 kV with the distance of 1 mm between the spyhole and the ion transfer capillary.

In summary, the optimized conditions are: ESI buffer: 50% MeOH, 49% H_2O, 1% Acetic acid; flow rate: 100 nL/min; ESI voltage: 3 kV, the AGC value: 10'000; vertical distance: 1 mm.

5.3.2. Sensitivity of spyhole-nanoESI MS

$$P_E = \frac{\sigma^2}{2\varepsilon_0} \geq P_L = 2\gamma/r \; ; \sigma = 2\sqrt{\frac{\gamma\varepsilon_0}{r}}$$

$$SSC = \frac{\text{surface charge number}}{\text{sample amount}} = \frac{4\pi r^2\sigma}{\frac{4}{3}\pi r^3 C} = \frac{3\sigma}{rC} = 6\frac{\sqrt{\gamma\varepsilon_0}}{C}\frac{1}{r^{3/2}}$$

Equation 5.1: P_E, electrostatic pressure; P_L, Laplace pressure; σ, surface charge density; ε_0, vacuum permittivity; r, the radius of the initial charged droplet; γ, the surface tension of the liquid; SSC, specific surface charge; C, the analyte concentration.

According to the Equation 5.1, the ionization efficiency can be generally determined by the specific surface charge (SSC), which means the surface charge number per unit amount of analytes obtained when the Rayleigh limit is reached for every initial droplet emitted from the Taylor Cone. The charge number per sample molecule is mainly determined by the radius of the charged droplet for a certain concentration of analyte and could be used to theoretically evaluate the overall ionization efficiency of an electrospray emitter. A larger proportion of analyte molecules could be ionized for MS detection when the initial droplets are smaller.

Table 5.1. LODs of Ang I in ESI buffer (50% MeOH, 49% H_2O, 1% Acetic acid) with various devices. The detection conditions for the four different devices were described in experimental parts of 5.2.2 and 5.2.3. i.d: internal diameter.

Device	Emitter size	Ang I Concentration	S/N @ 433	Flow rate
spyhole-nanoESI	12 μm i.d.	0.05 nM	4	100 nL/min
chiptip-ESI	110 μm × 50 μm	5 nM	10	1 μL/min
spyhole-nanoESTASI	11 μm i.d.	15 nM	5	200 nL/min
standard ESI	500 μm i.d.	30 nM	5	3 μL/min

Based on Equation 5.1, the sensitivity of spyhole-nanoESI was measured and compared to standard ESI from commercial ion source, chiptip-ESI and spyhole-nanoESTASI, under optimized analysis conditions. For chiptip-ESI, the tip of the sample

channel (110 μm × 50 μm) was cut into a V-shape as spray emitter. Ionization with spyhole-nanoESTASI was achieved using a recently developed method of electrostatic spray ionization (ESTASI).[29] The sample channel and the spyhole on the spyhole-nanoESTASI were the same as those of spyhole-nanoESI but no on-chip electrode was used. Instead, a disk metallic electrode (Ø, 1 mm) was placed below the microchip and in line with the spyhole and the "L-shaped" ion transfer capillary to induce the ESTASI by applying a pulsed high voltage of 10 kV.

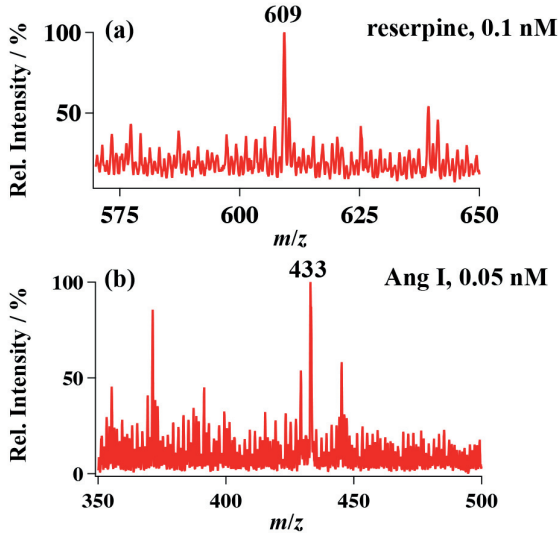

Figure 5.6. Detection of different molecules in ESI buffer (50% MeOH, 49% H_2O and 1% acetic acid) by the spyhole-nanoESI MS: **(a)** 0.1 nM reserpine, **(b)** 0.05 nM Ang I. The detection conditions were the same as the optimized one given in experimental part of 5.2.2.

Ang I in ESI buffer was analyzed with spyhole-nanoESI, chiptip-ESI and spyhole-nanoESTASI and standard ESI, respectively. The LODs of Ang I from its triply protonated ions (m/z =433) were listed in Table 5.1. From the results, the spyhole-nanoESI demonstrated the best sensitivity with the S/N of 4 for 0.05 nM Ang I, as shown in Figure 5.6 (b). In contrast, the LODs with chiptip-ESI, spyhole-nanoESTASI and standard ESI were determined to be 5 nM, 15 nM and 30 nM, respectively, for Ang I with S/N ≥3. It is worth mentioning that different flow rates were used for different setups. For the spyhole-nanoESI, the optimized flow rate was 100 nL/min; for spyhole-nanoESTASI, the optimized flow rate was 200 nL/min; for chiptip-ESI, the optimized flow rate was 1 μL/min; for standard ESI, the optimized flow rate was 3 μL/min. Therefore, the spyhole-nanoESI showed a LODs 600 times lower than standard ESI and 100 times than the previously developed chiptip-ESI.[25]

The sample consumption is decreased by ~1,000 times lower than chiptip-ESI, and ~20,000 time lower than the standard ESI considering the difference in flow rate. With such a high performance, the spyhole-nanoESI can bring additional value to the coupling of microfluidics with MS. Considering that the ion injection time was around 1 ms to generate a mass spectrum for 0.15 nM Ang I, the infused Ang I at 100 nL/min was ~150 molecules to generate a mass spectrum, which was comparable with other reported nanospray devices for peptide detection.[8,30,31]

The high sensitivity of the spyhole-nanoESI was also demonstrated with reserpine, a small drug molecule, with LOD as 0.1 nM, Figure 5.6(a). The good performance of spyhole-nanoESI stems from the advantages of nanoESI,[8] the well-controlled emitter geometry and the surface hydrophobic modification of microfluidic chips.

5.3.3. Detection of cancer biomarker with the spyhole-nanoESI MS/MS

With the high sensitivity, the spyhole-nanoESI MS could be applied to detect cancer biomarkers directly from body fluids. As a proof-of-concept, a lung cancer biomarker protein, neuron-specific enolase (NSE), at low abundance was detected by monitoring the transition of its unique peptide with spyhole-nanoESI MS/MS.

Signature peptide candidates were obtained by analysing 1 μg/mL NSE tryptic digest with spyhole-nanoESI MS. 9 peaks were found possibly originating from NSE by matching the experimental data to the peptide list from *in silico* proteolysis, as shown in Figure 5.7(b) in bold. The mass tolerance was less than 1 Da. Peptides with missed cleavage or any modification were not considered to ensure the quality of signature peptide candidates, for example the reproducibility or chemical stability. Uniqueness of these potential peptides was checked with the peptide search in UniprotKB and 8 of them were found specific for NSE, as the italic and bold parts in Figure 5.7(b). Finally, four highly detectable and unique peptides were selected and further identified by spyhole-nanoESI MS/MS, as the italic, bold and underlined parts in Figure 5.7(b).

CID-induced fragmentations of the four candidate signature peptides were performed individually and the optimal transition of each peptide was obtained through SRM by adjusting the collision energy. The fragments with m/z values too close to the precursor ions were not considered, as such transitions are usually noisy especially when analysing the rather complicated sample. The fragments with m/z values smaller than the precursors were

also avoided even though they are usually the predominant product ions, because they generally display worse selectivity and may come from the singly charged chemical background. Considering these factors and comparing the efficiency of the optimal transition for each candidate signature peptide, the peptide of IVIGMDVAASEFYR namely SP-14 was selected as the signature peptide of NSE and the transition of $785.8^{2+} \rightarrow 843.4^{+}$ with the optimal normalized collision energy of 20 and the isolated width of 1 *m*/*z* was monitored for the following NSE detection, as shown in Figure 5.7(c). The product ion at *m*/*z* 843.4 was further identified by spyhole-nanoESI MS^3 to ensure it actually came from the signature peptide instead of any other chemical background, in Figure 5.7(d).

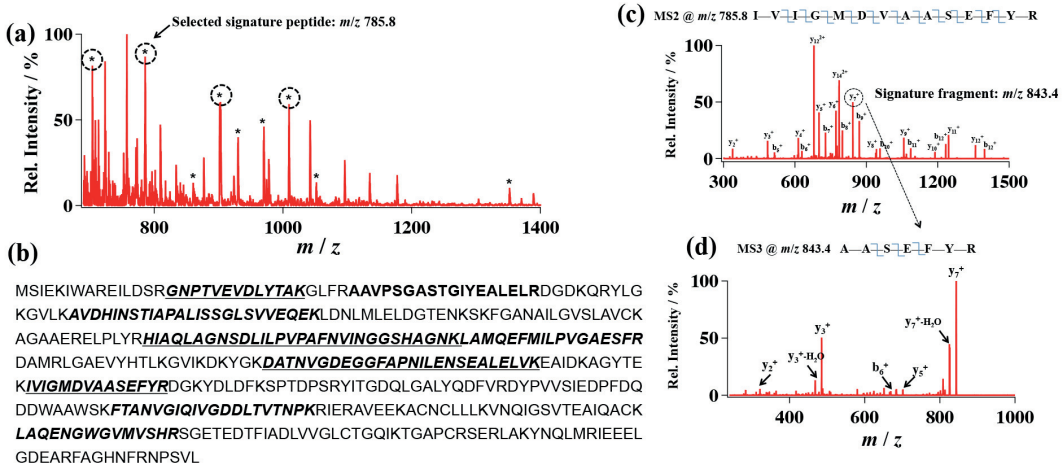

Figure 5.7. (a) Mass spectrum of 1 μg/mL NSE tryptic digests in ESI buffer (50% MeOH, 49% H_2O and 1% acetic acid) by spyhole-nanoESI MS. The peaks marked with stars were peptides potentially from NSE. The peaks marked with stars and circles were selected as candidate signature peptides. **(b)** NSE sequence. Bold parts: potential peptides of NSE observed by spyhole-nanoESI MS. Bold and italic parts: potential peptides specific for NSE. Bold, italic and underlined parts: signature peptides candidates. **(c)** Mass spectrum from the CID-induced fragmentation of the signature peptide SP-14 at *m*/*z* 785.8 in 100 ng/mL NSE digests with a normalized energy of 20 and the isolated width of 1 *m*/*z* by spyhole-nanoESI MS/MS. **(d)** Mass spectrum from the CID-induced fragmentation of the product ion at *m*/*z* 843.4 by spyhole-nanoESI MS3. The product ion at *m*/*z* 843.4 was selected from the fragmentation of the signature peptide SP-14 at *m*/*z* 785.8 by spyhole-nanoESI MS/MS. The detection conditions were described in experimental part of 5.2.2.

Under these conditions, the spyhole-nanoESI MS/MS was firstly used to detect NSE in water. With 10 ng/mL (0.2 nM) NSE tryptic digest, the fragment ion at *m*/*z* = 834.4 could be observed with good S/N of 50, as shown in Figure 5.8(a). In contrast, chiptip-ESI and standard ESI gave the S/N of 6 and 3 for 10 ng/mL NSE, respectively, as shown in Figure 5.8(b) and (c). As shown in Figure 5.8(d), the ESI buffer did not give any signal at *m*/*z* 834.4,

confirming that the fragment ion solely originating from NSE instead of contaminates in the microchip or MS instrument.

The LOD of NSE with the S/N of 3 by spyhole-nanoESI was then estimated as around 0.6 ng/mL (12 pM) and was comparable to that (0.4 ng/mL) reported with liquid chromatography (LC)-MS/MS based method.[32] In the literature, specific capture was firstly performed to collect the low abundant NSE (5-500 ng/mL, 1 mL), and then LC was applied to desalt and fractionate the 100 μL 10 times concentrated tryptic peptides before MS/MS analysis. In contrast, the spyhole-nanoESI MS/MS requires no additional sample pretreatment prior to analysis and provides good sensitivity even without any concentration step.

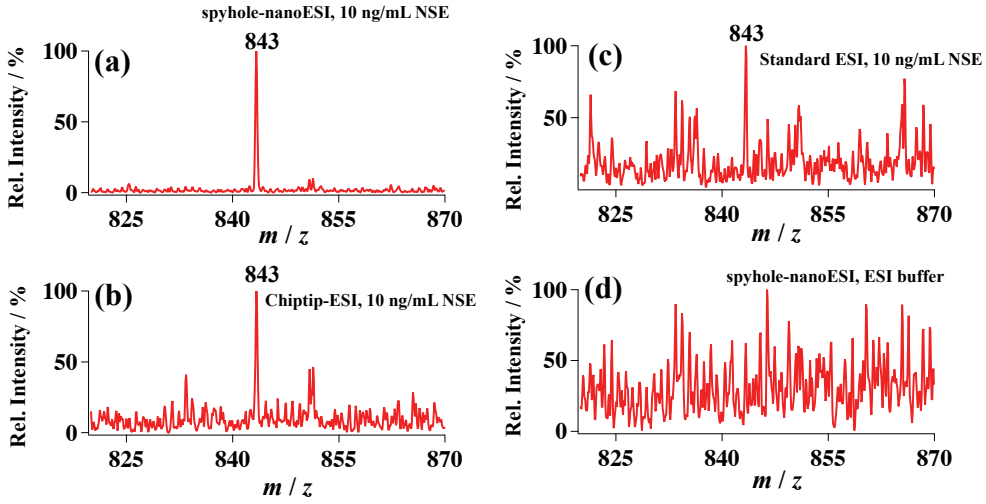

Figure 5.8. NSE detection by single reaction monitoring (SRM) of its signature peptide SP-14. 10 ng/mL NSE tryptic digest in ESI buffer (50% MeOH, 49% H_2O and 1% acetic acid) was used for the following tests. Mass spectra of the signature fragment ion of SP-14 at *m/z* 843.4 obtained by **(a)** spyhole-nanoESI MS/MS; **(b)** chiptip-ESI MS/MS; **(c)** standard ESI MS/MS. **(d)** Mass spectrum of the ESI buffer obtained by spyhole-nanoESI MS/MS.

The spyhole-nanoESI MS/MS was further applied to detect the biomarker directly from human serum to demonstrate its potential application in clinical diagnosis. Human serum from healthy individuals was spiked with 0, 100, or 200 ng/mL of NSE for test. To reduce the complexity of the human serum, the top 12 abundant proteins in the serum sample were first depleted with immune spin columns and then digested by trypsin. The tryptic digests were directly analyzed with spyhole-nanoESI MS/MS after being diluted 10 times with ESI buffer (50% MeOH, 49% H_2O and 1% acetic acid). For the 10 times diluted human serum without spiked NSE, there was no obvious signal of the signature fragment ion of SP-

14 at *m/z* = 834.4 observed in Figure 5.9(c), while the ion could be found from the serum spiked with 200 ng/mL NSE (S/N = 10) or 100 ng/mL NSE (S/N =3), Figure 5.9(a) and (b). Therefore, the elevated NSE at 100 ng/mL (2 nM) in 1 μL human serum could be detected with the spyhole-nanoESI MS/MS, which could be valuable for the fast and simple diagnosis of SCLC at the extensive stage (94.5+/-13.8 ng/mL)[27] and could also be used as the early indicator of the response rate to chemotherapy. In contrast, with the chiptip-ESI and standard ESI, no obvious signal of the fragment ion of SP-14 could be detected either from normal human serum or the serum spiked with 100 ng/mL NSE.

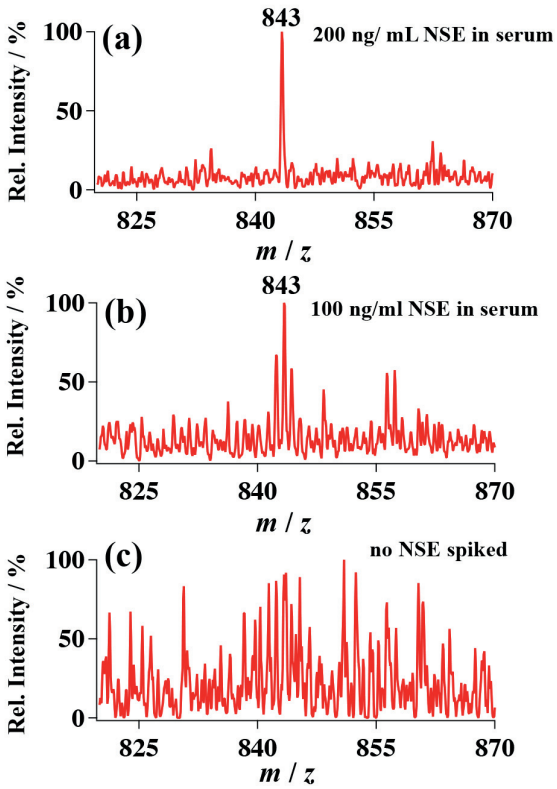

Figure 5.9. Detection of NSE in human serum with spyhole-nanoESI MS/MS. 1 μL of tryptic digests of human serum spiked with NSE was diluted by 10 times with ESI buffer (50% MeOH, 49% H_2O and 1% acetic acid) for spyhole-nanoESI MS/MS analysis. Mass spectra of the signature fragment ion of SP-14 at *m/z* 843.4 from serum sample spiked with **(a)** 200 ng/mL NSE; **(b)** 100 ng/mL NSE; **(c)** without NSE. The detection conditions were the same as those given in experimental part of 5.2.2.

Compared with the routine immunometric method for NSE determination, the present method requires no usage of expensive labelled antibodies and provides exact identification, avoiding possible false positive diagnosis from antibody cross reaction. Using LC-MS/MS based methods for NSE detection, numerous cleanup processes before analysis are rather

complicated, labour-extensive, time-consuming and can cause sample loss. A large volume of serum from several hundred microliters to millilitres was usually required for specific separation and concentration. In contrast, the spyhole-nanoESI MS/MS could offer direct and sensitive diagnosis of the low abundant biomarker in human serum and requires only one cleanup procedure of high abundant protein depletion. Owing to the simplified procedure and great sensitivity, only 1 μL of serum was consumed for a single diagnosis.

In addition, the laser ablation method for microchip fabrication offers a precise process control, wherein the spyhole-nanoESI devices were reproducible. Its easy fabrication, low cost and disposable nature make washing avoided and eliminate cross contamination between samples, which is highly suitable for clinical diagnosis application. Moreover, the spyhole-nanoESI device could be coupled with various MS instruments, such as high-resolution mass spectrometers for improved accuracy of the analyte identification, which are intensively required in clinical diagnosis from complex matrices.

5.4. Conclusions

In the present work, a microchip device was coupled with MS by drilling a spyhole with a diameter of 10-12 μm on top of the chip to form a nanoESI emitter for ultrasensitive analysis. The sample was infused at a nanoscale flow rate and emitted from the hydrophobic-treated spyhole into MS by a nanoelectrospray ionization. With the optimized detection conditions, peptides were detected with ultrahigh sensitivities. The LOD of Ang I was as low as 50 pM, which was 600 times lower comparing to standard ESI. The sample consumption for MS detection can be lowered 20,000 times compared to standard ESI. With the spyhole-nanoESI MS/MS, a lung cancer biomarker protein of NSE could be detected sensitively with a LOD of 12 pM by monitoring the transition of its signature peptide. The biomarker can also be detected from human serum with concentrations as low as 2 nM. Only 1 μL of serum digests was sufficient for a single diagnosis. The great sensitivity, low cost, disposal nature, compatible with various MS instruments, together with the overall simplicity of the direct analysis with few cleanup processes make spyhole-nanoESI MS/MS suitable for clinical diagnosis with a limited amount of samples.

5.5. References

(1) Liu, K. K.; Wu, R. G.; Chuang, Y. J.; Khoo, H. S.; Huang, S. H.; Tseng, F. G. *Sensors*. **2010**, 6623-6661.

(2) Su, W.; Gao, X.; Jiang, L.; Qin, J. *J. Chromatogr. A*. **2015**,13-26.

(3) Wu, J.; Gu, M. *J. Biomed. Opt.* **2011**, *16* (8), 80901.

(4) Johnson, M. E.; Landers, J. P. *Electrophoresis*. **2004**, 3513-3527.

(5) Wang, J. *Talanta*. **2002**, 223-231.

(6) Wang, X.; Yi, L.; Mukhitov, N.; Schrell, A. M.; Dhumpa, R.; Roper, M. G. *J. Chromatogr. A*. **2015**, 98-116.

(7) Freire, S. L. S.; Yang, H.; Wheeler, A. R. *Electrophoresis* **2008**, *29* (9), 1836-1843.

(8) Wilm, M.; Mann, M. *Anal. Chem.* **1996**, *68* (1), 1-8.

(9) Xue, Q.; Foret, F.; Dunayevskiy, Y. M.; Zavracky, P. M.; McGruer, N. E.; Karger, B. L. *Anal. Chem.* **1997**, *69* (3), 426-430.

(10) Rohner, T. C.; Rossier, J. S.; Girault, H. H. *Anal. Chem.* **2001**, *73* (22), 5353-5357.

(11) Chen, S. H.; Sung, W. C.; Lee, G. Bin; Lin, Z. Y.; Chen, P. W.; Liao, P. C. *Electrophoresis* **2001**, *22* (18), 3972-3977.

(12) Schilling, M.; Nigge, W.; Rudzinski, A.; Neyer, A.; Hergenroder, R. *Lab Chip* **2004**, *4* (3), 220-224.

(13) Yin, H.; Killeen, K.; Brennen, R.; Sobek, D.; Werlich, M.; Van De Goor, T. *Anal. Chem.* **2005**, *77* (2), 527-533.

(14) Bedair, M. F.; Oleschuk, R. D. *Anal. Chem.* **2006**, *78* (4), 1130-1138.

(15) Lazar, I. M.; Ramsey, R. S.; Sundberg, S.; Ramsey, J. M. *Anal. Chem.* **1999**, *71* (17), 3627-3631.

(16) Chan, J. H.; Timperman, A. T.; Qin, D.; Aebersold, R. *Anal. Chem.* **1999**, *71* (20), 4437-4444.

(17) Bings, N. H.; Wang, C.; Skinner, C. D.; Colyer, C. L.; Thibault, P.; Harrison, D. J. *Anal. Chem.* **1999**, *71* (15), 3292-3296.

(18) Kim, W.; Guo, M.; Yang, P.; Wang, D. *Anal. Chem.* **2007**, *79* (10), 3703-3707.

(19) Hoffmann, P.; Häusig, U.; Schulze, P.; Belder, D. *Angew. Chemie - Int. Ed.* **2007**, *46* (26), 4913-4916.

(20) Xie, J.; Miao, Y.; Shih, J.; Tai, Y. C.; Lee, T. D. *Anal. Chem.* **2005**, *77* (21), 6947-6953.

(21) Svedberg, M.; Veszelei, M.; Axelsson, J.; Vangbo, M.; Nikolajeff, F. *Lab Chip* **2004**, *4* (4), 322-327.

(22) Rohner, T.; Rossier, J.; Girault, H. H. *Anal. Chem.* **2001**, *73*, 5353-5357.

(23) Lion, N.; Gobry, V.; Jensen, H.; Rossier, J.; Girault, H. H. *Electrophoresis* **2002**, *23*, 3583-3588.

(24) Lion, N.; Gellon, J.; Jensen, H.; Girault, H. H. *J. Chromatogr. A.* **2003**, *1003*, 11-19.

(25) Gobry, V.; Van Oostrum, J.; Martinelli, M.; Rohner, T. C.; Reymond, F.; Rossier, J. S.; Girault, H. H. *Proteomics* **2002**, *2* (4), 405-412.

(26) Gasilova, N.; Qiao, L.; Momotenko, D.; Pourhaghighi, M. R.; Girault, H. H. *Anal. Chem.* **2013**, *85* (13), 6254-6263.

(27) Johnson, D. H.; Marangos, P. J.; Forbes, J. T.; Hainsworth, J. D.; Van Welch, R.; Hande, K. R.; Greco, F. A. *Cancer Res.* **1984**, *44* (11), 5409-5414.

(28) Gasilova, N.; Yu, Q.; Qiao, L.; Girault, H. H. *Angew. Chemie - Int. Ed.* **2014**, *53* (17), 4408-4412.

(29) Qiao, L.; Sartor, R.; Gasilova, N.; Lu, Y.; Tobolkina, E.; Liu, B.; Girault, H. H. *Anal. Chem.* **2012**, *84* (17), 7422-7430.

(30) Sun, L.; Zhu, G.; Zhao, Y.; Yan, X.; Mou, S.; Dovichi, N. J. *Angew. Chemie - Int. Ed.* **2013**, *52* (51), 13661-13664.

(31) Li, Y.; Champion, M. M.; Sun, L.; Champion, P. A. D.; Wojcik, R.; Dovichi, N. J. *Anal. Chem.* **2012**, *84* (3), 1617-1622.

(32) Torsetnes, S. B.; Løvbak, S. G.; Claus, C.; Lund, H.; Nordlund, M. S.; Paus, E.; Halvorsen, T. G.; Reubsaet, L. *J. Chromatogr. B Anal. Technol. Biomed. Life Sci.* **2013**, *929*, 125-132.

CHAPTER VI.

Summary & perspective

The main purpose of this thesis is to develop bioanalytical tools based on mass spectrometry. The first objective is to expand the application fields of ESTASI-MS exploiting the advantages of this ambient technique. Therefore, Chapter II & III describe the combination of ESTASI-MS or ESTASI-MSI with two classical analytical tools of TLC plates and 384-well plates. Coupling ESTASI-MS with 384-well plates, liquid samples could be sprayed directly from the unmodified wells, which acted as both containers and emitters for ionization without any liquid delivery interface. With both the qualification and quantification abilities, the integrated device is suitable for enzyme assay and drug metabolism studies, providing great potential value for drug development. In ESTASI-TLC-MS, dye spots separated on a high performance reverse phase C_{18} silica plate were profiled by ESTASI-MSI, which revealed the accurate sample location and is especially of great value when the samples are colorless and do not give a clear image under UV illumination. To analyze the normal phase silica TLC plates with ESTASI-MS, the surface modification with chlorotrimethylsilane was performed to render the normal phase TLC plates hydrophobic, which alleviated the strong adsorption of ESI buffer into the TLC plates and benefited the ESTASI-MS analyses with efficient sample extraction, reduced tailing effect and even the abilities of sample desalting, thus leading to an enhanced sensitivity.

Similarly, ambient surface analyses with ESTASI-MS could be extended to lateral flow tests, also known as lateral flow immunochromatographic assays, which is a rather inexpensive, simple and rapid device for clinical and point-of-care testing.[1] Typically, the analytes in biofluids were passing through a series of capillary beds spontaneously by a capillary pumping, binding with particle-labeled antibodies (Abs) or mixing with particle-labeled target analytes, and then finally captured in a format of sandwich assay or competitive assay. As mediums for signal reading out, latex or nanoparticles, including gold, fluorescent or magnetic particles, are often employed.

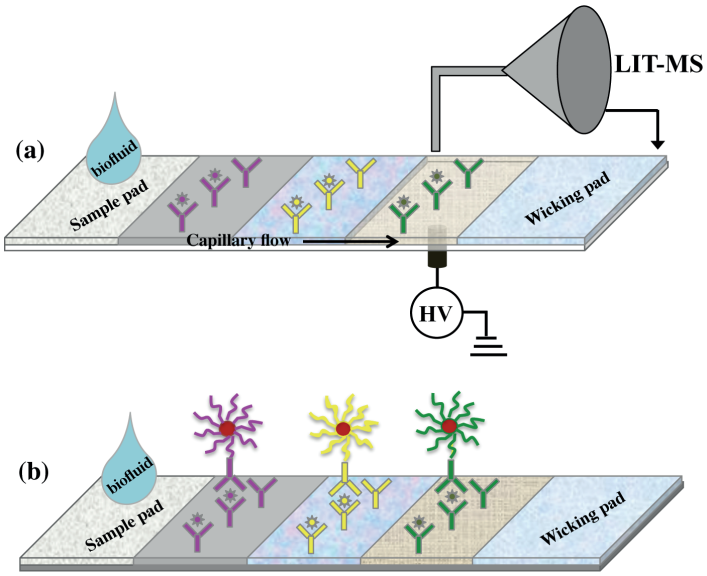

Figure 6.1. Direct coupling of ESTASI-MS with lateral flow tests. **(a)** High throughput analyses of multiple target analytes from biofluids captured and separated on a lateral flow strip. **(b)** Amplified ESTASI-MS signals with various mass barcoded particles for multiplex analyses of biofluids.

Compared to spectroscopic, magnetic or electronic detection methods, ESTASI-MS as a signal read out tool could provide accurate identification of analytes, as well as structural elucidation with tandem MS, avoiding false positive results often happened in reporter-labeled immunoassay. Moreover, high throughput and fast analysis could be easily realized within a single lateral flow strip, no requiring multiplex labels and expensive Abs, as shown in Figure 6.1(a). Coupling ESTASI-MS with lateral flow strips holds a wide range of applications in biochemical analyses, particularly for biofluid-based clinical tests, such as the allergy and allergen, biomarker, or pregnancy diagnosis in a component-resolved diagnosis way. Furthermore, mass barcode-based MS signal amplification strategy, described in Chapter II, could also be implanted into lateral flow strip ESTASI-MS to achieve ultrasensitive testing, which is very important for disease-related early diagnosis. Based on the sandwich or competitive assay, the mass barcodes could be grafted onto particles in a covalent or noncovalent way, and then desorbed for ESTASI-MS analysis, as shown in Figure 6.1(b).

Taking advantage of ESTASI-MS as an ambient surface analysis method, studies of solid-liquid reaction kinetics could also be performed to monitor intermediate products with short half-life time in real time.[2] Besides, large quantities of metabolic profiles of normal cells and cancerous cells at different stages could be differentiated with the 384-well plate ESTASI-MS in a high throughput way. Based on the differences of mass spectra profiles, the

potential metabolic biomarkers could be determined and their distributions of over normal and cancerous tissues would further be imaged with ESTASI-MSI to reveal the tumor margin, which should be helpful for the rapid intra-operative detection of residual cancer tissue during organ-conserving surgery.[3]

Chapter IV and V presented two strategies to enhance the MALDI-MS and ESI-MS signals, respectively. Combined with immunomagnetic separation, multiplex allergenic proteins in cow's milk were conjugated onto mass barcoded gold nanoparticles (Mb-AuNPs), captured by specific IgE Abs in only 1 μL of patient's blood serum, and then reported by simultaneous detection of corresponding mass barcodes from AuNPs in a highly sensitive manner for component resolved allergy diagnosis. This signal amplification strategy could also be applied for biomarker probing in cells or tissues, such as the melanoma cell diagnosis by labeling the biomarker of tyrosinase with Mb-AuNPs for sensitive MALDI-MS detection of the mass barcodes.

In Chapter V, an on-chip spyhole with a diameter around 10 μm was created by laser ablation method to work as an emitter for nanoESI, which acted as an efficient interface for coupling microfluidics with MS. With the spyhole-nanoESI-MS/MS, sensitive detection of lung cancer biomarker in small volumes of human serum was realized by monitoring the characteristic transition of a signature peptide without complicated sample pretreatments. Moreover, with the producible and precise control of the fabrication process by laser ablation, various functions could be easily integrated for different purposes. In proteomics, several on-chip sample treatments, such as proteolysis, purification, and fractionation, could be performed, following with sensitive spyhole-nanoESI-MS/MS analysis.

To develop novel emitters and improve the spray flux, macroporous ordered silica foams (MOSF) would be deposited on a substrate or modified onto capillary tips, and then act as multiplex emitters for nanoESTASI-MS analysis.[4]

All in all, as this thesis has shown, it is clear that mass spectrometry will become more and more an instrument of choice of bioanalytical chemistry, and will play a greater role in automated medical diagnostic laboratories.

References

(1) https://en.wikipedia.org/wiki/Lateral_flow_test

(2) Perry R. H.; Splendore, M.; Chien, A.; Davis, N. K.; Zare, R. N. *Angew. Chem.- Int. Ed.* **2011**, *50*, 250-254.

(3) Calligaris, D.; Caragacianu, D.; Liu, X.; Norton, I.; Thompson, C. J.; Richardson, A. L.; Golshan, M.; Easterling, M. L.; Santagata, S.; Dillon, D. A.; Jolesz, F. A.; Agar, N. *Proc. Natl. Acad. Sci. U.S.A.* **2014**, *111*, 15184-15189.

(4) Qian, K.;, Wan, J.; Qiao, L.;, Huang, X.; Tang, J.; Wang, Y.; Kong, J.; Yang, P.; Yu, C.; Liu, B. *Anal. Chem.* **2009**, *81*, 5749-5756.

Xiaoqin ZHONG

Female, Born on September 3rd, 1988 ; Tel: 0041-787353686 ; E-mail: xiaoqin.zhong@epfl.ch
Rue de l'envol 12, 1950 Sion, VS, Switzerland

PROFESSIONAL PROFILE

- Expertise in mass spectrometry (MS) and bioanalysis
- 6 years experience in matrix-assisted laser desorption/ionization time-of-flight (MALDI-TOF) mass spectrometer
- 4 years experience in electrospray ionization (ESI) ion trap mass spectrometer
- 2 years teaching assistant: méthodes de séparation analytique, in Ecole Polytechnique Fédérale de Lausanne, 2014-2016.

EDUCATION

École Polytechnique Fédérale de Lausanne (EPFL), Switzerland
Ph.D. in Chemistry and Chemical Engineering 11/2017

Nanjing University, Nanjing, China
M.Sc. & B.Sc. in Analytical Chemistry 06/2013

RESEARCH EXPERIENCE

Institute of Chemical Sciences and Engineering, EPFL Doctoral Assistant 2013-2017

Thesis: New ionization and tagging method for mass spectrometry
Supervisor: Prof. Hubert H. Girault

- Allergy diagnosis, cancer biomarker detection
- Drug metabolism study, enzyme assay and inhibitor screening
- Development of Electrostatic spray ionization (ESTASI)-MS imaging
- Coupling ESTASI-MS with thin layer chromatography and microtiter plate
- Coupling microfluidic chip with MS
- Synthesis of polymer-tagged nanoparticles for MALDI-MS signal amplification

Department of Chemistry, Nanjing University 2008-2013

Thesis: Aptamer-Functionalized Silver Nanocluster for Biosensing
Supervisor: Prof. Junjie Zhu

- Combining MS with fluorimeter for thrombin detection
- Fabrication of flexible PDMS-based soft electrode
- PDMS-gold nanoparticle composite for visual detection of biomolecules
- Silver nanocluster for fluorescence bioassay and cell imaging

TECHNICAL SKILLS Analytical and Bioanalytical Chemistry

Mass Spectrometer: electrospray ionization (ESI), matrix-assisted laser desorption ionization (MALDI), electrostatic spray ionization (ESTASI), time-of-flight (TOF), ion trap, quadrupole, orbitrap, collision induced dissociation, tandem MS

Chromatography: liquid chromatography (LC), gas chromatography (GC), thin layer chromatography (TLC)

Materials: immunoaffinity gold nanoparticles, polymer-coated gold nanoparticles, DNA-templated silver nanocluster, immunoaffinity magnetic beads

Microfabrication: clean room experience, laser ablation, microfluidic chip, soft electrode with PDMS

Application: proteomics, drug metabolism, enzyme assay, inhibitor screening, immunoassay, allergy diagnosis, biomarker detection, microfluidics, organic mixture separation and identification, MS imaging

Software: ExPASy Tools, MASCOT, Xcalibur, Photoshop, Illustrator, Chemdraw, Windows, Mac OS, Office, Igor Pro, Origin Pro

LANGUAGE

English Advanced (C1), French intermediate (B1), Chinese Native

PUBLICATION

1. X. Zhong, L. Qiao, B. Liu and H. Girault. Microfluidics nanoelectrospray mass spectrometry for biomarker diagnostics. *Under preparation*.

2. L. Qiao,[#] X. Zhong,[#] E. Belghith, Y. Deng, T.-E. Lin, E. Tobolkina, B. Liu and H. Girault. Electrostatic spray ionization from 384-well microtiter plates for mass spectrometry analysis based enzyme assay and drug metabolism screening. *Anal. Chem.*, **2017**, *89* (11), 5983-5990. #: Equal contribution.

3. X. Zhong, L. Qiao, N. Gasilova, B. Liu and H. Girault. Mass Barcode Signal Amplification for Multiplex Allergy Diagnosis by MALDI-MS. *Anal. Chem.*, **2016**, *88* (12), 6184-6189.

4. X. Zhong, L. Qiao, B. Liu and H. H. Girault. Ambient in situ analysis and imaging of both hydrophilic and hydrophobic thin layer chromatography plates by electrostatic spray ionization mass spectrometry. *RSC Advances*, **2015**, *5* (92), 75395-75402.

5. L. Qiao, E. Tobolkina, A. Lesch, A. Bondarenko, X. Zhong, B. Liu, H. Pick, H. Vogel and H. Girault. Electrostatic Spray Ionization Mass Spectrometry Imaging. *Anal. Chem.*, **2014**, *86* (4), 2033-2041.

6. J. Li, X. Zhong, F. Cheng, J. Zhang, L. Jiang, and J. Zhu. One-Pot Synthesis of Aptamer-Functionalized Silver Nanoclusters for Cell-Type-Specific Imaging. *Anal. Chem*., **2012**, *84* (9), 4140-4146.

7. J. Li, X. Zhong, H. Zhang, X. Le, and J. Zhu. Binding-Induced Fluorescence Turn-On Assay Using Aptamer-Functionalized Silver Nanocluster DNA Probes. *Anal. Chem.*, **2012**, *84* (12), 5170-5174.

8. W. Wu, X. Zhong, W. Wang, Q. Miao, J. Zhu. Flexible PDMS-based three-electrode sensor. *Electrochem commun*., **2010**, *12* (11), 1600-1604.

9. W. Wang, W. Wu, X. Zhong, W. Wang, Q. Miao, J. Zhu. Aptamer-based PDMS-gold nanoparticle composite as a platform for visual detection of biomolecules with silver enhancement. *Biosens Bioelectron*., 2011, *26* (7), 3110-3114.

CONFERENCE

- ASMS 2016: 64th American Society for Mass Spectrometry, San Antonio, USA.

Poster presentation: Mass Barcode Signal Amplification for Multiplex Allergy Diagnosis by

MALDI-MS.

- IMSC 2014: 20th International Mass Spectrometry Conference, Geneva, Switzerland.

Poster presentation: “Direct coupling of thin layer chromatography with electrostatic spray ionization mass spectrometry”.

- ISE 2014: 14th International Society of Electrochemistry, Nanjing, China.

Oral presentation: “Electrostatic spray ionization mass spectrometry imaging”.

- SGMS 2013: 31th Swiss Group for Mass Spectrometry, Interlaken, Switzerland.

PEER REVIEW JOURNAL REFEREE

Chemical Science & **Analytical Methods** RSC Publishing - Royal Society of Chemistry

SELECTED AWARDS

- Excellent Graduate of Nanjing University, top 3%, 2012 and 2011
- Excellent Leader of Student Union, 2012
- The Third-prize Scholarship of Nanjing University, top 5%, 2008 and 2007